ANL-GenIV-056

Initial Implementation of Multi-Channel Thermal-Hydraulics Capability in Frequency Domain SCWR Stability Analysis Code SCWRSA

W. S. Yang

Nuclear Engineering Division

Argonne National Laboratory
9700 S. Cass Avenue
Argonne, IL 60439

September 15, 2005

Initial Implementation of Multi-Channel Thermal-Hydraulics Capability in Frequency Domain SCWR Stability Analysis Code SCWRSA

W. S. Yang

Argonne National Laboratory

Abstract

A frequency domain linear stability analysis code for SCWR is being developed under the USDOE Generation IV Initiative. Based on single-channel coolant and water rod models, a thermal-nuclear coupled SCWR stability analysis code named SCWRSA was previously developed and applied to preliminary stability analyses of a U.S. Generation IV SCWR reference concept. In this work, a multi-channel thermal-hydraulics analysis capability has been developed and implemented into SCWRSA. An iterative solution scheme was developed to calculate the steady state flow distribution among parallel thermal-hydraulics channels under a fixed total flow rate and the equal pressure drop boundary condition. This scheme determines the coolant and water-rod flow rates simultaneously by taking into account the heat transfer between coolant and water rod. For linear stability analysis, perturbation calculation models for flow redistribution among parallel channels were developed along with an efficient scheme to solve the resulting system of linear equations. Time-dependent behavior of water in the lower plenum was approximated by two bounding inlet boundary conditions: instantaneous mixing and constant mixed-mean enthalpy of water in the lower plenum. The instantaneous mixing boundary condition neglects the time delay of the mixing in the lower plenum, and the constant mixed-mean enthalpy boundary condition assumes that the steady state mixed-mean enthalpy of water in the lower plenum is maintained during the time of interest.

The functionality of the modified SCWRSA code was confirmed by reproducing the previous single-channel analysis results. Preliminary verification tests of the new multi-channel

analysis capability have been performed using two-channel models derived from the U.S. Generation IV SCWR reference design. Although individual assemblies can be represented as separate channels, two-channel models were used in these tests for simplicity and because of lack of information on the core power distribution except for the target values of power peaking factors. The results showed that the iteration scheme for the steady state flow distribution produces the converged solution after only a few iterations. It was observed that the heat transfer between coolant and water rod has a non-negligible effect on the steady state flow distribution. The decay ratios obtained with multi-channel models were smaller than those determined with single average-channel models, since the multi-channel model includes hot channel assemblies that introduce larger Doppler and coolant density feedbacks than average channel assemblies. It was also observed that the effects of the inlet boundary condition are not monotonic; compared to the constant mixed-mean enthalpy approximation, the instantaneous mixing approximation produces smaller decay ratios for the Dittus-Boelter correlation but larger decay ratios for the Jackson correlation, although the difference is not so significant. The decay ratio for thermal-nuclear coupled stability estimated with two-channel models was less than 0.17, which is well below the limit (0.25) traditionally imposed for BWR stability.

Table of Contents

List of Figures

List of Tables

Nomenclature

A_c	coolant channel flow area
A_w	water rod flow area
a_w	water rod side length
D_h	coolant channel hydraulic diameter
D_w	water rod hydraulic diameter
P_h	coolant channel wetted perimeter
P_{hw}	water rod wetted perimeter
N_f	number of fuel rods per assembly
N_w	number of water rods per assembly
N_A	number of fuel assemblies in core
W_F	total feedwater flow
ω	water rod flow fraction
ρ_c	coolant density
ρ_w	water rod density
h	coolant enthalpy
h_w	water rod enthalpy
h_F	feedwater enthalpy
P	coolant pressure
P_w	water rod pressure
T_c	coolant temperature
T_w	water rod temperature
v	coolant velocity
v_w	water rod velocity
c_p^c	coolant specific heat capacity at constant pressure
μ	coolant viscosity
k_c	coolant conductivity
h_{cl}	cladding wall to coolant heat transfer coefficient

h_{cs}	coolant to water rod wall heat transfer coefficient
h_{sw}	water rod wall to water rod heat transfer coefficient
q''_f	heat flux at the fuel cladding
q''_{sc}	heat flux at the water rod wall (coolant side)
q''_{sw}	heat flux at the water rod wall (water rod side)
f	coolant channel friction factor
f_w	water rod friction factor
q'''_f	volumetric heat source in the fuel
ρ_f	fuel density
k_f	fuel conductivity
c_p^f	fuel specific heat capacity at constant pressure
T_f	fuel temperature
h_g	gap conductance
r_s	fuel pellet radius
r_g	cladding inner surface radius
ρ_{cl}	cladding density
k_{cl}	cladding conductivity
c_p^{cl}	cladding heat capacity
T_{cl}	cladding outer wall temperature
Δx	water rod wall thickness
ρ_s	water rod wall density
c_p^s	water rod wall specific heat
k_s	water rod wall heat conductivity
T_{sc}	water rod wall temperature (coolant side)
T_{sw}	water rod wall temperature (water rod side)
p	power amplitude function

ρ	core reactivity
Λ	prompt neutron generation time
β	effective delayed neutron fraction
c_k	reduced concentration for the precursor group k
β_k	delayed neutron fraction for the precursor group k
λ_k	decay constant for the precursor group k
Nu	Nusselt number
Re	Reynolds number
Pr	Prandtl number
T_{pc}	pseudo-critical temperature
P_{crit}	critical pressure
$\overline{p}_r$	reduced pressure

1. Introduction

The supercritical water cooled reactor (SCWR) is one of six Generation IV nuclear systems currently being considered internationally. It has unique features that may offer advantages compared to state-of-the-art light water reactors: a higher thermal efficiency, a lower coolant mass flow rate per unit core thermal power, and a simpler plant with fewer major components. On the other hand, because of a large variation of water density across the core, the possibility of density-wave instabilities and coupled thermal-hydraulics and neutronics instabilities exists, as discussed in the Generation IV roadmap [1]. Consistent with the U.S. NRC approach to Boiling Water Reactor (BWR) licensing, the licensing of SCWR will probably require, at a minimum, demonstration of the ability to predict the onset of instabilities. Therefore, it is necessary to understand the instability phenomena in SCWR, to identify the important variables affecting these phenomena, and ultimately to generate the maps identifying the stable operating conditions of the different SCWR designs [2].

A frequency domain linear stability analysis code for SCWR is being developed under the USDOE Generation IV Initiative. Based on single-channel coolant and water rod models, a thermal-nuclear coupled SCWR stability analysis code named SCWRSA was previously developed and applied to preliminary stability analyses of a U.S. Generation IV SCWR reference concept [3,4]. In the current reference SCWR concept, descending-flow water rods are introduced to achieve high coolant outlet temperature, to prevent thermal fatigue of control rod tubes, and to provide good neutron moderation in the upper core [5]. Thus, an ascending-flow coolant channel and a descending-flow water rod are modeled based on the single-channel mass, momentum, and energy conservation equations [6]. The heat transfer between coolant and water rod is considered by the one-dimensional heat conduction in the water rod wall and the heat convections at both sides of the wall. The NIST/ASME STEAM package [7] is used to determine supercritical water properties, and Dittus-Boelter [8,9] and Jackson [10] correlations are optionally used to determine convective heat transfer coefficients. For the coupled thermal-hydraulics and neutronics stability analysis, a point kinetics model with six delayed neutron groups is used. Reactivity feedbacks due to the Doppler effects and the coolant and water-rod density variations are considered.

The objective of this work is to investigate the parallel channel effects on the SCWR stability by improving the previous single-channel coolant and water rod thermal-hydraulics models [3,4] for multi-channel analysis. The computational model has been extended for multi-channel analysis by including the steady state and perturbation models for the flow redistribution among parallel thermal-hydraulics channels. An iterative solution scheme was developed to calculate the steady state flow distribution among parallel thermal-hydraulics channels under a fixed total flow rate and the equal pressure drop boundary condition. This scheme determines the coolant and water-rod flow rates simultaneously by taking into account the heat transfer between coolant and water rod. For linear stability analysis, perturbation calculation models for flow redistribution among parallel channels were developed along with an efficient scheme to solve the resulting system of linear equations. The extended computational models have been implemented into the frequency domain linear stability analysis code SCWRSA.

The functionality of the modified SCWRSA was confirmed by reproducing the previous single-channel analysis results. Preliminary tests of the new multi-channel analysis capability have been performed using two-channel models derived from the U.S. Generation IV SCWR reference design [11]. Although individual assemblies can be represented as separate channels, two-channel models were used in these tests for simplicity and because of lack of information on the core power distribution except for the target values of power peaking factors. The iteration scheme to determine the flow rates of individual thermal-hydraulic channels was tested. Initial verification tests for calculated response functions were performed by comparing the near-zero frequency responses with the steady state gains obtained from direct perturbation calculations. The thermal-nuclear coupled stability was estimated by using the stability criteria for BWR.

Section 2 describes the computational models including steady-state flow solution schemes. The frequency domain linear stability analysis methods are discussed in Section 3 along with the solution schemes for the linear perturbation equations. Preliminary test results are presented in Section 4. The conclusions and future work are summarized in Section 5.

2. Computational Models

The current U.S. SCWR reference design is a thermal-spectrum reactor with a rated core thermal power of 3575 MW and a rated core flow of 1843 kg/s [11]. The core includes 145 fuel assemblies. The SCWR fuel assembly is surrounded by a flow box to avoid cross flow from one assembly to its surroundings. Fuel rods are arranged in the square lattice, and square "water rod" boxes are introduced for neutron moderation, as shown in Figure 2-1. Each fuel assembly has 300 fuel rods arranged in the square lattice and 36 square water rods. The water rods are introduced to provide good neutron moderation in the upper core. Control rods are inserted in the guide tubes located in water rods. About 90% of feedwater flows downward through the water rods into the lower plenum, and then it is mixed with the rest of the feedwater from the downcomer in the lower plenum as shown in Figure 2-2. The mixed coolant flows upward through the fuel channels.

Since each fuel assembly is separated from its surroundings, every assembly flow box can be simulated as a separate channel. Thus, the SCWR core can be simulated as a parallel channel system connected only in the lower and upper plenums as shown in Figure 2-3. For parallel channel analyses, the previous thermal-nuclear coupled stability model based on single-channel coolant and water rod models has been extended by including the steady state and perturbation calculation models for the flow redistribution among parallel thermal-hydraulics channels under a fixed total flow rate and the equal pressure boundary condition. In the new multi-channel model, every assembly or several assemblies of similar power and flow conditions can be represented as a thermal-hydraulics channel.

As discussed in Reference 12, the water rod density variations due to external perturbations is important for the coupled nuclear and thermal stability of SCWR, since major neutron moderation is provided by water rods. Thus, each thermal-hydraulic channel is represented by a single fuel pin cell and a water rod, and the heat transfer between coolant and water rod is taken into account. The single pin cell representation is made such that the area of water rod wall per pin cell is preserved. Figure 2-4 shows the single pin cell model used in SCWRSA. The heat transfer between coolant and water rod is taken into account in determining the coolant and water-rod pressure drops in each thermal-hydraulics channel. The system

equations of these extended models and the numerical solution schemes are described in the following sections.

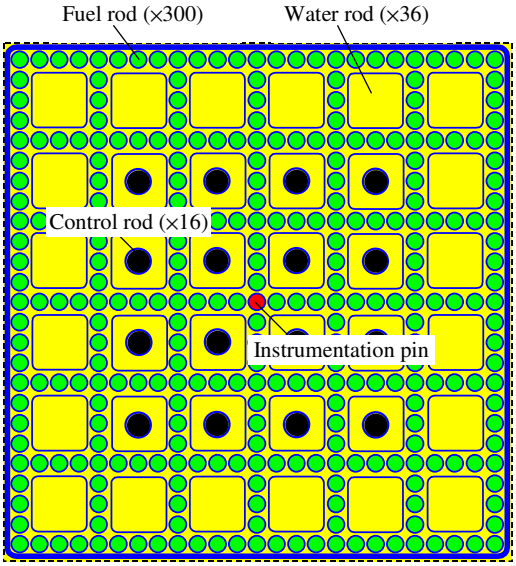

Figure 2-1 SCWR Fuel Assembly Design

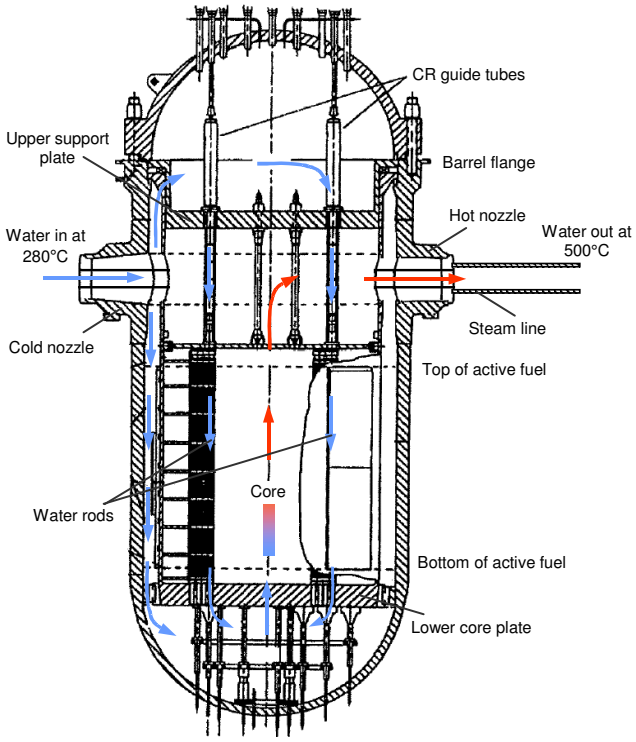

Figure 2-2 Vertical View of SCWR Reactor Pressure Vessel

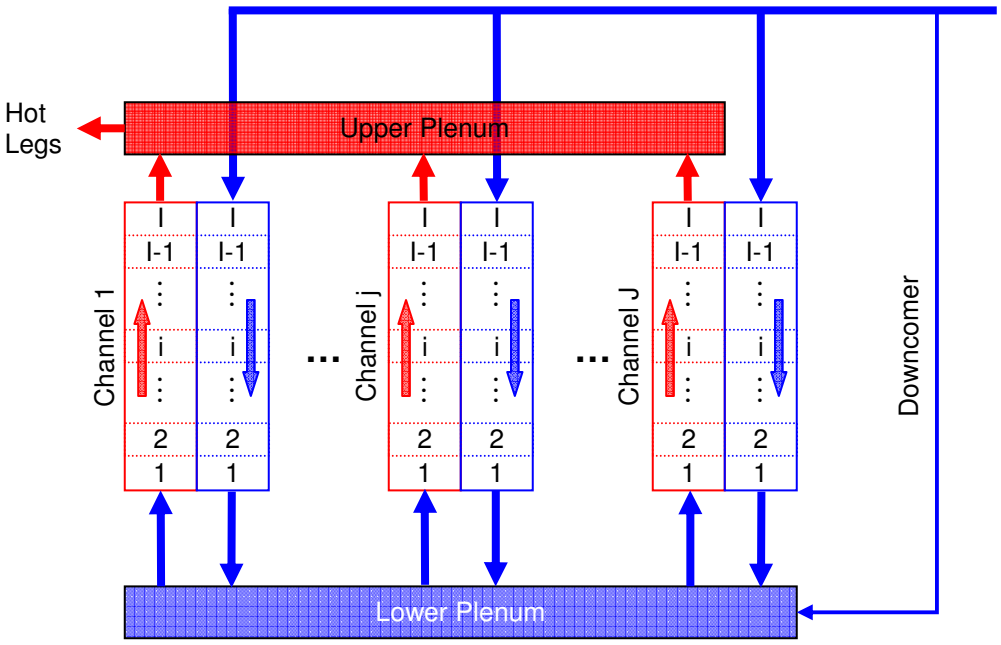

Figure 2-3 Parallel Channel Model of SCWR Core

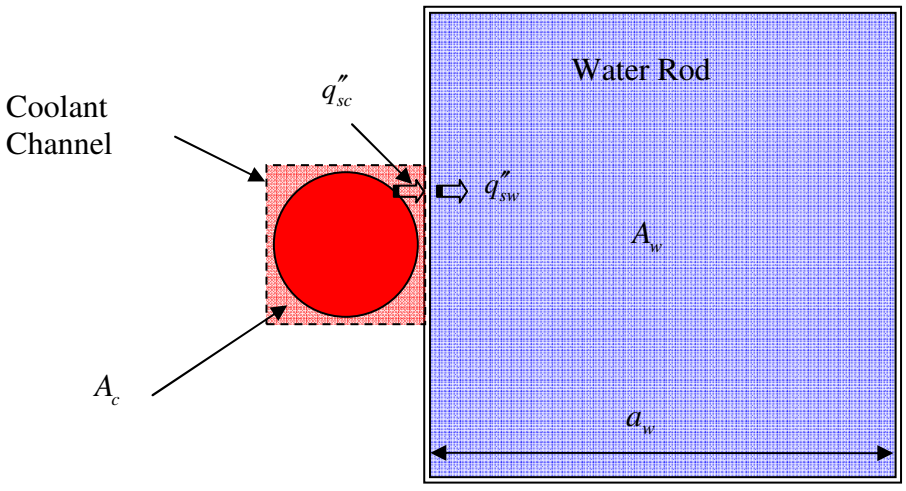

Figure 2-4 Coolant Channel and Water Rod Geometry

2.1. Governing Equations

2.1.1. Thermal-Hydraulics Equations

Neglecting axial heat conduction, energy variation due to pressure changes and frictional dissipation, and shear forces due to velocity gradients in the fluid at open portions of the surface area, the mass, momentum, and energy balance equations for one-dimensional flow in a coolant channel can be written as

$$\frac{\partial \rho_c}{\partial t} + \frac{\partial}{\partial z}(\rho_c v) = 0 \tag{2.1}$$

$$\rho_c \frac{\partial v}{\partial t} + \rho_c v \frac{\partial v}{\partial z} = -\frac{\partial P}{\partial z} - \rho_c g - \frac{f \rho_c v^2}{2D_h} \tag{2.2}$$

$$\rho_c \frac{\partial h}{\partial t} + \rho_c v \frac{\partial h}{\partial z} = \frac{q''_f P_h}{A_c} - \frac{q''_{sc} a_1}{A_c} \tag{2.3}$$

where z is the axial coordinate in flow direction and ρ_c, v, P and h are the coolant density, velocity, pressure, and enthalpy, respectively. The variable q''_f is the heat flux at the fuel cladding wall, and q''_{sc} is the heat flux at the outer (i.e., coolant channel side) surface of water rod wall. (See Fig. 2-4.) The parameters D_h, P_h, and A_c respectively denote the hydraulic diameter, perimeter, and cross-sectional area of the coolant channel; f is the turbulent friction factor, g is the acceleration due to gravity, and a_1 is the average interface area per unit height between a coolant channel and a water rod.

Similarly, the mass, momentum, and energy conservation equations for one-dimensional flow in a water rod can be written as

$$\frac{\partial \rho_w}{\partial t} + \frac{\partial}{\partial z}(\rho_w v_w) = 0 \tag{2.4}$$

$$\rho_w \frac{\partial v_w}{\partial t} + \rho_w v_w \frac{\partial v_w}{\partial z} = -\frac{\partial P_w}{\partial z} + \rho_w g - \frac{f_w \rho_w v_w^2}{2D_w} \tag{2.5}$$

$$\rho_w \frac{\partial h_w}{\partial t} + \rho_w v_w \frac{\partial h_w}{\partial z} = \frac{q''_{sw} P_{hw}}{A_w} \tag{2.6}$$

where ρ_w, v_w, P_w and h_w are the water density, velocity, pressure, and enthalpy in the water rod, respectively, and q''_{sw} is the heat flux at the inner (i.e., water rod side) surface of water rod wall. Note that the axial coordinate z and velocities are in the downward direction. The parameters D_w, P_{hw}, and A_w represent the hydraulic diameter, perimeter, and cross-sectional area of the water rod, respectively. Denoting the inside side length of water rod by a_w, then $A_w = a_w^2$, $P_{hw} = 4a_w$, and $D_w = 4A_w / P_{hw} = a_w$. Since the whole assembly is represented by a single coolant channel and a water rod, the average interface area per unit height between a coolant channel and a water rod, i.e., a_1 in Eq. (2.3), can be represented as

$$a_1 = \frac{4}{N_f}(a_w + 2\Delta x)N_w \tag{2.7}$$

where N_f and N_w are the numbers of fuel and water rods in an assembly, respectively, and Δx is the thickness of water rod wall. The mass, momentum, and energy conservation equations of coolant and water rod channels are closed by the equation of state for supercritical water. In this study, supercritical water properties are determined using the NIST/ASME STEAM package [7].

As the boundary conditions for these conservation equations, the inlet flow rate, inlet enthalpy, and outlet pressure are used. These boundary conditions are determined using the given system outlet pressure and total coolant and water rod flow rates. As mentioned above, a large fraction of feedwater flows downward through the water rods and is mixed with the rest of the feedwater from the downcomer in the lower plenum. The mixed water from the lower plenum then enters the coolant region of all fuel assemblies. Thus, the inlet enthalpy of coolants into all fuel assemblies is assumed to be constant at the mixed-mean enthalpy of water in the lower plenum. As a result, the mass and energy conservation equations in the lower plenum are approximated as

$$\frac{dm}{dt} = \sum_{j=1}^{J} w_{wj} + w_{dc} - \sum_{j=1}^{J} w_{cj} \tag{2.8}$$

$$\frac{d}{dt}(mh_{c0}) = \sum_{j=1}^{J} h_{w0,j} w_{wj} + h_{dc} w_{dc} - h_{c0} \sum_{j=1}^{J} w_{cj} \tag{2.9}$$

$$P_{w0,j} = P_{LP} \tag{2.10}$$

where m is the lower plenum mass, w_{cj} and w_{wj} flow rates of thermal-hydraulic channel j, h_{c0} and $h_{w0,j}$ are the coolant inlet and water-rod outlet enthalpies, and J is the number of thermal-hydraulic channels. The pressure P_{LP} and enthalpy h_{c0} are inlet values to the orifices of coolant channels, while P_{w0} and $h_{w0,j}$ are water-rod outlet values. The coolant and water-rod flow rates of each thermal-hydraulic channel are determined under a fixed total flow rate and the equal pressure boundary condition. For given total coolant flow rate w_T and water-rod flow rate w_w, the mass conservation and equal pressure drop boundary conditions are given by

$$\Delta P_{c1} = \Delta P_{c2} = \cdots = \Delta P_{cJ} \tag{2.11}$$

$$\Delta P_{w1} = \Delta P_{w2} = \cdots = \Delta P_{wJ} \tag{2.12}$$

$$\sum_{j=1}^{J} w_{cj} = w_T \tag{2.13}$$

$$\sum_{j=1}^{J} w_{wj} = w_w = w_T - w_{dc} \tag{2.14}$$

2.1.2. Heat Conduction Equations

Neglecting axial conduction, the heat conduction in the fuel pellet and cladding is determined by the following one-dimensional radial heat conduction equation:

$$\rho_r c_p^r \frac{\partial T_r}{\partial t} = \frac{1}{r}\frac{\partial}{\partial r}\left[k_r(T) r \frac{\partial T_r}{\partial r} \right] + q_f''' \tag{2.15}$$

where ρ_r, c_p^r, and k_r are respectively the density, specific heat, and heat conductivity of fuel pellet or cladding, and q_f''' is the volumetric heat source. The fuel and cladding heat conduction equations are coupled through the interface condition at the gas gap given by

$$q_s'' = -\left(k_f \frac{\partial T_f}{\partial r} \right)_s = h_g (T_s - T_g) \tag{2.16}$$

Here h_g is the gap conductance, T_s is the temperature at the fuel pellet surface, and T_g is the temperature at the inner surface of the cladding. This equation provides a boundary condition for the second order differential equation for the heat conduction in fuel pellet. Another boundary condition is given by the symmetry condition (i.e., $\partial T / \partial r = 0$) at the center of fuel pellet.

The heat conduction equation for cladding is coupled with the coolant energy equation in Eq. (2.3) through the Newton's law for heat convection at the cladding wall

$$q''_f = -\left(k_{cl} \frac{\partial T}{\partial r} \right)_{cl} = h_{cl}(T_{cl} - T_c) \tag{2.17}$$

where T_{cl} is the cladding outer wall temperature, T_c is the bulk temperature of coolant, and h_{cl} is the heat transfer coefficient at the cladding wall. This equation provides a boundary condition for the second order differential equation for the heat conduction in cladding. Another boundary condition is given by the heat flux condition at the inner surface of cladding $q''_g = q''_s r_s / r_g$, where r_s and r_g are the fuel pellet radius and the cladding inner surface radius, respectively.

Since the water-rod wall thickness (0.4 mm) is much smaller than the side length (33.6 mm), the axial and azimuthal heat conductions in the water rod wall can be neglected. Thus, the heat conduction in the water rod wall can be determined by the following one-dimensional heat conduction equation:

$$\rho_s c_p^s \frac{\partial T_s}{\partial t} = \frac{\partial}{\partial x}\left[k_s(T) \frac{\partial T_s}{\partial x} \right] \tag{2.18}$$

where ρ_s, c_p^s, and k_s are the density, specific heat, and heat conductivity of water rod wall, respectively. This heat conduction equation is coupled with the coolant channel and water-rod energy equations in Eqs. (2.3) and (2.6) through the heat fluxes at the surfaces of water rod wall

$$q''_{sc} = -\left(k_s \frac{\partial T}{\partial x} \right)_c = h_{sc}(T_c - T_{sc}) \tag{2.19}$$

$$q''_{sw} = -\left(k_s \frac{\partial T}{\partial x} \right)_w = h_{sw}(T_{sw} - T_w) \tag{2.20}$$

Here T_{sc} and T_{sw} are the temperatures at the outer (i.e., coolant channel side) and inner (i.e., water rod side) surfaces of water rod wall, respectively, and T_c and T_w are the bulk temperatures of coolant and water rod. The heat transfer coefficients h_{sc} and h_{sw} are the values at the outer and inner surfaces of water rod wall, respectively. Equations (2.19) and (2.20) provide boundary conditions for the second order differential equation in Eq. (2.18).

2.1.3. Point Kinetics Equations

The temporal variation of the core power is determined by the following point kinetics equations with six delayed neutron groups [13]

$$\frac{dp(t)}{dt} = \frac{\rho(t) - \beta}{\Lambda} p(t) + \sum_{k=1}^{6} \lambda_k c_k(t) \tag{2.21}$$

$$\frac{dc_k(t)}{dt} = \frac{\beta_k}{\Lambda} p(t) - \lambda_k c_k(t), \quad k = 1, 2, \cdots, 6 \tag{2.22}$$

where p is the flux amplitude function, ρ is the core reactivity, β is the effective delayed neutron fraction, Λ is the prompt neutron generation time. The variables $c_k(t)$, β_k, and λ_k represent the reduced precursor concentration, delayed neutron fraction, and decay constant of each delayed neutron group k, respectively. These point kinetics equations are coupled with the coolant and water-rod conservation equations and the fuel heat-conduction equation through the Doppler, and coolant and water-rod density reactivity feedbacks.

2.1.4. Friction Factor and Heat Transfer Correlations

The turbulent friction factor f in Eqs. (2.2) and (2.5) for a smooth tube can be obtained from the Blasius and McAdams relations

$$f = \begin{cases} 0.316 Re^{-0.25}, & Re < 30,000 \\ 0.184 Re^{-0.2}, & 30,000 < Re < 10^6 \end{cases} \tag{2.23}$$

where Re is the Reynolds number defined as

$$Re = \frac{\rho v D}{\mu} \tag{2.24}$$

with fluid density ρ, velocity v, viscosity μ, and hydraulic diameter D.

The heat transfer coefficients h in Eqs. (2.17), (2.19) and (2.20) are determined by either the Dittus-Boelter correlation [8,9] or the Jackson correlation [10]. The Dittus-Boelter correlation is given by

$$Nu = 0.023 Re^{0.8} Pr^{0.33} \tag{2.25}$$

where Nu and Pr are Nusselt and Prandtl numbers defined by

$$Nu = \frac{hD}{k} \tag{2.26}$$

$$Pr = \frac{\mu c_p}{k} \tag{2.27}$$

with fluid conductivity k and specific heat c_p. This correlation is known to be not accurate enough for SCWR heat transfer calculations [10,14,15].

The Jackson correlation, which is considered more appropriate for SCWR in a wide range of operating conditions [10], was developed for forced convection heat transfer from tubes to supercritical water and supercritical carbon dioxide. The correlation is

$$Nu_b = 0.0183\, Re_b^{0.82} Pr_b^{0.5} \left(\frac{\rho_w}{\rho_b}\right)^{0.3} \left(\frac{\overline{c}_p}{c_{pb}}\right)^n \tag{2.28}$$

where $\overline{c}_p$ is defined by

$$\overline{c}_p = \frac{h_w - h_b}{T_w - T_b} \tag{2.29}$$

and the exponent n is defined as

$$n = \begin{cases} 0.4 & \text{for } T_b < T_w < T_{pc} \\ 0.4 + 0.2(T_w / T_{pc} - 1) & \text{for } T_b < T_{pc} < T_w \\ 0.4 + 0.2(T_w / T_{pc} - 1)(1 - 5(T_b / T_{pc} - 1)) & \text{for } T_{pc} < T_b < 1.2T_{pc} \text{ and } T_b < T_w \\ 0.4 & \text{for } 1.2T_{pc} < T_b < T_w \end{cases} \tag{2.30}$$

where T_{pc} is the pseudo-critical temperature. Here the subscripts b and w denote the properties at bulk coolant and local wall temperatures, respectively. The pseudo-critical temperature is defined as the temperature at which the specific heat capacity at constant pressure is maximized. It is obtained from the correlation of Howell and Lee [16]

$$T_{pc} = 547.27 + 114.97\,\overline{p}_r - 15.216\,\overline{p}_r^2 \tag{2.31}$$

where T_{pc} is in degrees K and $\overline{p}_r$ is the reduced pressure, which is calculated as

$$\overline{p}_r = \frac{P}{P_c} \tag{2.32}$$

where P is the pressure and P_c is the critical pressure. The Jackson correlation is applied at the fuel cladding and coolant interface and at the water rod wall and water rod interface. At the

coolant and water rod interface, the Dittus-Boelter correlation is used, since the Jackson correlation given by Eqs. (2.28) to (2.32) is not defined for heat transfer from hot liquid to colder surface.

2.2. Spatial Discretization

The governing equations discussed in the previous section form a system of nonlinear equations. This system of nonlinear equations cannot be solved analytically, and thus need to be solved numerically. In this section, the spatial discretization schemes employed to solve this system of equations are discussed.

2.2.1. Thermal-Hydraulics Equations

To derive the finite difference approximations of coolant conservation equations, the problem domain is divided into axial computational nodes as shown in Figure 2-3. In order to facilitate the frequency domain analysis, the finite difference equations are derived in terms of the state variables at node surfaces such that the variables of only two meshes are coupled. Applying the upwind differencing scheme to Eqs. (2.1), (2.2), and (2.3), the finite difference equations for coolant channel node i are obtained as

$$\frac{d\rho_{c,i}}{dt} = \frac{1}{\Delta z_i}(\rho_{c,i-1}v_{c,i-1} - \rho_{c,i}v_{c,i}) \tag{2.33}$$

$$\rho_{c,i}\frac{dv_{c,i}}{dt} = \frac{\rho_{c,i}v_{c,i}}{\Delta z_i}(v_{c,i-1} - v_{c,i}) + \frac{1}{\Delta z_i}(P_{c,i-1} - P_{c,i}) - \rho_{c,i-1}g - \frac{f_{c,i-1}\rho_{c,i-1}v_{c,i-1}^2}{2D_h} \tag{2.34}$$

$$\rho_{c,i}\frac{dh_{c,i}}{dt} = \frac{\rho_{c,i}v_{c,i}}{\Delta z_i}(h_{c,i-1} - h_{c,i}) + \frac{\overline{q}''_{f,i}P_h}{A_c} - \frac{\overline{q}''_{sc,i}a_1}{A_c} \tag{2.35}$$

Here the variables with bar denote node averaged values, and those without bar denote the values at node surfaces.

Applying the upwind differencing scheme to Eqs. (2.4), (2.5), and (2.6), the finite difference equations for water rod nodes are obtained as

$$\frac{d\rho_{w,i}}{dt} = \frac{1}{\Delta z_{i+1}}(\rho_{w,i+1}v_{w,i+1} - \rho_{w,i}v_{w,i}) \tag{2.36}$$

$$\rho_{w,i}\frac{dv_{w,i}}{dt}=\frac{\rho_{w,i}v_{w,i}}{\Delta z_{i+1}}(v_{w,i+1}-v_{w,i})+\frac{1}{\Delta z_{i+1}}(P_{w,i+1}-P_{w,i})+\rho_{w,i+1}g-\frac{f_{w,i+1}\rho_{w,i+1}v_{w,i+1}^2}{2D_{hw}} \tag{2.37}$$

$$\rho_{w,i}\frac{dh_{w,i}}{dt}=\frac{\rho_{w,i}v_{w,i}}{\Delta z_{i+1}}(h_{w,i+1}-h_{w,i})+\frac{\overline{q}''_{sw,i+1}P_{hw}}{A_w} \tag{2.38}$$

2.2.2. Heat Conduction Equations

For each axial coolant node, the heat conduction equations for fuel pellet and cladding are discretized in the radial direction as shown in Figure 2-5. The pellet region is divided into n equidistance meshes and the temperatures are defined at the mesh boundaries. Two meshes are used for the cladding region. Therefore, the total number of mesh points including the fuel center is $n+4$. Among $n+1$ fuel temperatures, one is at the center, T_1, and one is at the outer surface T_{fs}. The cladding temperatures at the inner, middle, and outer wall are denoted as T_g, T_m, and T_{cl}, respectively.

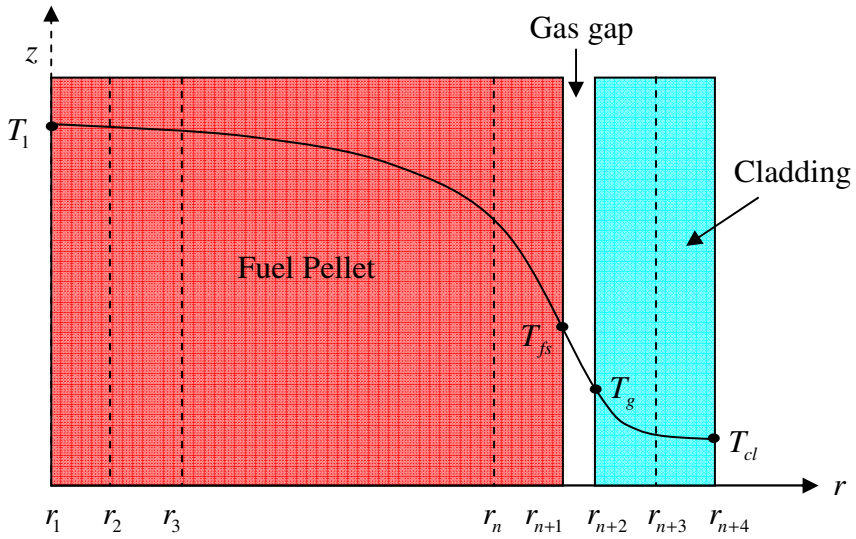

Figure 2-5 Radial Mesh Structure for Heat Conduction Calculation

The central differencing scheme, which has a second order accuracy, is used for the spatial differencing of Eq. (2.15). At each interior mesh point j, the second order derivative term of Eq. (2.15) is approximated as

$$\frac{1}{r}\frac{\partial}{\partial r}\left[k(T)r\frac{\partial T}{\partial r}\right]_j = e_{l,j}T_{j-1} + e_{d,j}T_j + e_{u,j}T_{j+1} \tag{2.39}$$

$$e_{l,j} = \frac{k_{j-1/2}}{(\Delta r)^2}\left(1-\frac{\Delta r}{2r_j}\right) \tag{2.40a}$$

$$e_{d,j} = -\frac{1}{(\Delta r)^2}\left[\left(1-\frac{\Delta r}{2r_j}\right)k_{j-1/2} + \left(1+\frac{\Delta r}{2r_j}\right)k_{j+1/2}\right] \tag{2.40b}$$

$$e_{u,j} = \frac{k_{j+1/2}}{(\Delta r)^2}\left(1+\frac{\Delta r}{2r_j}\right) \tag{2.40c}$$

where $k_{j+1/2}$ is the heat conductivity at the middle of two mesh points j and $j+1$, which is approximated by the mean value of k_j and k_{j+1}.

At the center of the fuel pellet, a symmetric boundary condition is used. Based on the symmetric property and the second-order differencing, a parabolic shape can be assumed for the temperature variation near the central point as

$$T(r) = ar^2 + T_1 \tag{2.41}$$

By applying this parabolic shape to the neighboring mesh point, the coefficient a can be determined, and thus the coefficients of Eq. (2.39) can be expressed as

$$e_{l,1} = 0,\ e_{d,1} = -\frac{4k_{3/2}}{(\Delta r)^2},\ e_{u,1} = \frac{4k_{3/2}}{(\Delta r)^2} \tag{2.42}$$

Similarly, the finite difference equations for the mesh points at the fuel pellet surface and the inner and outer surfaces of cladding are derived by using parabolic temperature shapes and applying the heat flux boundary conditions discussed above. The resulting approximations of the second order derivative term of Eq. (2.15) are summarized below.

(1) $j = n+1$ ($r = r_s$, fuel pellet surface),

$$\frac{2k_{n+1}}{(\Delta r)^2}T_n - \left[\frac{2k_{n+1}}{(\Delta r)^2} + \frac{h_g}{\Delta r}\left(3+\frac{1}{n}-\frac{k_n}{k_{n+1}}\right)\right]T_{n+1} + \frac{h_g}{\Delta r}\left(3+\frac{1}{n}-\frac{k_n}{k_{n+1}}\right)T_{n+2} \tag{2.43}$$

(2) $j = n+2$ ($r = r_g$, cladding inner surface),

$$\left[\frac{2h_g r_s}{r_g d}\left(3-\frac{k_m}{k_g}\right)-\frac{h_g r_s}{r_g^2}\right]T_{n+1}-\left[\frac{2h_g r_s}{r_g d}\left(3-\frac{k_m}{k_g}\right)-\frac{h_g r_s}{r_g^2}+\frac{8k_g}{d^2}\right]T_{n+2}+\frac{8k_g}{d^2}T_{n+3} \tag{2.44}$$

(3) $j=n+4$ ($r=r_{cl}$, cladding outer surface),

$$\frac{8k_{cl}}{d^2}T_{n+3}-\left[\frac{8k_{cl}}{d^2}+\frac{h_{cl}}{r_{cl}}+\frac{2h_{cl}}{d}\left(3-\frac{k_m}{k_{cl}}\right)\right]T_{n+4}+\left[\frac{h_{cl}}{r_{cl}}+\frac{2h_{cl}}{d}\left(3-\frac{k_m}{k_{cl}}\right)\right]T_c \tag{2.45}$$

Here d is the thickness of cladding, k_g is the heat conductivity of cladding at the inner surface, and k_w is the heat conductivity of cladding at the outer surface.

The above finite difference approximations for the Laplacian term of Eq. (2.15) couple each mesh temperature with two neighboring mesh temperatures. By combining the temporal derivative and volumetric heat source terms with these approximations of Laplacian term, the difference equations for individual mesh points can be represented as a tri-diagonal system of equations as

$$\rho_j c_{p,j}\ \frac{dT_j}{dt}=e_{l,j}T_{j-1}+e_{d,j}T_j+e_{u,j}T_{j+1}+s_j,\quad j=1,2,\cdots,n+4 \tag{2.46}$$

The coefficients in this system of equations are determined by the thermal properties of fuel and cladding and the heat transfer coefficients in the gas gap and cladding wall. Since the thermal properties are temperature-dependent, Eq. (2.46) is a system of non-linear equations. It can be seen from Eq. (2.45) that the source term s_{n+4} of Eq. (2.46) includes the bulk coolant temperature while the other source terms include the volumetric heat source only.

Therefore, denoting the radial temperature distribution vector by $\mathbf{T}_{f,i}$, Eq. (2.46) for the axial node i can be rewritten as

$$\mathbf{D}_{f,i}\frac{d\mathbf{T}_{f,i}}{dt}=\mathbf{E}_{f,i}\mathbf{T}_{f,i}+\mathbf{r}_{f,i}\overline{q}'''_{f,i}+\mathbf{b}_{f,i}T_{c,i} \tag{2.47}$$

where $\mathbf{D}_{f,i}$ is a diagonal matrix including the product of density and specific heat, $\mathbf{E}_{f,i}$ is a tri-diagonal matrix with elements depending on the heat conductivity and mesh size, and $T_{c,i}$ is the bulk coolant temperature that can be determined from the node average enthalpy $\overline{h}_{c,i}$. The vector

$\mathbf{r}_{f,i}$ represents the radial distribution of the volumetric heat source, and the vector $\mathbf{b}_{f,i}$ represents the convection boundary condition at the cladding wall.

Dividing the water rod wall into two equal meshes and applying the central differencing scheme to (2.18), the finite difference equation for the mid-wall temperature $T_{s,i}$ of axial node i can be obtained as

$$\rho_{s,i} c_{p,i}^{s} \frac{dT_{s,i}}{dt} = \frac{4k_{s,i}}{(\Delta x)^2}(T_{sc,i} - 2T_{s,i} + T_{sw,i}) \tag{2.48}$$

where the variation of heat conductivity over a thin wall is assumed negligible and $k_{s,i}$ evaluated at temperature $T_{s,i}$ is used. Using parabolic temperature shapes and applying the heat flux boundary conditions given in Eqs. (2.19) and (2.20), the finite difference equations for the temperatures at inner and outer surfaces are derived as

$$\rho_{sc,i} c_{p,i}^{s} \frac{dT_{sc,i}}{dt} = \frac{8k_{s,i}}{(\Delta x)^2} T_{s,i} - \left[\frac{8k_{s,i}}{(\Delta x)^2} + \frac{4h_{sc,i}}{\Delta x} \right] T_{sc,i} + \frac{4h_{sc,i}}{\Delta x} T_{c,i} \tag{2.49}$$

$$\rho_{sw,i} c_{p,i}^{s} \frac{dT_{sw,i}}{dt} = \frac{8k_{s,i}}{(\Delta x)^2} T_{s,i} - \left[\frac{8k_{s,i}}{(\Delta x)^2} + \frac{4h_{sw,i}}{\Delta x} \right] T_{sw,i} + \frac{4h_{sw,i}}{\Delta x} T_{w,i+1} \tag{2.50}$$

Note that the node average coolant and water rod temperatures are approximated by the upwind surface values. Denoting the temperatures of water rod wall meshes by a vector $\mathbf{T}_{s,i} = (T_{sc,i}, T_{s,i}, T_{sw,i})^T$, Eqs. (2.48) to (2.50) can be rewritten in a matrix form as

$$\mathbf{D}_{s,i} \frac{d\mathbf{T}_{s,i}}{dt} = \mathbf{E}_{s,i} \mathbf{T}_{s,i} + \mathbf{b}_{sc,i} T_{c,i} + \mathbf{b}_{sw,i} T_{w,i+1} \tag{2.51}$$

where $\mathbf{D}_{s,i}$ is a 3×3 diagonal matrix including the product of density and specific heat, $\mathbf{E}_{s,i}$ is a 3×3 tri-diagonal matrix, and $\mathbf{b}_{sc,i}$ and $\mathbf{b}_{sw,i}$ are 3×1 column vectors.

2.3. Steady-State Solution Scheme

At the steady state, all the heat generated in the fuel is deposited in the coolant, and hence the cladding-wall heat flux is directly represented by the volumetric heat source. As a result, the fuel conduction equations are decoupled from the other equations. Therefore, the axial distributions of coolant and water rod temperature, pressure, density, and velocity can be determined first for given inlet flow rate, inlet enthalpy (or temperature), and outlet pressure.

Then, for each axial node, the radial distribution of fuel pin temperature can be determined by solving the fuel conduction equations with the boundary condition provided by the coolant temperature of each axial node.

The Dittus-Boelter correlation depends on the bulk temperature only. Thus the cladding wall temperature is directly determined from Eq. (2.17). For the Jackson heat transfer correlation, the heat transfer coefficient is dependent on both the coolant and cladding temperatures. Therefore, Eq. (2.17) needs to be solved iteratively for the cladding temperature.

The inlet flow rates and enthalpy of individual thermal-hydraulics channels are determined by solving Eqs. (2.8) to (2.14) iteratively for given total coolant flow rate w_T and water rod flow rate w_w. Note that the time derivatives in Eqs. (2.8) and (2.9) are zero at a steady state. Figure 2-6 depicts the overall iteration scheme for the steady state solution, which can be summarized as

(1) At the beginning, initial guesses for the coolant and water-rod flow rates of individual channels are made.
(2) With known flow rates, feedwater enthalpy, system outlet pressure, and power distributions, the coolant and water rod thermal-hydraulic equations in Eqs. (2.1) to (2.6) are solved for every channel. Since the heat transfer between coolant and water rod depends on the coolant and water rod temperatures, these equations are solved iteratively as described in Section 2.3.2.
(3) Using the pressure solutions for individual channels, it is tested whether the equal pressure drop boundary conditions are satisfied.
(4) If the pressure drop boundary conditions are satisfied within specified convergence criteria, then the fuel-pin temperature equation is solved for each channel, using the known heat source and coolant temperature distributions. The solution scheme is described in Section 2.3.3.
(5) If not, the coolant and water-rod flow rates of each channel are updated as described in Section 2.3.1. Using the updated flow rates, the mixed-mean enthalpy of water in the lower plenum is updated. Go back to the step (2).

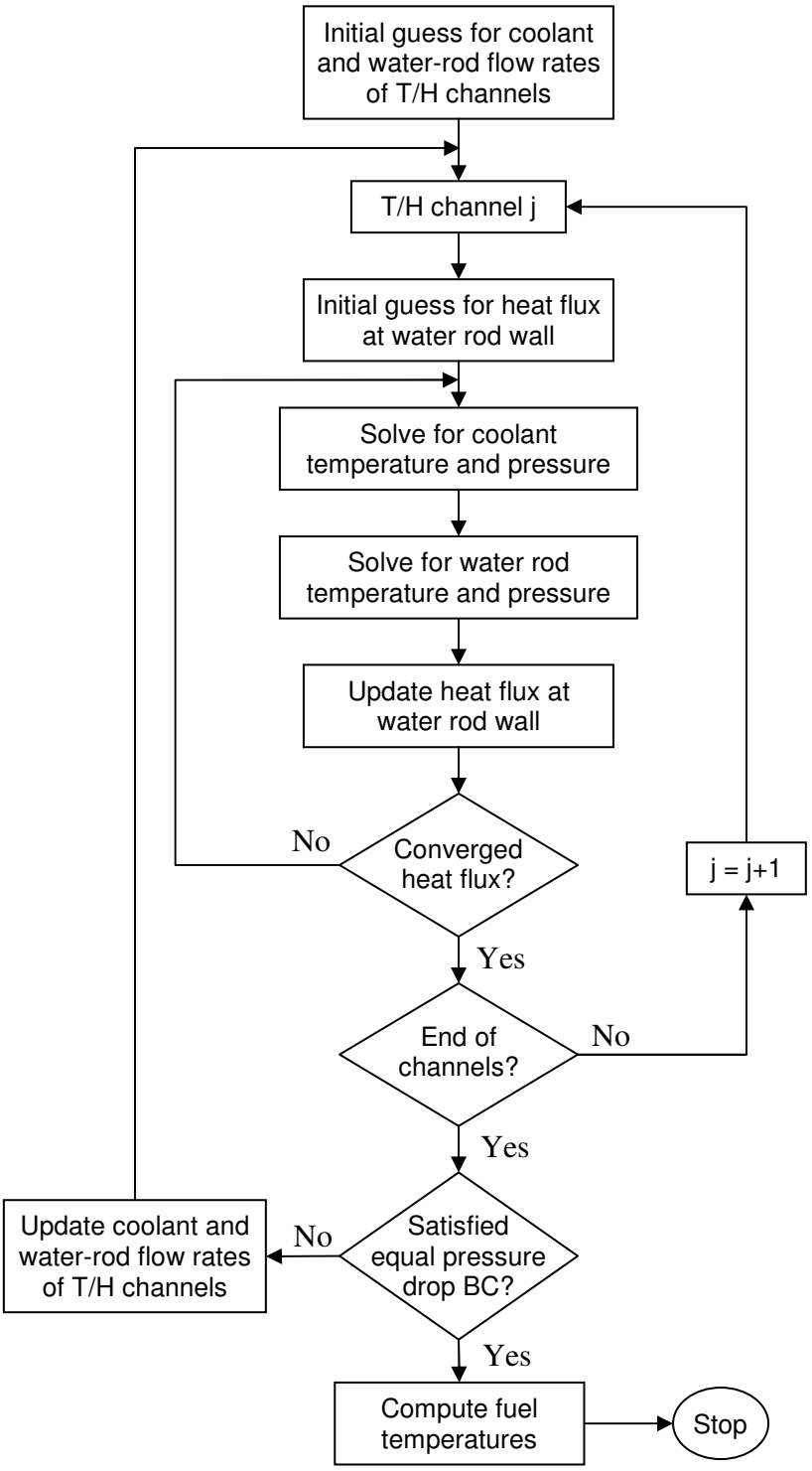

Figure 2-6 Overall Iteration Scheme for Steady State Solution

2.3.1. Coolant and Water Rod Flow Rates

Perturbation of coolant or water-rod flow rate in a channel changes the amount of heat transferred between coolant and water rod, which in turn changes the coolant and water-rod pressure drops of that channel through water density variations. Thus, the coolant pressure drop ΔP_{cj} and water-rod pressure drop ΔP_{wj} of each channel j are a function of coolant mass flux G_{cj} and water rod mass flux G_{wj}. As a result, for given total coolant flow rate w_T and water-rod flow rate w_w, the mass conservation and equal pressure drop boundary conditions to be satisfied can be represented by the following system of equations:

$$\Delta P_{c1}(G_{c1}, G_{w1}) = \Delta P_{c2}(G_{c2}, G_{w2}) = \cdots = \Delta P_{cJ}(G_{cJ}, G_{wJ}) \tag{2.52}$$

$$\Delta P_{w1}(G_{c1}, G_{w1}) = \Delta P_{w2}(G_{c2}, G_{w2}) = \cdots = \Delta P_{wJ}(G_{cJ}, G_{wJ}) \tag{2.53}$$

$$\sum_{j=1}^{J} N_j A_{cj} G_{cj} = w_T \tag{2.54}$$

$$\sum_{j=1}^{J} N_j A_{wj} G_{wj} = w_w \tag{2.55}$$

where N_j is the number of assemblies in channel j, and A_{cj} and A_{wj} are the total coolant and water rod flow areas of an assembly in channel j, respectively.

Expanding each channel pressure drop as a first-order Taylor series of mass flux, this system of nonlinear equations can be solved iteratively using the Newton-Raphson method as

$$\Delta P_{cj}^{(n+1)} = \Delta P_{cj}^{(n)} + a_j^{(n)}(G_{cj}^{(n+1)} - G_{cj}^{(n)}) + b_j^{(n)}(G_{wj}^{(n+1)} - G_{wj}^{(n)}), \quad j = 1, 2, \cdots, J \tag{2.56}$$

$$\Delta P_{wj}^{(n+1)} = \Delta P_{wj}^{(n)} + c_j^{(n)}(G_{cj}^{(n+1)} - G_{cj}^{(n)}) + d_j^{(n)}(G_{wj}^{(n+1)} - G_{wj}^{(n)}), \quad j = 1, 2, \cdots, J \tag{2.57}$$

$$\sum_{j=1}^{J} N_j A_{cj} G_{cj}^{(n+1)} = w_T \tag{2.58}$$

$$\sum_{j=1}^{J} N_j A_{wj} G_{wj}^{(n+1)} = w_w \tag{2.59}$$

where n is the iteration index and $a_j^{(n)}$, $b_j^{(n)}$, $c_j^{(n)}$, and $d_j^{(n)}$ are expansion coefficients that can be determined as described below. For known mass fluxes and pressure drops of the nth iteration, this system of linear equations can be solved for new mass fluxes $G_{cj}^{(n+1)}$ and $G_{wj}^{(n+1)}$ as

$$G_{cj}^{(n+1)} = G_{cj}^{(n)} + \frac{1}{D_j^{(n)}}\left[d_j^{(n)}(\overline{\Delta P}_c^{(n+1)} - \Delta P_{cj}^{(n)}) - b_j^{(n)}(\overline{\Delta P}_w^{(n+1)} - \Delta P_{wj}^{(n)}) \right], \quad j = 1, 2, \cdots, J \tag{2.60}$$

$$G_{wj}^{(n+1)} = G_{wj}^{(n)} - \frac{1}{D_j^{(n)}}\left[c_j^{(n)}(\overline{\Delta P}_c^{(n+1)} - \Delta P_{cj}^{(n)}) - a_j^{(n)}(\overline{\Delta P}_w^{(n+1)} - \Delta P_{wj}^{(n)}) \right], \quad j = 1, 2, \cdots, J \tag{2.61}$$

where $D_j^{(n)} = a_j^{(n)} d_j^{(n)} - b_j^{(n)} c_j^{(n)}$. The core average pressure drops $\overline{\Delta P}_c^{(n+1)}$ and $\overline{\Delta P}_w^{(n+1)}$ are given by

$$\overline{\Delta P}_c^{(n+1)} = \frac{1}{\alpha^{(n)}\delta^{(n)} - \beta^{(n)}\gamma^{(n)}}\left[\delta^{(n)}(\xi^{(n)} - \eta^{(n)}) - \beta^{(n)}(\zeta^{(n)} - \omega^{(n)}) \right] \tag{2.62}$$

$$\overline{\Delta P}_w^{(n+1)} = \frac{1}{\alpha^{(n)}\delta^{(n)} - \beta^{(n)}\gamma^{(n)}}\left[\gamma^{(n)}(\xi^{(n)} - \eta^{(n)}) - \alpha^{(n)}(\zeta^{(n)} - \omega^{(n)}) \right] \tag{2.63}$$

$$\alpha^{(n)} = \sum_j \frac{d_j^{(n)} N_j A_{cj}}{D_j^{(n)}}, \ \beta^{(n)} = \sum_j \frac{b_j^{(n)} N_j A_{cj}}{D_j^{(n)}}, \ \gamma^{(n)} = \sum_j \frac{c_j^{(n)} N_j A_{wj}}{D_j^{(n)}}, \ \delta^{(n)} = \sum_j \frac{a_j^{(n)} N_j A_{wj}}{D_j^{(n)}} \tag{2.64}$$

$$\begin{aligned} \xi^{(n)} &= \sum_j \frac{d_j^{(n)} N_j A_{cj} \Delta P_{cj}^{(n)}}{D_j^{(n)}}, \quad \eta^{(n)} = \sum_j \frac{b_j^{(n)} N_j A_{cj} \Delta P_{wj}^{(n)}}{D_j^{(n)}}, \\ \zeta^{(n)} &= \sum_j \frac{c_j^{(n)} N_j A_{wj} \Delta P_{cj}^{(n)}}{D_j^{(n)}}, \quad \omega^{(n)} = \sum_j \frac{a_j^{(n)} N_j A_{wj} \Delta P_{wj}^{(n)}}{D_j^{(n)}} \end{aligned} \tag{2.65}$$

The initial guesses of coolant and water rod mass fluxes are made such that the flow rates of each channel are proportional to the channel power.

The expansion coefficients $a_j^{(n)}$, $b_j^{(n)}$, $c_j^{(n)}$, and $d_j^{(n)}$ in Eqs. (2.56) and (2.57) are determined approximately by expanding the pressure drops of previous two iterations $\Delta P_{cj}^{(n-1)}$, $\Delta P_{wj}^{(n-1)}$, $\Delta P_{cj}^{(n-2)}$, and $\Delta P_{wj}^{(n-2)}$ as first order Taylor series around the mass fluxes $G_{cj}^{(n)}$ and $G_{wj}^{(n)}$. The resulting coefficients are given by

$$a_j^{(n)} = \frac{1}{\Delta_j^{(n)}}\left[(G_{wj}^{(n)} - G_{wj}^{(n-2)})(\Delta P_{cj}^{(n)} - \Delta P_{cj}^{(n-1)}) - (G_{wj}^{(n)} - G_{wj}^{(n-1)})(\Delta P_{cj}^{(n)} - \Delta P_{cj}^{(n-2)}) \right] \tag{2.66}$$

$$b_j^{(n)} = -\frac{1}{\Delta_j^{(n)}}\left[(G_{cj}^{(n)} - G_{cj}^{(n-2)})(\Delta P_{cj}^{(n)} - \Delta P_{cj}^{(n-1)}) - (G_{cj}^{(n)} - G_{cj}^{(n-1)})(\Delta P_{cj}^{(n)} - \Delta P_{cj}^{(n-2)}) \right] \tag{2.67}$$

$$c_j^{(n)} = \frac{1}{\Delta_j^{(n)}}\left[(G_{wj}^{(n)} - G_{wj}^{(n-2)})(\Delta P_{wj}^{(n)} - \Delta P_{wj}^{(n-1)}) - (G_{wj}^{(n)} - G_{wj}^{(n-1)})(\Delta P_{wj}^{(n)} - \Delta P_{wj}^{(n-2)}) \right] \tag{2.68}$$

$$d_j^{(n)} = -\frac{1}{\Delta_j^{(n)}}\left[(G_{cj}^{(n)} - G_{cj}^{(n-2)})(\Delta P_{wj}^{(n)} - \Delta P_{wj}^{(n-1)}) - (G_{cj}^{(n)} - G_{cj}^{(n-1)})(\Delta P_{wj}^{(n)} - \Delta P_{wj}^{(n-2)}) \right] \tag{2.69}$$

where $\Delta_j^{(n)} = (G_{cj}^{(n)} - G_{cj}^{(n-1)})(G_{wj}^{(n)} - G_{wj}^{(n-2)}) - (G_{wj}^{(n)} - G_{wj}^{(n-1)})(G_{cj}^{(n)} - G_{cj}^{(n-2)})$. For the first two iterations, these coefficients are approximated as

$$a_j^{(1)} = \frac{\Delta P_{cj}^{(1)}}{G_{cj}^{(1)}},\ b_j^{(1)} = c_j^{(1)} = 0,\ d_j^{(1)} = \frac{\Delta P_{wj}^{(1)}}{G_{wj}^{(1)}} \tag{2.70}$$

$$a_j^{(2)} = \frac{\Delta P_{cj}^{(2)} - \Delta P_{cj}^{(1)}}{G_{cj}^{(2)} - G_{cj}^{(1)}},\ b_j^{(2)} = c_j^{(2)} = 0,\ d_j^{(2)} = \frac{\Delta P_{wj}^{(2)} - \Delta P_{wj}^{(1)}}{G_{wj}^{(2)} - G_{wj}^{(1)}} \tag{2.71}$$

2.3.2. Coolant Channel and Water Rod Equations

At a steady state, all the time derivatives are zero, and hence the coolant conservation equations in Eqs. (2.33) to (2.35) are decoupled from each other. Therefore, for given inlet flow rate ($w_{c,in}$), inlet enthalpy ($h_{c,in}$), and outlet pressure ($P_{c,out}$), they are reduced to

$$w_{c,i} = w_{c,in} \tag{2.72}$$

$$P_{c,i} = P_{c,i-1} - \frac{w_{c,in}^2}{A_c^2}\left(\frac{1}{\rho_{c,i}} - \frac{1}{\rho_{c,i-1}}\right) - \bar{\rho}_{c,i} g \Delta z_i - \frac{\bar{f}_{c,i} \Delta z_i w_{c,in}^2}{2 D_h \bar{\rho}_{c,i} A_c^2} \tag{2.73}$$

$$h_{c,i} = h_{c,i-1} + \frac{\bar{q}''_{f,i} P_h \Delta z_i}{w_{c,in}} - \frac{\bar{q}''_{sc,i} a_1 \Delta z_i}{w_{c,in}} \tag{2.74}$$

Since the NIST/ASME STEAM package is adopted in this study to provide the water properties for given pressure and temperature, it is more convenient to use the temperature as a state variable rather than the enthalpy. In this case, the energy equation in Eq. (2.74) is represented by an integral equation as

$$\int_{T_{c,i-1}}^{T_{c,i}} c_p(\bar{P}_{c,i}, T) dT = \frac{\bar{q}''_{f,i} P_h \Delta z_i}{w_{c,in}} - \frac{\bar{q}''_{sc,i} a_1 \Delta z_i}{w_{c,in}} \tag{2.75}$$

In the same way, the water-rod conservation equations are reduced to

$$w_{w,i} = w_{w,in} \tag{2.76}$$

$$P_{w,i-1} = P_{w,i} - \frac{w_{w,in}^2}{A_w^2}\left(\frac{1}{\rho_{w,i-1}} - \frac{1}{\rho_{w,i}}\right) + \bar{\rho}_{w,i} g \Delta z_i - \frac{\bar{f}_{w,i} \Delta z_i w_{w,in}^2}{2 D_{hw} \bar{\rho}_{w,i} A_w^2} \tag{2.77}$$

$$\int_{T_{w,i}}^{T_{w,i-1}} c_p(\bar{P}_{w,i}, T) dT = \frac{\bar{q}''_{sw,i} P_{hw} \Delta z_i}{w_{w,in}} \tag{2.78}$$

The conservation equations for coolant channel are coupled with those for water rod only by the heat transfer through water rod wall. Once the heat fluxes at the water rod wall are known, the conservation equations for coolant channel and water rod can be solved independently in a way described in the previous study [17]. In addition, most of the heat deposited in coolant is removed by convection, and only a small fraction of it is transferred by the conduction through the water rod wall. Therefore, the conservation equations for coolant channel and water rod can be solved iteratively by a few iterations on the heat flux at the water rod wall. For given heat fluxes at water rod wall, the momentum and energy equations for coolant channel and water rod are solved by two-step iterations as described below; one is an outer iteration for the overall axial pressure distribution, and the other is an inner iteration for the temperature or pressure of each node. These iterative solution schemes provide the temperature, pressure, and density at each node surface. The enthalpy at each node surface is determined from the equation of state using the known pressure and temperature. Each node-average value is approximated by the arithmetic average of the upper and lower surface values.

Iteration Scheme for Water-Rod Wall Heat Flux

Since the heat flux in the water rod wall is constant at a steady state, the coolant and water-rod momentum and energy equations in Eqs. (2.73), (2.75), (2.77), and (2.78) can be solved by iteration on the heat flux $\overline{q}''_{sc,i} = \overline{q}''_{sw,i}$ as

(1) Make initial guesses for the heat flux, water rod pressure and temperature, and water rod wall temperatures in each axial node

$$\overline{q}''^{(0)}_{sc,i} = \overline{q}''^{(0)}_{sw,i} = 0 \tag{2.79a}$$

$$T^{(0)}_{w,i} = T_{in} \tag{2.79b}$$

$$P^{(0)}_{w,i} = P_{out} \tag{2.79c}$$

$$T^{(0)}_{sw,i} = T^{(0)}_{s,i} = T^{(0)}_{sc,i} = T_{in} \tag{2.79d}$$

(2) With known $\overline{q}''^{(k)}_{sc,i}$, solve iteratively the coolant channel equations in Eqs. (2.73) and (2.75) for $T^{(k+1)}_{c,i}$ and $P^{(k+1)}_{c,i}$ using the "iteration scheme for temperature and pressure distributions" described below.

(3) With new coolant channel solutions and previous water rod solutions, determine the

heat transfer coefficients at wall surfaces and wall heat conductivity:

$$h_{sc,i}^{(k+1)} = h_{sc,i}[\overline{T}_{c,i}^{(k+1)}, \overline{P}_{c,i}^{(k+1)}, \overline{v}_{c,i}^{(k+1)}] \tag{2.80a}$$

$$h_{sw,i}^{(k)} = h_{sw,i}[\overline{T}_{w,i}^{(k)}, \overline{P}_{w,i}^{(k)}, \overline{v}_{w,i}^{(k)}] \tag{2.80b}$$

$$k_{s,i}^{(k)} = k_{s,i}[T_{s,i}^{(k)}] \tag{2.80c}$$

(4) Solve the water-rod wall conduction equation in Eq. (2.51) for $\mathbf{T}_{s,i}^{(k+1)}$, and update heat flux using Eqs. (2.19) and (2.20). Since the spatial variation of heat conductivity is neglected, the heat flux and temperatures can be determined as

$$\overline{q}''^{(k+1)}_{sc,i} = \overline{q}''^{(k+1)}_{sw,i} = \left[\frac{1}{h_{sc,i}^{(k+1)}} + \frac{\Delta x}{k_{s,i}^{(k)}} + \frac{1}{h_{sw,i}^{(k)}} \right]^{-1} [T_{c,i}^{(k+1)} - T_{w,i}^{(k)}] \tag{2.81a}$$

$$T_{sc,i}^{(k+1)} = \overline{T}_{c,i}^{(k+1)} - \frac{\overline{q}''^{(k+1)}_{sc,i}}{h_{sc,i}^{(k+1)}} \tag{2.81b}$$

$$T_{sw,i}^{(k+1)} = \overline{T}_{w,i}^{(k)} + \frac{\overline{q}''^{(k)}_{sw,i}}{h_{sw,i}^{(k)}} \tag{2.81c}$$

$$T_{s,i}^{(k+1)} = \frac{1}{2}[T_{sc,i}^{(k+1)} + T_{sw,i}^{(k+1)}] \tag{2.81d}$$

(5) With updated heat flux $\overline{q}''^{(k+1)}_{sw,i}$, solve iteratively the water rod equations in Eqs. (2.77) and (2.78) for $T_{w,i}^{(k+1)}$ and $P_{w,i}^{(k+1)}$ using the "iteration scheme for temperature and pressure distributions" described below.

(6) If $\left| T_{w,i}^{(k+1)} - T_{w,i}^{(k)} \right|$ is less than a specified convergence criterion for all nodes, stop; otherwise go back to the step (2).

Iteration Scheme for Temperature and Pressure Distributions

For given heat fluxes at water rod wall, the momentum and energy equations for coolant channel and water rod are solved by two-step iterations: an outer iteration for the overall axial pressure distribution and an inner iteration for the temperature or pressure of each node. In the following description of these iteration schemes, the outer and inner iterations are denoted by the indices l and m, respectively.

(1) Make an initial guess for the pressure P_i at each node surface be equal to the given

outlet pressure

$$P_i^{(0)} = P_{out} \tag{2.82}$$

(2) By sweeping from the inlet node to the outlet node successively (i.e., from bottom to top for coolant channel, and from top to bottom for water rod), determine the outlet temperature of each node using known inlet temperature and cladding wall heat flux. That is, solve Eq. (2.75) for $T_i^{(l+1)}$ using known $T_{i-1}^{(l+1)}$ and $\overline{q}''_{f,i}$ for a coolant channel node or solve Eq. (2.78) for $T_{i-1}^{(l+1)}$ using known $T_i^{(l+1)}$ and $\overline{q}''_{f,i}$ for a water rod node. For each node, the outlet temperature is iteratively determined using the "iteration scheme for outlet temperature of a node" described below.

(3) By sweeping from the outlet node to the inlet node successively, determine the inlet pressure of each node using known outlet pressure and inlet temperature. That is, solve Eq. (2.73) for $P_{i-1}^{(l+1)}$ using known $T_{i-1}^{(l+1)}$ and $P_i^{(l+1)}$ for a coolant node or solve Eq. (2.77) for $P_i^{(l+1)}$ using known $T_i^{(l+1)}$ and $P_{i-1}^{(l+1)}$ for a coolant node. For each node, the inlet pressure is iteratively determined using the "iteration scheme for inlet pressure of a node" described below.

(4) If $\left|P_i^{(l+1)} - P_i^{(l)}\right|$ is less than a specified convergence criterion for all nodes, then return; otherwise go back to the step (2).

Iteration Scheme for Outlet Temperature of a Node

For given inlet temperature $T_{in,i}^{(l+1)}$, the outlet temperature $T_{out,i}^{(l+1)}$ of a coolant or water rod node is determined iteratively as follows:

(1) Make an initial guess for $T_{out,i}^{(l+1,0)}$ by evaluating the specific heat with the inlet temperature $T_{in,i}^{(l+1)}$ and the node average pressure approximated by the mean value of inlet and outlet pressures as

$$\overline{P}_i^{(l)} = [P_{in,i}^{(l)} + P_{out,i}^{(l)}]/2 \tag{2.83}$$

$$T_{out,i}^{(l+1,0)} = T_{in,i}^{(l+1)} + \frac{\overline{q}''_{f,i} P_h \Delta z_i}{c_p[\overline{P}_i^{(l)}, T_{in,i}^{(l+1)}] w_{in}} \tag{2.84}$$

(2) Re-evaluate the specific heat with the previous inner iteration temperature $T_{out,i}^{(l+1,m)}$ and

determine an updated temperature $T_{out,i}^{(l+1,m+1)}$ as

$$T_{out,i}^{(l+1,m+1)} = T_{out,i}^{(l+1,m)} + \frac{1}{c_p[\overline{P}_i^{(l)}, T_{out,i}^{(l+1,m)}]}\left[\frac{\overline{q}''_{f,i} P_h \Delta z_i}{w_{in}} - \int_{T_{in,i}^{(l+1)}}^{T_{out,i}^{(l+1,m)}} c_p[\overline{P}_i^{(l)}, T]dT\right] \tag{2.85}$$

(3) If $\left|\overline{T}_{out,i}^{(l+1,m+1)} - \overline{T}_{out,i}^{(l+1,m)}\right|$ is less than a specified convergence criterion, then return; otherwise go back to the step (2).

Iteration Scheme for Inlet Pressure of a Node

For given outlet pressure $P_{out,i}^{(l+1)}$, the inlet pressure $P_{in,i}^{(l+1)}$ of a coolant or water rod node is determined iteratively as follows:

(1) Make an initial guess for the inlet pressure $P_{in,i}^{(l+1,0)}$ be equal to the outlet pressure $P_{out,i}^{(l+1)}$

$$P_{in,i}^{(l+1,0)} = P_{out,i}^{(l+1)} \tag{2.86}$$

(2) Estimate $\rho_{in,i}$, $\overline{\rho}_i$, and $\overline{\mu}_i$ with the previous inner iteration pressure $P_{in,i}^{(l+1,m)}$ and calculate $\bar{f}_i$ as

$$\rho_{in,i}^{(l+1,m)} = \rho[P_{in,i}^{(l+1,m)}, T_{in,i}^{(l+1)}] \tag{2.87}$$

$$\overline{\rho}_i^{(l+1,m)} = [\rho_{out,i}^{(l+1)} + \rho_{in,i}^{(l+1,m)}]/2 \tag{2.88}$$

$$\overline{T}_i^{(l+1)} = [T_{out,i}^{(l+1)} + T_{in,i}^{(l+1)}]/2 \tag{2.89}$$

$$\overline{\mu}_i^{(l+1,m)} = \mu[\overline{\rho}_i^{(l+1,m)}, \overline{T}_i^{(l+1)}] \tag{2.90}$$

$$\overline{f}_i^{(l+1,m)} = C\left[\frac{w_{in} D_h}{A\overline{\mu}_i^{(l+1,m)}}\right]^{-\alpha} \tag{2.91}$$

(3) Calculate the pressure loss in the node as

$$\Delta P_{loss}[P_{in,i}^{(l+1,m)}] = \frac{w_{in}^2}{A^2}\left(\frac{1}{\rho_{out,i}^{(l+1)}} - \frac{1}{\rho_{in,i}^{(l+1,m)}}\right) \pm \overline{\rho}_i^{(l+1,m)} g \Delta z_i + \frac{\overline{f}_i^{(l+1,m)} \Delta z_i w_{in}^2}{2 D_h \overline{\rho}_i^{(l+1,m)} A^2} \tag{2.92}$$

where the gravitational term is negative for a coolant node and positive for a water rod node.

(4) Update the lower surface pressure $P_{in,i}^{(l+1,m+1)}$

$$P_{in,i}^{(l+1,m+1)} = P_{out,i}^{(l+1)} + \Delta P_{loss}[P_{in,i}^{(l+1,m)}] \tag{2.93}$$

(5) If $\left|P_{in,i}^{(l+1,m+1)} - P_{in,i}^{(l+1,m)}\right|$ is less than a specified convergence criterion, then return;

otherwise go back to the step (2).

2.3.3. Fuel Conduction Equations

For each axial node i, the fuel-pin temperature equation given in Eq. (2.47) is solved with the known volumetric heat source distribution and coolant temperature. Since the time derivative is zero at a steady state, Eq. (2.47) is reduced to a system of non-linear algebraic equations. This system of equations is solved iteratively as follows:

(1) Make an initial guess for the fuel pin temperature vector $\mathbf{T}_{f,i}^{(0)}$

(2) Estimate the fuel and cladding properties using the previous iteration temperature vector and compute the coefficient matrix $\mathbf{E}_{f,i}^{(l)}[\mathbf{T}_{f,i}^{(l)}]$

(3) Solve the resulting tri-diagonal system of linear equations by a single sweep of forward elimination and backward substitution

$$\mathbf{T}_{f,i}^{(l+1)} = -[\mathbf{E}_{f,i}^{(l)}]^{-1}(\mathbf{r}_{f,i}\overline{q}'''_{f,i} + \mathbf{b}_{f,i}T_{c,i}) \tag{2.94}$$

(4) If $\left|\mathbf{T}_{f,i}^{(l+1)} - \mathbf{T}_{f,i}^{(l)}\right|$ is less than a specified convergence criterion, stop; otherwise, go back to the step (2).

3. Frequency Domain Linear Analysis

The frequency domain linear system of equations is obtained by linearizing the differential equations and the constitutive equations near the steady state solution and subsequently applying the Laplace transformation to the resulting linear equations. Each equation is linearized by representing each state variable with its steady state values and a deviation from steady state, expanding nonlinear terms in Taylor series, and neglecting higher order terms. The frequency domain linear system of equations is obtained by applying the Laplace transformation to the resulting linear equations. The frequency responses of state variables to the external perturbations are determined by solving this linear system of perturbation equations. The determinant of the coefficient matrix of this system of equations is the system characteristic equation that determines the system stability.

The frequency responses of state variables and the system characteristic equation are discussed in the following sections along with the detailed derivation of the frequency domain linear system of equations.

3.1. Linear Perturbation Equations

3.1.1. Coolant Perturbation Equations

In order to derive the perturbation equations of the coolant conservation equations, each of density, velocity, enthalpy, pressure, and heat flux is represented by its steady state value and a deviation from steady state as

$$\begin{aligned} \rho_i(t) &= \rho_{i0} + \delta\rho_i(t) \\ v_i(t) &= v_{i0} + \delta v_i(t) \\ h_i(t) &= h_{i0} + \delta h_i(t) \\ P_i(t) &= P_{i0} + \delta P_i(t) \\ \overline{q}''_{f,i}(t) &= \overline{q}''_{f,i0} + \delta\overline{q}''_{f,i}(t) \\ \overline{q}''_{sc,i}(t) &= \overline{q}''_{sc,i0} + \delta\overline{q}''_{sc,i}(t) \end{aligned} \tag{3.1}$$

Here the subscript *c* for coolant is omitted for simplicity. By substituting these perturbation expressions into Eqs. (2.33) to (2.35), expanding nonlinear terms in Taylor series, and neglecting

higher order terms, we obtain the linearized perturbation equations for the mass, energy, and momentum conservation equations as

$$\frac{d}{dt}\delta\rho_i = -\frac{v_{i0}}{\Delta z_i}\delta\rho_i - \frac{\rho_{i0}}{\Delta z_i}\delta v_i + \frac{v_{i-1,0}}{\Delta z_i}\delta\rho_{i-1} + \frac{\rho_{i-1,0}}{\Delta z_i}\delta v_{i-1} \tag{3.2}$$

$$\begin{aligned}\rho_{i0}\frac{d}{dt}\delta h_i = {} & \frac{v_{i0}(h_{i-1,0}-h_{i0})}{\Delta z_i}\delta\rho_i + \frac{\rho_{i0}(h_{i-1,0}-h_{i0})}{\Delta z_i}\delta v_i - \frac{\rho_{i0}v_{i0}}{\Delta z_i}\delta h_i \\ & + \frac{\rho_{i0}v_{i0}}{\Delta z_i}\delta h_{i-1} + \frac{P_h}{A}\delta\overline{q}''_{f,i} - \frac{a_1}{A}\delta\overline{q}''_{sc,i}\end{aligned} \tag{3.3}$$

$$\begin{aligned}\rho_{i0}\frac{d}{dt}\delta v_i = {} & \frac{v_{i0}(v_{i-1,0}-v_{i0})}{\Delta z_i}\delta\rho_i + \frac{\rho_{i0}(v_{i-1,0}-2v_{i0})}{\Delta z_i}\delta v_i - \frac{1}{\Delta z_i}\delta P_i \\ & - \left[g + (1+\alpha)\frac{f_{i-1,0}v_{i-1,0}^2}{2D_h}\right]\delta\rho_{i-1} + \left[\frac{\rho_{i0}v_{i0}}{\Delta z_i} - (2+\alpha)\frac{f_{i-1,0}\rho_{i-1,0}v_{i-1,0}}{2D_h}\right]\delta v_{i-1} \\ & + \left[\frac{1}{\Delta z_i} + \alpha\frac{f_{i-1,0}\rho_{i-1,0}v_{i-1,0}^2\gamma_{i-1,0}}{2D_h\mu_{i-1,0}}\right]\delta P_{i-1} + \alpha\frac{f_{i-1,0}\rho_{i-1,0}v_{i-1,0}^2\beta_{i-1,0}}{2D_h\mu_{i-1,0}}\delta h_{i-1}\end{aligned} \tag{3.4}$$

For the derivation of Eq. (3.4), the variation of the turbulent friction factor for a smooth tube given in Eq. (2.23) is determined as

$$\delta f = \frac{\alpha f}{\rho_c}\delta\rho_c + \frac{\alpha f}{v}\delta v - \frac{\alpha f\beta}{\mu}\delta h - \frac{\alpha f\gamma}{\mu}\delta P \tag{3.5}$$

where α is the exponent of Reynolds number in Eq. (2.24), β is the partial derivative of the viscosity with respect to enthalpy at a constant pressure, and γ is the partial derivative of the viscosity with respect to pressure at a constant enthalpy

$$\beta = \left.\frac{\partial\mu}{\partial h}\right|_P, \quad \gamma = \left.\frac{\partial\mu}{\partial P}\right|_h \tag{3.6}$$

The coolant density variation $\delta\rho_c$ can be obtained from a pressure-enthalpy state relation as

$$\delta\rho_c = \left.\frac{\partial\rho_c}{\partial h}\right|_P \delta h + \left.\frac{\partial\rho_c}{\partial P}\right|_h \delta P = \xi\delta h + \eta\delta P \tag{3.7}$$

By eliminating $\delta\rho_c$ using this relation, therefore, Eqs. (3.2), (3.3), and (3.4) can be reduced to

$$\xi_{i0}\frac{d}{dt}\delta h_i+\eta_{i0}\frac{d}{dt}\delta P_i=-\frac{v_{i0}\xi_{i0}}{\Delta z_i}\delta h_i-\frac{v_{i0}\eta_{i0}}{\Delta z_i}\delta P_i-\frac{\rho_{i0}}{\Delta z_i}\delta v_i + \frac{v_{i-1,0}\xi_{i-1,0}}{\Delta z_i}\delta h_{i-1}+\frac{v_{i-1,0}\eta_{i-1,0}}{\Delta z_i}\delta P_{i-1}+\frac{\rho_{i-1,0}}{\Delta z_i}\delta v_{i-1} \tag{3.8}$$

$$\frac{d}{dt}\delta h_i=\frac{v_{i0}}{\Delta z_i}\left[\frac{(h_{i-1,0}-h_{i0})\xi_{i0}}{\rho_{i0}}-1\right]\delta h_i+\frac{v_{i0}(h_{i-1,0}-h_{i0})\eta_{i0}}{\Delta z_i\rho_{i0}}\delta P_i+\frac{(h_{i-1,0}-h_{i0})}{\Delta z_i}\delta v_i + \frac{v_{i0}}{\Delta z_i}\delta h_{i-1}+\frac{P_h}{A\rho_{i0}}\delta\overline{q}''_{f,i}-\frac{a_1}{A\rho_{i0}}\delta\overline{q}''_{sc,i} \tag{3.9}$$

$$\frac{d}{dt}\delta v_i=\frac{v_{i0}(v_{i-1,0}-v_{i0})\xi_{i0}}{\Delta z_i\rho_{i0}}\delta h_i+\frac{1}{\rho_{i0}\Delta z_i}\left[v_{i0}(v_{i-1,0}-v_{i0})\eta_{i0}-1\right]\delta P_i+\frac{(v_{i-1,0}-2v_{i0})}{\Delta z_i}\delta v_i + b_{31}^i\delta h_{i-1}+b_{32}^i\delta P_{i-1}+b_{33}^i\delta v_{i-1} \tag{3.10}$$

where

$$b_{31}^i=\frac{1}{\rho_{i0}}\left[\frac{f_{i-1,0}v_{i-1,0}^2}{2D_h}\left(\frac{\alpha\rho_{i-1,0}\beta_{i-1,0}}{\mu_{i-1,0}}-(1+\alpha)\xi_{i-1,0}\right)-g\xi_{i-1,0}\right]$$

$$b_{32}^i=\frac{1}{\rho_{i0}}\left[\frac{1}{\Delta z_i}+\frac{f_{i-1,0}v_{i-1,0}^2}{2D_h}\left(\frac{\alpha\rho_{i-1,0}\gamma_{i-1,0}}{\mu_{i-1,0}}-(1+\alpha)\eta_{i-1,0}\right)-g\eta_{i-1,0}\right]$$

$$b_{33}^i=\frac{v_{i0}}{\Delta z_i}-(2+\alpha)\frac{f_{i-1,0}\rho_{i-1,0}v_{i-1,0}}{2D_h\rho_{i0}}$$

Substituting Eq. (3.9) into (3.8), the time derivative of pressure perturbation is obtained as

$$\frac{d}{dt}\delta P_i=-\frac{v_{i0}(h_{i-1,0}-h_{i0})\xi_{i0}^2}{\Delta z_i\rho_{i0}\eta_{i0}}\delta h_i-\frac{v_{i0}}{\Delta z_i\rho_{i0}}\left[\rho_{i0}+(h_{i-1,0}-h_{i0})\xi_{i0}\right]\delta P_i - \frac{\rho_{i0}+(h_{i-1,0}-h_{i0})\xi_{i0}}{\Delta z_i\eta_{i0}}\delta v_i+\frac{v_{i-1,0}\xi_{i-1,0}-v_{i0}\xi_{i0}}{\Delta z_i\eta_{i0}}\delta h_{i-1} + \frac{v_{i-1,0}\eta_{i-1,0}}{\Delta z_i\eta_{i0}}\delta P_{i-1}+\frac{\rho_{i-1,0}}{\Delta z_i\eta_{i0}}\delta v_{i-1}-\frac{P_h\xi_{i0}}{A\rho_{i0}\eta_{i0}}\delta\overline{q}''_{f,i}+\frac{a_1\xi_{i0}}{A\rho_{i0}\eta_{i0}}\delta\overline{q}''_{sc,i} \tag{3.11}$$

Equations (3.9), (3.10), and (3.11) form a system of linear equations for the perturbations of enthalpy, pressure, and velocity. This system of equations can be written in a matrix form as

$$\frac{d}{dt}\delta\mathbf{x}_{c,i}=\mathbf{A}_{c,i}\delta\mathbf{x}_{c,i}+\mathbf{B}_{c,i}\delta\mathbf{x}_{c,i-1}+\mathbf{c}_{f,i}\delta\overline{q}''_{f,i}-\mathbf{c}_{sc,i}\delta\overline{q}''_{sc,i} \tag{3.12}$$

where $\delta \mathbf{x}_{c,i}$ is the vector representing the enthalpy, pressure, and velocity perturbations in the coolant node i and is defined as

$$\delta \mathbf{x}_{c,i}(t) = [\delta h_{c,i}(t), \delta P_{c,i}(t), \delta v_{c,i}(t)]^T \tag{3.13}$$

The 3×3 matrices $\mathbf{A}_{c,i}$ and $\mathbf{B}_{c,i}$ and 3×1 vectors $\mathbf{c}_{f,i}$ and $\mathbf{c}_{sc,i}$ are given by

$$\mathbf{A}_{c,i} = \begin{bmatrix} \frac{v_{i0}}{\Delta z_i}\left[\frac{(h_{i-1,0}-h_{i0})\xi_{i0}}{\rho_{i0}}-1\right] & \frac{v_{i0}(h_{i-1,0}-h_{i0})\eta_{i0}}{\Delta z_i \rho_{i0}} & \frac{(h_{i-1,0}-h_{i0})}{\Delta z_i} \\ -\frac{v_{i0}(h_{i-1,0}-h_{i0})\xi_{i0}^2}{\Delta z_i \rho_{i0}\eta_{i0}} & -\frac{v_{i0}}{\Delta z_i \rho_{i0}}\left[\rho_{i0}+(h_{i-1,0}-h_{i0})\xi_{i0}\right] & -\frac{\rho_{i0}+(h_{i-1,0}-h_{i0})\xi_{i0}}{\Delta z_i \eta_{i0}} \\ \frac{v_{i0}(v_{i-1,0}-v_{i0})\xi_{i0}}{\Delta z_i \rho_{i0}} & \frac{1}{\Delta z_i \rho_{i0}}\left[v_{i0}(v_{i-1,0}-v_{i0})\eta_{i0}-1\right] & \frac{(v_{i-1,0}-2v_{i0})}{\Delta z_i} \end{bmatrix} \tag{3.14}$$

$$\mathbf{B}_{c,i} = \begin{bmatrix} \frac{v_{i0}}{\Delta z_i} & 0 & 0 \\ \frac{v_{i-1,0}\xi_{i-1,0}-v_{i0}\xi_{i0}}{\Delta z_i \eta_{i0}} & \frac{v_{i-1,0}\eta_{i-1,0}}{\Delta z_i \eta_{i0}} & \frac{\rho_{i-1,0}}{\Delta z_i \eta_{i0}} \\ b_{31}^i & b_{32}^i & b_{33}^i \end{bmatrix} \tag{3.15}$$

$$\mathbf{c}_{f,i} = \left[\frac{P_h}{A_c \rho_{i0}}, -\frac{P_h \xi_{i0}}{A_c \rho_{i0}\eta_{i0}}, 0\right]^T \tag{3.16}$$

$$\mathbf{c}_{sc,i} = \left[\frac{a_1}{A_c \rho_{i0}}, -\frac{a_1 \xi_{i0}}{A_c \rho_{i0}\eta_{i0}}, 0\right]^T \tag{3.17}$$

Note that all the variables in these matrices are those for coolant channel nodes.

For an un-heated node i with an orifice, the coolant conservation equations can be represented as

$$\rho_i v_i = \rho_{i-1} v_{i-1} \tag{3.18}$$

$$h_i = h_{i-1} \tag{3.19}$$

$$P_i = P_{i-1} - \frac{1}{2}\zeta_i \rho_{i-1} |v_{i-1}| v_{i-1} \tag{3.20}$$

where ζ_i is the pressure loss coefficient of orifice. These equations can be linearized as

$$v_{i0}\delta\rho_i + \rho_{i0}\delta v_i = v_{i-1,0}\delta\rho_{i-1} + \rho_{i-1,0}\delta v_{i-1} \tag{3.21}$$

$$\delta h_i = \delta h_{i-1} \tag{3.22}$$

$$\delta P_i = \delta P_{i-1} - \frac{1}{2}\zeta_i \left|v_{i-1,0}\right| v_{i-1,0}\delta\rho_{i-1} - \zeta_i \rho_{i-1,0}\left|v_{i-1,0}\right|\delta v_{i-1} \tag{3.23}$$

Eliminating the coolant density variation $\delta\rho_c$ from Eqs. (3.21) to (3.23) using Eq. (3.7), the resulting system of equations for enthalpy, pressure, and velocity perturbations can be written in a matrix form as

$$\mathbf{A}_{c,i}\delta\mathbf{x}_{c,i} + \mathbf{B}_{c,i}\delta\mathbf{x}_{c,i-1} = 0 \tag{3.24}$$

where

$$\mathbf{A}_{c,i} = \begin{bmatrix} -v_{i0}\xi_{i0} & -v_{i0}\eta_{i0} & -\rho_{i0} \\ -1 & 0 & 0 \\ 0 & -1 & 0 \end{bmatrix} \tag{3.25}$$

$$\mathbf{B}_{c,i} = \begin{bmatrix} v_{i-1,0}\xi_{i-1,0} & v_{i-1,0}\eta_{i-1,0} & \rho_{i-0} \\ 1 & 0 & 0 \\ -\zeta_i v_{i-1,0}^2 \xi_{i-1,0}/2 & 1-\zeta_i v_{i-1,0}^2 \eta_{i-1,0}/2 & -\zeta_i \rho_{i-1,0} v_{i-1,0} \end{bmatrix} \tag{3.26}$$

3.1.2. Water Rod Perturbation Equations

Applying the same procedure used in deriving the coolant perturbation equations, the water-rod perturbation equations can be derived from Eqs. (2.36) to (2.38) as

$$\frac{d}{dt}\delta\mathbf{x}_{w,i} = \mathbf{A}_{w,i}\delta\mathbf{x}_{w,i} + \mathbf{B}_{w,i}\delta\mathbf{x}_{w,i+1} + \mathbf{c}_{sw,i}\delta\overline{q}''_{sw,i+1} \tag{3.27}$$

where

$$\delta\mathbf{x}_{w,i}(t) = [\delta h_{w,i}(t), \delta P_{w,i}(t), \delta v_{w,i}(t)]^T \tag{3.28}$$

The 3×3 matrices $\mathbf{A}_{w,i}$ and $\mathbf{B}_{w,i}$ and the 3×1 vector $\mathbf{c}_{sw,i}$ are given by

$$\mathbf{A}_{w,i} = \begin{bmatrix} \frac{v_{i0}}{\Delta z_{i+1}}\left[\frac{(h_{i+1,0}-h_{i0})\xi_{i0}}{\rho_{i0}} - 1\right] & \frac{v_{i0}(h_{i+1,0}-h_{i0})\eta_{i0}}{\Delta z_{i+1}\rho_{i0}} & \frac{(h_{i+1,0}-h_{i0})}{\Delta z_{i+1}} \\ -\frac{v_{i0}(h_{i+1,0}-h_{i0})\xi_{i0}^2}{\Delta z_{i+1}\rho_{i0}\eta_{i0}} & -\frac{v_{i0}}{\Delta z_{i+1}\rho_{i0}}\left[\rho_{i0} + (h_{i+1,0}-h_{i0})\xi_{i0}\right] & -\frac{\rho_{i0} + (h_{i+1,0}-h_{i0})\xi_{i0}}{\Delta z_{i+1}\eta_{i0}} \\ \frac{v_{i0}(v_{i+1,0}-v_{i0})\xi_{i0}}{\Delta z_{i+1}\rho_{i0}} & \frac{1}{\Delta z_{i+1}\rho_{i0}}\left[v_{i0}(v_{i+1,0}-v_{i0})\eta_{i0} - 1\right] & \frac{(v_{i+1,0}-2v_{i0})}{\Delta z_{i+1}} \end{bmatrix} \tag{3.29}$$

$$\mathbf{B}_{w,i} = \begin{bmatrix} \dfrac{v_{i0}}{\Delta z_{i+1}} & 0 & 0 \\ \dfrac{v_{i+1,0}\xi_{i+1,0} - v_{i0}\xi_{i0}}{\Delta z_{i+1}\eta_{i0}} & \dfrac{v_{i+1,0}\eta_{i+1,0}}{\Delta z_{i+1}\eta_{i0}} & \dfrac{\rho_{i+1,0}}{\Delta z_{i+1}\eta_{i0}} \\ b_{31}^{i} & b_{32}^{i} & b_{33}^{i} \end{bmatrix} \tag{3.30}$$

$$\mathbf{c}_{sw,i} = \left[\frac{P_{hw}}{A_w \rho_{i0}}, -\frac{P_{hw}\xi_{i0}}{A_w \rho_{i0}\eta_{i0}}, 0 \right]^T \tag{3.31}$$

where

$$b_{31}^{i} = \frac{1}{\rho_{i0}} \left[\frac{f_{i+1,0} v_{i+1,0}^2}{2D_h} \left(\frac{\alpha \rho_{i+1,0} \beta_{i+1,0}}{\mu_{i+1,0}} - (1+\alpha)\xi_{i+1,0} \right) + g\xi_{i+1,0} \right]$$

$$b_{32}^{i} = \frac{1}{\rho_{i0}} \left[\frac{1}{\Delta z_i} + \frac{f_{i+1,0} v_{i+1,0}^2}{2D_h} \left(\frac{\alpha \rho_{i+1,0} \gamma_{i+1,0}}{\mu_{i+1,0}} - (1+\alpha)\eta_{i+1,0} \right) + g\eta_{i+1,0} \right]$$

$$b_{33}^{i} = \frac{v_{i0}}{\Delta z_i} - (2+\alpha) \frac{f_{i+1,0} \rho_{i+1,0} v_{i+1,0}}{2D_h \rho_{i0}}$$

Note that all the variables in these matrices are those for water rod nodes.

3.1.3. Fuel Temperature Perturbation Equations

The fuel temperature perturbation equation is derived from the time-dependent fuel temperature equation in Eq. (2.47) by representing the radial temperature distribution vector, volumetric heat source, and coolant temperature as

$$\begin{aligned} \mathbf{T}_{f,i}(t) &= \mathbf{T}_{f,i0} + \delta\mathbf{T}_{f,i}(t) \\ \overline{q}'''_{f,i}(t) &= \overline{q}'''_{f,i0} + \delta\overline{q}'''_{f,i}(t) \\ T_{c,i}(t) &= T_{c,i0} + \delta T_{c,i}(t) \end{aligned} \tag{3.32}$$

Expanding the temperature dependent coefficient matrix $\mathbf{E}_{f,i}$ in Taylor series, and neglecting higher order terms, we obtain a linear system of differential equation for the fuel temperature perturbations in the axial node i as

$$\mathbf{D}_{f,i} \frac{d}{dt} \delta\mathbf{T}_{f,i} = \mathbf{F}_{f,i} \delta\mathbf{T}_{f,i} + \delta\mathbf{s}_{f,i} \tag{3.33}$$

where $\mathbf{F}_{f,i}$ is a tri-diagonal matrix and $\delta\mathbf{s}_{f,i}$ is a source vector, which are discussed below.

Elements of the tri-diagonal matrix $\mathbf{F}_{f,i}$ depend on the steady state fuel temperatures, heat conductivities, and their temperature derivatives. Explicit expressions of these elements can be obtained using Eqs. (2.40) to (2.45). The resulting expressions of these elements and source terms are summarized below. The axial node index i is omitted for simplicity in these expressions, and all the temperatures represent steady state values. For each row j, $f_{l,j}$, $f_{d,j}$, and $f_{u,j}$ denote the lower-triangular, diagonal, and upper-triangular elements, respectively.

(1) $j=1$ (fuel pellet center)

$$f_{l,j}=0$$

$$f_{d,j}=e_{d,j}-\frac{2}{(\Delta r)^2}\frac{\partial k_j}{\partial T}(T_{f,j}-T_{f,j+1})$$

$$f_{u,j}=e_{u,j}-\frac{2}{(\Delta r)^2}\frac{\partial k_{j+1}}{\partial T}(T_{f,j}-T_{f,j+1})$$

$$\delta s_{f,j}=\delta\overline{q}'''_{f,j}$$

(2) $j=2,3,\cdots,n$ (interior mesh points of fuel pellet)

$$f_{l,j}=e_{l,j}-\frac{1}{2(\Delta r)^2}\left(1-\frac{\Delta r}{2r_j}\right)\frac{\partial k_{j-1}}{\partial T}(T_{f,j}-T_{f,j-1})$$

$$f_{d,j}=e_{d,j}-\frac{1}{2(\Delta r)^2}\frac{\partial k_j}{\partial T}\left[2T_{f,j}-\left(1-\frac{\Delta r}{2r_j}\right)T_{f,j-1}-\left(1+\frac{\Delta r}{2r_j}\right)T_{f,j+1}\right]$$

$$f_{u,j}=e_{u,j}-\frac{1}{2(\Delta r)^2}\left(1+\frac{\Delta r}{2r_j}\right)\frac{\partial k_{j+1}}{\partial T}(T_{f,j}-T_{f,j+1})$$

$$\delta s_{f,j}=\delta\overline{q}'''_{f,j}$$

(3) $j=n+1$ (fuel pellet surface)

$$f_{l,j}=e_{l,j}-\frac{1}{\Delta r}\frac{h_g}{k_j}\frac{\partial k_{j-1}}{\partial T}(T_{f,j+1}-T_{f,j})$$

$$f_{d,j}=e_{d,j}-\frac{2}{(\Delta r)^2}\frac{\partial k_j}{\partial T}(T_{f,j}-T_{f,j-1})-\frac{1}{\Delta r}\frac{h_g k_{j-1}}{(k_j)^2}\frac{\partial k_j}{\partial T}(T_{f,j}-T_{f,j+1})$$

$$f_{u,j} = e_{u,j}$$

$$\delta s_{f,j} = \delta \overline{q}'''_{f,j}$$

(4) $j = n+2$ (cladding inner surface)

$$f_{l,j} = e_{l,j}$$

$$f_{d,j} = e_{d,j} - \frac{8}{d^2}\frac{\partial k_j}{\partial T}(T_{f,j} - T_{f,j+1}) - \frac{2}{d}\frac{r_s}{r_g}\frac{h_g k_{j+1}}{k_j^2}\frac{\partial k_j}{\partial T}(T_{f,j} - T_{f,j-1})$$

$$f_{u,j} = e_{u,j} - \frac{2}{d}\frac{h_g}{k_j}\frac{r_s}{r_g}\frac{\partial k_{j+1}}{\partial T}(T_{f,j-1} - T_{f,j})$$

$$\delta s_{f,j} = 0$$

(5) $j = n+3$ (cladding mid-point)

$$f_{l,j} = e_{l,j} - \frac{1}{2d^2}\frac{\partial k_{j-1}}{\partial T}\left(4 - \frac{d}{r_g + d/2}\right)(T_{f,j} - T_{f,j-1})$$

$$f_{d,j} = e_{d,j} - \frac{1}{d^2}\frac{\partial k_j}{\partial T}\left[4T_{f,j} - \frac{1}{2}\left(4 - \frac{d}{r_g + d/2}\right)T_{f,j-1} - \frac{1}{2}\left(4 + \frac{d}{r_g + d/2}\right)T_{f,j+1}\right]$$

$$f_{u,j} = e_{u,j} - \frac{1}{2d^2}\frac{\partial k_{j+1}}{\partial T}\left(4 + \frac{d}{r_g + d/2}\right)(T_{f,j} - T_{f,j+1})$$

$$\delta s_{f,j} = 0$$

(6) $j = n+4$ (cladding outer surface)

$$f_{l,j} = e_{l,j} - \frac{2}{d}\frac{h_{cl}}{k_j}\frac{\partial k_{j-1}}{\partial T}(T_c - T_{cl})$$

$$f_{d,j} = e_{d,j} - \frac{8}{d^2}\frac{\partial k_j}{\partial T}(T_{cl} - T_{f,j-1}) - \left[\frac{1}{r_{cl}}\frac{\partial h_{cl}}{\partial T_{cl}} + \frac{2}{d}\left(3 - \frac{k_m}{k_{cl}}\right)\frac{\partial h_{cl}}{\partial T_{cl}} + \frac{2}{d}\frac{h_{cl}k_{j-1}}{k_j^2}\frac{\partial k_j}{\partial T_{cl}}\right](T_{cl} - T_c)$$

$$f_{u,j} = 0$$

$$\delta s_{f,j} = \delta s_{f,h} + \delta s_{f,P} + \delta s_{f,v} \tag{3.34}$$

The source term in Eq. (3.34) for the mesh point at the cladding outer surface arises from the boundary condition perturbation at the cladding outer surface. Since the heat transfer coefficient at the cladding wall is changed by the coolant enthalpy, pressure, and velocity perturbations, it can be decomposed into three terms due to enthalpy perturbation δh_c, pressure perturbation δP_c, and velocity perturbation δv_c. Representing δT_c in terms of δh_c and δP_c using the relation

$$dh = \left.\frac{\partial h}{\partial T}\right|_P dT + \left.\frac{\partial h}{\partial P}\right|_T dP = c_p dT + \frac{1-\alpha T}{\rho} dP$$

the explicit expressions of these source terms can be written as

(1) Coolant enthalpy perturbation

$$\delta s_{f,h} = \left[\frac{1}{r_{cl}} + \frac{2}{d}\left(3 - \frac{k_m}{k_{cl}}\right)\right]\left[\frac{\partial h_{cl}}{\partial h_c}(T_c - T_{cl}) + \frac{h_{cl}}{c_p^c}\right]\delta h_c \tag{3.35}$$

(2) Coolant pressure perturbation

$$\delta s_{f,P} = \left[\frac{1}{r_{cl}} + \frac{2}{d}\left(3 - \frac{k_m}{k_{cl}}\right)\right]\left[\frac{\partial h_{cl}}{\partial P_c}(T_c - T_{cl}) - \frac{h_{cl}}{\rho_c c_p^c}(1 - \alpha_c T_c)\right]\delta P_c \tag{3.36}$$

(3) Coolant velocity perturbation

$$\delta s_{f,v} = \left[\frac{1}{r_{cl}} + \frac{2}{d}\left(3 - \frac{k_m}{k_{cl}}\right)\right]\left[\frac{\partial h_{cl}}{\partial v_c}(T_c - T_{cl})\right]\delta v_c \tag{3.37}$$

where c_p^c is the coolant specific heat capacity and α_c is the coolant volume expansivity. The derivatives of the heat transfer coefficient h_{cl} are computed using the steady state conditions, as described in Appendix A.

3.1.4. Water Rod Wall Temperature Perturbation Equations

Applying the same procedure used in deriving the fuel temperature perturbation equations, the perturbation equations for water-rod wall temperatures can be derived from Eqs. (2.48) to (2.50) as

$$\mathbf{D}_{s,i}\frac{d}{dt}\delta\mathbf{T}_{s,i} = \mathbf{F}_{s,i}\delta\mathbf{T}_{s,i} + \delta\mathbf{s}_{s,i} \tag{3.38}$$

where

$$\mathbf{F}_{s,i}=\begin{bmatrix} f_{11} & \dfrac{8}{(\Delta x)^2}\left[k_{s,i}+\dfrac{\partial k_{s,i}}{\partial T_{s,i}}(T_{s,i}-T_{sc,i})\right] & 0 \\ \dfrac{4k_{s,i}}{(\Delta x)^2} & \dfrac{4}{(\Delta x)^2}\left[-2k_{s,i}+\dfrac{\partial k_{s,i}}{\partial T_{s,i}}(T_{sc,i}-2T_{s,i}+T_{sw,i})\right] & \dfrac{4k_{s,i}}{(\Delta x)^2} \\ 0 & \dfrac{8}{(\Delta x)^2}\left[k_{s,i}+\dfrac{\partial k_{s,i}}{\partial T_{s,i}}(T_{s,i}-T_{sw,i})\right] & f_{33} \end{bmatrix} \tag{3.39}$$

$$f_{11}=-\frac{4}{\Delta x}\left[\frac{2k_{s,i}}{\Delta x}+h_{sc,i}+\frac{\partial h_{sc,i}}{\partial T_{sc,i}}(T_{sc,i}-T_{c,i})\right]$$

$$f_{33}=-\frac{4}{\Delta x}\left[\frac{2k_{s,i}}{\Delta x}+h_{sw,i}+\frac{\partial h_{sw,i}}{\partial T_{sw,i}}(T_{sw,i}-T_{w,i})\right]$$

The source term $\delta\mathbf{s}_{s,i}$ arises from the perturbations of heat transfer coefficients at wall surfaces. Since the heat transfer coefficients are changed by the enthalpy, pressure, and velocity of coolant and water rod, it can be decomposed as

$$\delta\mathbf{s}_{s,i}=\begin{bmatrix} s_{1h} \\ 0 \\ 0 \end{bmatrix}\delta h_{c,i}+\begin{bmatrix} s_{1p} \\ 0 \\ 0 \end{bmatrix}\delta P_{c,i}+\begin{bmatrix} s_{1v} \\ 0 \\ 0 \end{bmatrix}\delta v_{c,i}+\begin{bmatrix} 0 \\ 0 \\ s_{3h} \end{bmatrix}\delta h_{w,i+1}+\begin{bmatrix} 0 \\ 0 \\ s_{3P} \end{bmatrix}\delta P_{w,i+1}+\begin{bmatrix} 0 \\ 0 \\ s_{3v} \end{bmatrix}\delta v_{w,i+1} \tag{3.40}$$

where

$$s_{1h}=\frac{4}{\Delta x}\left[\frac{\partial h_{sc,i}}{\partial h_{c,i}}(T_{c,i}-T_{sc,i})+\frac{h_{sc,i}}{c^c_{p,i}}\right]$$

$$s_{1P}=\frac{4}{\Delta x}\left[\frac{\partial h_{sc,i}}{\partial P_{c,i}}(T_{c,i}-T_{sc,i})-\frac{h_{sc,i}}{\rho_{c,i}c^c_{p,i}}(1-\alpha_{c,i}T_{c,i})\right]$$

$$s_{1v}=\frac{4}{\Delta x}\frac{\partial h_{sc,i}}{\partial v_{c,i}}(T_{c,i}-T_{sc,i})$$

$$s_{3h}=\frac{4}{\Delta x}\left[\frac{\partial h_{sw,i}}{\partial h_{w,i+1}}(T_{w,i+1}-T_{sw,i})+\frac{h_{sw,i}}{c^w_{p,i+1}}\right]$$

$$s_{3P}=\frac{4}{\Delta x}\left[\frac{\partial h_{sw,i}}{\partial P_{w,i+1}}(T_{w,i+1}-T_{sw,i})-\frac{h_{sw,i}}{\rho_{w,i+1}c^w_{p,i+1}}(1-\alpha_{w,i+1}T_{w,i+1})\right]$$

$$s_{3v}=\frac{4}{\Delta x}\frac{\partial h_{sw,i}}{\partial v_{w,i+1}}(T_{w,i+1}-T_{sw,i})$$

3.2. Frequency Domain Linear Equations

3.2.1. System of Linear Perturbation Equations for a Channel

The frequency domain linear equations are obtained by applying the Laplace transformation to the linearized perturbation equations discussed above. For each axial node i, the coolant perturbation equations are obtained by the Laplace transformation of Eq. (3.12) as

$$s\delta\tilde{\mathbf{x}}_{c,i}(s) = \mathbf{A}_{c,i}\delta\tilde{\mathbf{x}}_{c,i}(s) + \mathbf{B}_{c,i}\delta\tilde{\mathbf{x}}_{c,i-1}(s) + \mathbf{c}_{f,i}\delta\tilde{q}''_{f,i}(s) - \mathbf{c}_{cs,i}\delta\tilde{q}''_{sc,i}(s) \tag{3.41}$$

where s is the complex variable of the Laplace transform, the tilde denotes the Laplace transformed variables, and $\delta\tilde{\mathbf{x}}_{c,i} = (\delta\tilde{h}_{c,i}, \delta\tilde{P}_{c,i}, \delta\tilde{v}_{c,i})^T$. Similarly, the water-rod perturbation equations are obtained by the Laplace transform of Eq. (3.27) as

$$s\delta\tilde{\mathbf{x}}_{w,i}(s) = \mathbf{A}_{w,i}\delta\tilde{\mathbf{x}}_{w,i}(s) + \mathbf{B}_{w,i}\delta\tilde{\mathbf{x}}_{w,i+1}(s) + \mathbf{c}_{sw,i}\delta\tilde{q}''_{sw,i+1}(s) \tag{3.42}$$

The fuel temperature perturbation equations are obtained by applying the Laplace transformation to Eq. (3.33) and can be written in a matrix form as

$$s\mathbf{D}_{f,i}\delta\tilde{\mathbf{T}}_{f,i}(s) = \mathbf{A}_{f,i}\delta\tilde{\mathbf{T}}_{f,i}(s) + \mathbf{B}_{f,i}\delta\tilde{\mathbf{x}}_{c,i}(s) + \mathbf{r}_{f,i}\delta\tilde{q}'''_{f,i}(s) \tag{3.43}$$

Equation (3.43) includes the coolant variable perturbations $\delta\tilde{\mathbf{x}}_{c,i}$ because of the source terms shown in Eqs. (3.35) to (3.37) resulting from the variation of the heat transfer coefficient. Similarly, the Laplace-transformed perturbation equations for water-rod wall temperatures can be obtained using Eqs. (3.38) and (3.40) as

$$s\mathbf{D}_{s,i}\delta\tilde{\mathbf{T}}_{s,i}(s) = \mathbf{F}_{s,i}\delta\tilde{\mathbf{T}}_{s,i}(s) + \mathbf{S}_{c,i}\delta\tilde{\mathbf{x}}_{c,i}(s) + \mathbf{S}_{w,i}\delta\tilde{\mathbf{x}}_{w,i+1}(s) \tag{3.44}$$

The perturbation equation for the heat flux at the cladding wall is determined in a similar manner. Linearizing Eq. (2.17) around the steady state solution and applying the Laplace transformation to the resulting equation, we obtain the following equation for the heat flux perturbation

$$\begin{aligned}\delta\tilde{q}''_{f,i} = &\left[h_{cl,i} + \frac{\partial h_{cl,i}}{\partial T_{cl.i}}(T_{cl,i} - T_{c,i})\right]\delta\tilde{T}_{cl,i} + \left[\frac{\partial h_{cl,i}}{\partial h_{c,i}}(T_{cl,i} - T_{c,i}) - \frac{h_{cl,i}}{c^c_{p,i}}\right]\delta\tilde{h}_{c,i} \\ &+ \left[\frac{\partial h_{cl,i}}{\partial P_{c,i}}(T_{cl,i} - T_{c,i}) + \frac{h_{cl,i}}{\rho_{c,i}c^c_{p,i}}(1 - \alpha_{c,i}T_{c,i})\right]\delta\tilde{P}_{c,i} + \frac{\partial h_{cl,i}}{\partial v_{c,i}}(T_{cl,i} - T_{c,i})\delta\tilde{v}_{c,i}\end{aligned} \tag{3.45}$$

This equation can be written in a matrix notation consistent with Eqs. (3.41) and (3.43) as

$$\delta\tilde{q}''_{f,i}(s) = a_{q,i}\delta\tilde{T}_{cl,i}(s) + \mathbf{d}^T_{q,i}\delta\tilde{\mathbf{x}}_{c,i}(s) \tag{3.46}$$

The Laplace-transformed perturbation equations for the heat fluxes at the water-rod wall surfaces can be obtained from Eqs. (2.19) and (2.20) as

$$\begin{aligned}\delta\tilde{q}''_{sc,i} = &-\left[h_{sc,i} + \frac{\partial h_{sc,i}}{\partial T_{sc.i}}(T_{sc,i} - T_{c,i})\right]\delta\tilde{T}_{sc,i} + \left[\frac{\partial h_{sc,i}}{\partial h_{c,i}}(T_{c,i} - T_{sc,i}) + \frac{h_{sc,i}}{c^c_{p,i}}\right]\delta\tilde{h}_{c,i} \\ &+\left[\frac{\partial h_{sc,i}}{\partial P_{c,i}}(T_{c,i} - T_{sc,i}) - \frac{h_{sc,i}}{\rho_{c,i}c^c_{p,i}}(1-\alpha_{c,i}T_{c,i})\right]\delta\tilde{P}_{c,i} + \frac{\partial h_{sc,i}}{\partial v_{c,i}}(T_{c,i} - T_{sc,i})\delta\tilde{v}_{c,i}\end{aligned} \tag{3.47}$$

$$\begin{aligned}\delta\tilde{q}''_{sw,i} = &\left[h_{sw,i} + \frac{\partial h_{sw,i}}{\partial T_{sw.i}}(T_{sw,i} - T_{w,i+1})\right]\delta\tilde{T}_{sw,i} + \left[\frac{\partial h_{sw,i}}{\partial h_{c,i+1}}(T_{sw,i} - T_{w,i+1}) - \frac{h_{sw,i}}{c^w_{p,i+1}}\right]\delta\tilde{h}_{w,i+1} \\ &+\left[\frac{\partial h_{sw,i}}{\partial P_{c,i+1}}(T_{sw,i} - T_{w,i+1}) + \frac{h_{sw,i}}{\rho_{w,i+1}c^w_{p,i+1}}(1-\alpha_{w,i+1}T_{w,i+1})\right]\delta\tilde{P}_{w,i+1} + \frac{\partial h_{sw,i}}{\partial v_{c,i+1}}(T_{sw,i} - T_{w,i+1})\delta\tilde{v}_{w,i+1}\end{aligned} \tag{3.48}$$

These equations can be written in a matrix notation as

$$\delta\tilde{q}''_{sc,i}(s) = a_{sc,i}\delta\tilde{T}_{sc,i}(s) + \mathbf{d}^T_{sc,i}\delta\tilde{\mathbf{x}}_{c,i}(s) \tag{3.49}$$

$$\delta\tilde{q}''_{sw,i}(s) = a_{sw,i}\delta\tilde{T}_{sw,i}(s) + \mathbf{d}^T_{sw,i}\delta\tilde{\mathbf{x}}_{w,i+1}(s) \tag{3.50}$$

To make the overall computation easier, we first determine the component-wise fuel temperature transfer functions by solving Eq. (3.43) separately for individual perturbations of the coolant enthalpy, pressure, and velocity, as well as the volumetric heat source. Then the transfer functions for the coolant and the water-rod state variables are obtained by substituting these fuel temperature transfer functions into the corresponding thermal hydraulics and heat flux equations. The component-wise fuel temperature transfer functions are determined as:

(1) The coolant enthalpy to fuel temperature transfer function is computed by solving Eq. (3.43) with a unit enthalpy perturbation, i.e., $\delta\tilde{h}_{c,i} = 1$, $\delta\tilde{P}_{c,i} = 0$, $\delta\tilde{v}_{c,i} = 0$, and $\delta\tilde{q}'''_{f,i} = 0$. The average fuel temperature transfer function $\tilde{a}^i_{Tf} = \delta\tilde{T}^{avg}_{f,i} / \delta\tilde{h}_{c,i}$ is determined by a weighted average of fuel temperature perturbations as

$$\delta\tilde{T}^{avg}_{f,i} = \sum_{j=1}^{n} w^r_j \delta\tilde{T}^i_{f,j} \tag{3.51}$$

where w^r_j is the weighting factor for the radial mesh j. A volume-weighted average

was used in this study. The cladding-wall temperature transfer function $\tilde{a}^i_{Tcl} = \delta\tilde{T}_{cl,i} / \delta\tilde{h}_{c,i}$ is determined by the resulting cladding-wall temperature perturbation.

(2) The coolant pressure to fuel temperature transfer function is computed for a unit pressure perturbation $\delta\tilde{P}_{c,i} = 1$, with $\delta\tilde{h}_{c,i} = 0$, $\delta\tilde{v}_{c,i} = 0$, and $\delta\tilde{q}'''_{f,i} = 0$. The average fuel temperature transfer function $\tilde{b}^i_{Tf} = \delta\tilde{T}^{avg}_{f,i} / \delta\tilde{P}_{c,i}$ and the cladding-wall temperature transfer function $\tilde{b}^i_{Tcl} = \delta\tilde{T}_{cl,i} / \delta\tilde{P}_{c,i}$ are determined as in (1).

(3) The coolant velocity to fuel temperature transfer functions are computed for a unit coolant velocity perturbation $\delta\tilde{v}_{c,i} = 1$, with $\delta\tilde{h}_{c,i} = 0$, $\delta\tilde{P}_{c,i} = 0$, and $\delta\tilde{q}'''_{f,i} = 0$. The average fuel temperature transfer function $\tilde{c}^i_{Tf} = \delta\tilde{T}^{avg}_{f,i} / \delta\tilde{v}_{c,i}$ and the cladding-wall temperature transfer function $\tilde{c}^i_{Tcl} = \delta\tilde{T}_{cl,i} / \delta\tilde{v}_{c,i}$ are determined as in (1).

(4) The power to fuel temperature transfer functions are computed for a unit power perturbation $\delta\tilde{q}'''_{f,i} = 1$, with $\delta\tilde{h}_{c,i} = 0$, $\delta\tilde{P}_{c,i} = 0$, and $\delta\tilde{v}_{c,i} = 0$. The average fuel temperature transfer function $\tilde{d}^i_{Tf} = \delta\tilde{T}^{avg}_{f,i} / \delta\tilde{q}'''_{f,i}$ and the cladding-wall temperature transfer function $\tilde{d}^i_{Tcl} = \delta\tilde{T}_{cl,i} / \delta\tilde{q}'''_{f,i}$ are determined as in (1).

Using these component-wise transfer functions, the total perturbations of the average fuel temperature and cladding wall temperature in the axial node i are obtained as

$$\delta\tilde{T}^{avg}_{f,i} = \tilde{a}^i_{Tf}\delta\tilde{h}_{c,i} + \tilde{b}^i_{Tf}\delta\tilde{P}_{c,i} + \tilde{c}^i_{Tf}\delta\tilde{v}_{c,i} + \tilde{d}^i_{Tf}\delta\tilde{q}'''_{f,i} \tag{3.52}$$

$$\delta\tilde{T}_{cl,i} = \tilde{a}^i_{Tcl}\delta\tilde{h}_{c,i} + \tilde{b}^i_{Tcl}\delta\tilde{P}_{c,i} + \tilde{c}^i_{Tcl}\delta\tilde{v}_{c,i} + \tilde{d}^i_{Tcl}\delta\tilde{q}'''_{f,i} \tag{3.53}$$

Substituting Eq. (3.53) into Eq. (3.46), the perturbation of heat flux at the cladding wall is determined as

$$\delta\tilde{q}''_{f,i} = \tilde{\mathbf{a}}^T_{q,i}\delta\tilde{\mathbf{x}}_{c,i} + \tilde{d}_{q,i}\delta\tilde{q}'''_{f,i} \tag{3.54}$$

where

$$\tilde{d}_{q,i} = \left[h_{cl,i} + \frac{\partial h_{cl.i}}{\partial T_{cl.i}}(T_{cl,i} - T_{c,i}) \right] \tilde{d}^i_{Tcl}$$

$$\tilde{\mathbf{a}}_{q,i}=\begin{bmatrix} \dfrac{\partial h_{cl,i}}{\partial h_{c,i}}(T_{cl,i}-T_{c,i})-\dfrac{h_{cl,i}}{c^{c}_{p,i}}+\left[h_{cl,i}+\dfrac{\partial h_{cl.i}}{\partial T_{cl.i}}(T_{cl,i}-T_{c,i})\right]\tilde{a}^{i}_{Tcl} \\ \dfrac{\partial h_{cl,i}}{\partial P_{c,i}}(T_{cl,i}-T_{c,i})+\dfrac{h_{cl,i}}{\rho_{c,i}c^{c}_{p,i}}(1-\alpha_{c}T_{c,i})+\left[h_{cl,i}+\dfrac{\partial h_{cl.i}}{\partial T_{cl.i}}(T_{cl,i}-T_{c,i})\right]\tilde{b}^{i}_{Tcl} \\ \dfrac{\partial h_{cl,i}}{\partial v_{v,i}}(T_{cl,i}-T_{c,i})+\left[h_{cl,i}+\dfrac{\partial h_{cl.i}}{\partial T_{cl.i}}(T_{cl,i}-T_{c,i})\right]\tilde{c}^{i}_{Tcl} \end{bmatrix}$$

Similarly, by solving Eq. (3.44), the component-wise water-rod wall temperature transfer functions are determined as

$$\delta\tilde{\mathbf{T}}_{s,i}=\mathbf{A}_{s,i}\delta\tilde{\mathbf{x}}_{c,i}+\mathbf{B}_{s,i}\delta\tilde{\mathbf{x}}_{w,i+1} \tag{3.55}$$

where

$$\mathbf{A}_{s,i}=(s\mathbf{D}_{s,i}-\mathbf{F}_{s,i})^{-1}\mathbf{S}_{c,i}$$

$$\mathbf{B}_{s,i}=(s\mathbf{D}_{s,i}-\mathbf{F}_{s,i})^{-1}\mathbf{S}_{w,i}$$

Substituting Eq. (3.55) into Eqs. (3.49) and (3.50), the perturbations of heat fluxes at the water rod wall are determined as

$$\delta\tilde{q}''_{sc,i}=\tilde{\mathbf{a}}^{T}_{sc,i}\delta\tilde{\mathbf{x}}_{c,i}+\tilde{\mathbf{b}}^{T}_{sc,i}\delta\tilde{\mathbf{x}}_{w,i} \tag{3.56}$$

$$\delta\tilde{q}''_{sw,i}=\tilde{\mathbf{a}}^{T}_{sw,i}\delta\tilde{\mathbf{x}}_{c,i}+\tilde{\mathbf{b}}^{T}_{sw,i}\delta\tilde{\mathbf{x}}_{w,i} \tag{3.57}$$

where

$$\tilde{\mathbf{a}}^{T}_{sc,i}=[a_{sc,i},0,0]\mathbf{A}_{s,i}+\mathbf{d}^{T}_{sc,i}$$

$$\tilde{\mathbf{b}}^{T}_{sc,i}=[a_{sc,i},0,0]\mathbf{B}_{s,i}$$

$$\tilde{\mathbf{a}}^{T}_{sw,i}=[0,0,a_{sw,i}]\mathbf{A}_{s,i}$$

$$\tilde{\mathbf{b}}^{T}_{sw,i}=[0,0,a_{sw,i}]\mathbf{B}_{s,i}+\mathbf{d}^{T}_{sw,i}$$

Eliminating $\delta\tilde{q}''_{f,i}$ using Eq. (3.54) and $\delta\tilde{q}^{"}_{sc,i}$ using Eq. (3.56), the Laplace-transformed coolant perturbation equations in Eq. (3.41) are reduced to

$$(s\mathbf{I}-\mathbf{A}_{c,i}-\mathbf{D}_{c,i})\delta\tilde{\mathbf{x}}_{c,i}-\mathbf{B}_{c,i}\delta\tilde{\mathbf{x}}_{c,i-1}+\mathbf{C}_{c,i}\delta\tilde{\mathbf{x}}_{w,i}=\tilde{\mathbf{d}}_{f,i}\delta\tilde{q}'''_{f,i} \tag{3.58}$$

where

$$\mathbf{D}_{c,i}=\mathbf{c}_{f,i}\tilde{\mathbf{a}}^{T}_{q,i}-\mathbf{c}_{sc,i}\tilde{\mathbf{a}}^{T}_{sc,i}$$

$$\mathbf{C}_{c,i} = \mathbf{c}_{sc,i}\tilde{\mathbf{b}}_{sc,i}^{T}$$

$$\tilde{\mathbf{d}}_{f,i} = \tilde{d}_{q,i}\mathbf{c}_{f,i}$$

and $\mathbf{I}$ is the 3×3 identity matrix. In a similar way, the Laplace-transformed water-rod perturbation equations can be written as

$$(s\mathbf{I} - \mathbf{A}_{w,i})\delta\tilde{\mathbf{x}}_{w,i}(s) - (\mathbf{B}_{w,i} + \mathbf{D}_{w,i})\delta\tilde{\mathbf{x}}_{w,i+1}(s) - \mathbf{C}_{w,i}\delta\tilde{\mathbf{x}}_{c,i+1}(s) = 0 \tag{3.59}$$

where

$$\mathbf{D}_{w,i} = \mathbf{c}_{sw,i}(\mathbf{a}_{sw,i+1}^{T} + \mathbf{d}_{sw,i+1}^{T})$$

$$\mathbf{C}_{w,i} = \mathbf{c}_{sw,i}\mathbf{a}_{sw,i+1}^{T}$$

Defining a combined unknown vector $\delta\mathbf{x}_{i,j}$ for each node i of a thermal-hydraulic channel j as $\delta\mathbf{x}_{i,j} = (\delta\tilde{\mathbf{x}}_{c,i,j}, \delta\tilde{\mathbf{x}}_{w,i-1,j})^{T}$, Eqs. (3.58) and (3.59) can be written in a single matrix equation as

$$\begin{bmatrix} \mathbf{D}_{1,j} & \mathbf{U}_{1,j} & 0 & \cdots & 0 & 0 & 0 \\ \mathbf{L}_{2,j} & \mathbf{D}_{2,j} & \mathbf{U}_{2,j} & \cdots & 0 & 0 & 0 \\ 0 & \mathbf{L}_{3,j} & \mathbf{D}_{3,j} & \cdots & 0 & 0 & 0 \\ \vdots & \vdots & \ddots & \ddots & \ddots & \vdots & \vdots \\ 0 & 0 & 0 & \cdots & \mathbf{D}_{I-2,j} & \mathbf{U}_{I-2,j} & 0 \\ 0 & 0 & 0 & \cdots & \mathbf{L}_{I-1,j} & \mathbf{D}_{I-1,j} & \mathbf{U}_{I-1,j} \\ 0 & 0 & 0 & \cdots & 0 & \mathbf{L}_{I,j} & \mathbf{D}_{I,j} \end{bmatrix} \begin{bmatrix} \delta\mathbf{x}_{1,j} \\ \delta\mathbf{x}_{2,j} \\ \delta\mathbf{x}_{3,j} \\ \vdots \\ \delta\mathbf{x}_{I-2,j} \\ \delta\mathbf{x}_{I-1,j} \\ \delta\mathbf{x}_{I,j} \end{bmatrix} = \begin{bmatrix} \mathbf{s}_{1,j} - \mathbf{L}_{1,j}\delta\mathbf{x}_{0,j} \\ \mathbf{s}_{2,j} \\ \mathbf{s}_{3,j} \\ \vdots \\ \mathbf{s}_{I-2,j} \\ \mathbf{s}_{I-1,j} \\ \mathbf{s}_{I,j} - \mathbf{U}_{I,j}\delta\mathbf{x}_{I+1,j} \end{bmatrix} \tag{3.60}$$

where

$$\mathbf{L}_{i,j} = \begin{bmatrix} -\mathbf{B}_{ci,j} & 0 \\ 0 & 0 \end{bmatrix}, \quad \mathbf{D}_{i,j} = \begin{bmatrix} s\mathbf{I} - \mathbf{A}_{ci,j} - \mathbf{D}_{ci,j} & 0 \\ -\mathbf{C}_{wi,j} & s\mathbf{I} - \mathbf{A}_{wi,j} \end{bmatrix}, \quad \mathbf{U}_{i} = \begin{bmatrix} 0 & \mathbf{C}_{ci,j} \\ 0 & -(\mathbf{B}_{wi,j} + \mathbf{D}_{wi,j}) \end{bmatrix} \tag{3.61}$$

$$\mathbf{s}_{i,j} = \begin{bmatrix} \tilde{\mathbf{d}}_{f,i,j} f_{ij} \\ 0 \end{bmatrix} \delta\tilde{q}_{j} \tag{3.62}$$

Here, q_j is the pin power of the channel j and f_{ij} is the power fraction of axial node i in the channel j. Note that the term $\mathbf{U}_{I,j}\delta\mathbf{x}_{I+1,j}$ includes the water-rod inlet perturbations $\delta\tilde{\mathbf{x}}_{wI,j}$ only, since

$$\mathbf{U}_{I,j}\delta\mathbf{x}_{I+1,j} = \begin{bmatrix} 0 & \mathbf{C}_{cI,j} \\ 0 & -(\mathbf{B}_{wI,j} + \mathbf{D}_{wI,j}) \end{bmatrix} \begin{bmatrix} \delta\tilde{\mathbf{x}}_{c,I+1,j} \\ \delta\tilde{\mathbf{x}}_{wI,j} \end{bmatrix} = \begin{bmatrix} \mathbf{C}_{cI,j}\delta\tilde{\mathbf{x}}_{wI,j} \\ -(\mathbf{B}_{wI,j} + \mathbf{D}_{wI,j})\delta\tilde{\mathbf{x}}_{wI,j} \end{bmatrix} \tag{3.63}$$

Similarly, $\mathbf{L}_{1,j}\delta\mathbf{x}_{0,j}$ includes the coolant channel inlet perturbations $\delta\tilde{\mathbf{x}}_{c,0,j}$ only, since

$$\mathbf{L}_{1,j}\delta\mathbf{x}_{0,j}=\begin{bmatrix}-\mathbf{B}_{c1,j} & 0\\ 0 & 0\end{bmatrix}\begin{bmatrix}\delta\tilde{\mathbf{x}}_{c0,j}\\ \delta\tilde{\mathbf{x}}_{w0,j}\end{bmatrix}=\begin{bmatrix}-\mathbf{B}_{c1,j}\delta\tilde{\mathbf{x}}_{c0,j}\\ 0\end{bmatrix} \tag{3.64}$$

By solving Eq. (3.60) for the unit perturbation of each input parameter, the partial derivatives of state variables with respect to input parameters can be determined as:

$$\frac{\partial\mathbf{x}_{i,j}}{\partial h_{c0,j}} \text{ with } \delta\mathbf{x}_{c0,j}=(1,0,0)^T,\ \delta\mathbf{x}_{wI,j}=(0,0,0)^T,\ \mathbf{s}_{i,j}=0 \tag{3.65.a}$$

$$\frac{\partial\mathbf{x}_{i,j}}{\partial P_{c0,j}} \text{ with } \delta\mathbf{x}_{c0,j}=(0,1,0)^T,\ \delta\mathbf{x}_{wI,j}=(0,0,0)^T,\ \mathbf{s}_{i,j}=0 \tag{3.65.b}$$

$$\frac{\partial\mathbf{x}_{i,j}}{\partial v_{c0,j}} \text{ with } \delta\mathbf{x}_{c0,j}=(0,0,1)^T,\ \delta\mathbf{x}_{wI,j}=(0,0,0)^T,\ \mathbf{s}_{i,j}=0 \tag{3.65.c}$$

$$\frac{\partial\mathbf{x}_{i,j}}{\partial h_{wI,j}} \text{ with } \delta\mathbf{x}_{c0,j}=(0,0,0)^T,\ \delta\mathbf{x}_{wI,j}=(1,0,0)^T,\ \mathbf{s}_{i,j}=0 \tag{3.65.d}$$

$$\frac{\partial\mathbf{x}_{i,j}}{\partial P_{wI,j}} \text{ with } \delta\mathbf{x}_{c0,j}=(0,0,0)^T,\ \delta\mathbf{x}_{wI,j}=(0,1,0)^T,\ \mathbf{s}_{i,j}=0 \tag{3.65.e}$$

$$\frac{\partial\mathbf{x}_{i,j}}{\partial v_{wI,j}} \text{ with } \delta\mathbf{x}_{c0,j}=(0,0,0)^T,\ \delta\mathbf{x}_{wI,j}=(0,0,1)^T,\ \mathbf{s}_{i,j}=0 \tag{3.65.f}$$

$$\frac{\partial\mathbf{x}_{i,j}}{\partial q_j} \text{ with } \delta\mathbf{x}_{c0,j}=(0,0,0)^T,\ \delta\mathbf{x}_{wI,j}=(0,0,0)^T,\ \mathbf{s}_{i,j}=[\tilde{\mathbf{d}}^T_{f,i,j}f_{ij},0]^T \tag{3.65.g}$$

These partial derivatives are the responses of state variables to the channel input parameters. The responses of state variables to the external input parameters (e.g., core power, total flow rates, feed water enthalpy, etc.) can be determined using these partial derivatives and the responses of channel input parameters to the external parameters.

The transfer functions for the unheated orifice node are determined by the Laplace transform of the linearized equation given in Eq. (3.24) as

$$\delta\tilde{\mathbf{x}}_0=-\mathbf{A}_0^{-1}\mathbf{B}_0\delta\tilde{\mathbf{x}}_{in}=\mathbf{H}\delta\tilde{\mathbf{x}}_{in} \tag{3.66}$$

Inverting Eq. (3.24) analytically, Eq. (3.66) can be written as

$$\delta\tilde{h}_0=\delta\tilde{h}_{in} \tag{3.67a}$$

$$\delta\tilde{P}_0 = H_{Ph}\delta\tilde{h}_{in} + H_{PP}\delta\tilde{P}_{in} + H_{Pv}\delta\tilde{v}_{in} \tag{3.67b}$$

$$\delta\tilde{v}_0 = H_{vh}\delta\tilde{h}_{in} + H_{vP}\delta\tilde{P}_{in} + H_{vv}\delta\tilde{v}_{in} \tag{3.67c}$$

where

$$H_{Ph} = -\zeta\xi_{in}v_{in}^2/2 \tag{3.68a}$$

$$H_{PP} = 1-\zeta\eta_{in}v_{in}^2/2 \tag{3.68b}$$

$$H_{Pv} = -\zeta\rho_{in}v_{in} \tag{3.68c}$$

$$H_{vh} = \frac{1}{\rho_0}\left(-\xi_0 v_0 + \xi_{in}v_{in} + \frac{1}{2}\zeta\eta_0\xi_{in}v_0v_{in}^2\right) \tag{3.68d}$$

$$H_{vP} = \frac{1}{\rho_0}\left(-\eta_0 v_0 + \eta_{in}v_{in} + \frac{1}{2}\zeta\eta_0\eta_{in}v_0v_{in}^2\right) \tag{3.68e}$$

$$H_{vv} = \frac{\rho_{in}}{\rho_0}(1+\zeta\eta_0 v_0 v_{in}) \tag{3.68f}$$

At the non-heated inlet orifice node, the coolant is subcooled and thus it is almost incompressible. As a result, H_{Ph}, H_{vh}, and H_{vP} are almost zero, but H_{PP} and H_{vv} are almost one. Consequently, Eq. (3.67) can be approximated as

$$\delta\tilde{h}_0 = \delta\tilde{h}_{in} \tag{3.69a}$$

$$\delta\tilde{P}_0 = \delta\tilde{P}_{in} + H_{Pv}\delta\tilde{v}_{in} \tag{3.69b}$$

$$\delta\tilde{v}_0 = \delta\tilde{v}_{in} \tag{3.69c}$$

3.2.2. Inlet Boundary Condition Perturbations

Under the assumption of complete mixing, the mass and energy conservation equations in the lower plenum can be represented as in Eqs. (2.8) and (2.9). These equations include the time variations of the water mass and enthalpy in the lower plenum. However, as the initial implementation of multi-channel capability in SCWRSA, the time derivatives were neglected, and the equations were replaced with the algebraic boundary equations for two bounding approximations. One is the instantaneous mixing approximation in which the lower plenum mass is assumed to be zero. The other is the constant mixed-mean enthalpy approximation, which is equivalent to an assumption of infinite lower plenum mass.

Under the instantaneous mixing approximation, the conservation equations for the lower plenum can be approximated as

$$\sum_{j=1}^{J} w_{cj} = \sum_{j=1}^{J} w_{wj} + w_{dc} = w_T \tag{3.70}$$

$$h_{c0} \sum_{j=1}^{J} w_{cj} = \sum_{j=1}^{J} h_{w0,j} w_{wj} + h_{dc} w_{dc} \tag{3.71}$$

$$P_{w0,j} = P_{LP} \tag{3.72}$$

Taking the variations of Eq. (3.70) to (3.72) yields

$$\sum_{j=1}^{J} \delta w_{cj} = \sum_{j=1}^{J} \delta w_{wj} + \delta w_{dc} = \delta w_T \tag{3.73}$$

$$\delta h_{c0} w_T = \sum_{j=1}^{J} \delta h_{w0,j} w_{wj} + \sum_{j=1}^{J} (h_{w0,j} - h_{c0}) \delta w_{wj} + \delta h_{dc} w_{dc} + (h_{dc} - h_{c0}) \delta w_{dc} \tag{3.74}$$

$$\delta P_{w0,j} = \delta P_{LP} \tag{3.75}$$

The flow rate variations are determined to satisfy the equal pressure drop boundary conditions. The steady state solution satisfies the equal pressure drop boundary condition, and thus the variations of individual channel pressure drops should satisfy the equal pressure drop boundary condition.

$$\delta \Delta P_{c1} = \delta \Delta P_{c2} = \cdots = \delta \Delta P_{cJ} \tag{3.76}$$

$$\delta \Delta P_{w1} = \delta \Delta P_{w2} = \cdots = \delta \Delta P_{wJ} \tag{3.77}$$

In the constant mixed-mean enthalpy approximation, the inlet enthalpy of coolants into all the fuel assemblies is held constant at the steady-state mixed-mean enthalpy of water in the lower plenum in view of large capacitance of the lower plenum. Thus, Eq. (3.71) is reduced to

$$h_{c0} = \text{constant} \tag{3.78}$$

and the variation of mixed-mean enthalpy of water in the lower plenum becomes

$$\delta h_{c0} = 0 \tag{3.79}$$

3.3. Transfer Functions and Frequency Responses

The inlet boundary condition perturbations given in Eqs. (3.73) to (3.77) depend on the state variable perturbations determined by Eq. (3.60). Thus, these equations should be solved simultaneously with Eq. (3.60). As discussed in Section 3.2.1, the partial derivatives of state variables with respect to input parameters can be determined by solving Eq. (3.60) for the unit perturbation of each input parameter. Using these partial derivatives, Eqs. (3.73) to (3.77) are reduced to a system of equations for inlet parameter perturbations. By solving these equations for a unit perturbation of each of external parameters (e.g., core power, total flow rates, feed water enthalpy, etc.), the responses of channel input parameters to the external parameters are determined. The responses of state variables to the external input parameters are then obtained by combining the responses of channel input parameters to the external parameters and the partial derivatives of state variables with respect to input parameters.

The coolant outlet pressure of every channel is held constant, and thus its variation due to the flow perturbations should be zero. Using the partial derivatives in Eq. (3.65), this condition can be written as

$$\begin{aligned}\delta P_{cI,j} &= c_{cj}^0\delta v_{c0,j} + c_{cj}^2\delta v_{wI,j} + c_{cj}^3\delta h_{c0} + c_{cj}^4\delta P_{c0} + c_{cj}^5\delta P_{wI} + c_{cj}^6\delta h_{wI} + c_{cj}^7\delta p \\ &= c_{cj}^0\delta v_{c0,j} + c_{cj}^2\delta v_{wI,j} + c_{cj}^3\delta h_{c0} + c_{cj}^4(\delta P_{LP} + H_{pv,j}\delta v_{c0,j}) + c_{cj}^5\delta P_{wI} + c_{cj}^6\delta h_{wI} + c_{cj}^7\delta p \\ &= c_{cj}^1\delta v_{c0,j} + c_{cj}^2\delta v_{wI,j} + c_{cj}^3\delta h_{c0} + c_{cj}^4\delta P_{LP} + c_{cj}^5\delta P_{wI} + c_{cj}^6\delta h_{wI} + c_{cj}^7\delta p = 0\end{aligned} \quad (3.80)$$

where

$$c_{cj}^0 = \frac{\partial P_{cI,j}}{\partial v_{c0,j}},\ c_{cj}^2 = \frac{\partial P_{cI,j}}{\partial v_{wI,j}},\ c_{cj}^3 = \frac{\partial P_{cI,j}}{\partial h_{c0,j}},\ c_{cj}^4 = \frac{\partial P_{cI,j}}{\partial P_{c0,j}},$$

$$c_{cj}^5 = \frac{\partial P_{cI,j}}{\partial P_{wI,j}},\ c_{cj}^6 = \frac{\partial P_{cI,j}}{\partial h_{wI,j}},\ c_{cj}^7 = \frac{\partial P_{cI,j}}{\partial q_j}\frac{dq_j}{dp},\ c_{cj}^1 = c_{cj}^0 + c_{cj}^4 H_{pv,j},$$

$H_{pv,j}$ is the response of the channel j orifice outlet pressure to the inlet velocity, and p is the core thermal power. Similarly, the outlet pressure perturbation of water rod given in Eq. (3.75) can be written as

$$\delta P_{w0,j} = c_{wj}^1\delta v_{c0,j} + c_{wj}^2\delta v_{wI,j} + c_{wj}^3\delta h_{c0} + c_{wj}^4\delta P_{LP} + c_{wj}^5\delta P_{wI} + c_{wj}^6\delta h_{wI} + c_{wj}^7\delta p = \delta P_{LP} \quad (3.81)$$

where

$$c_{wj}^1 = \frac{\partial P_{w0,j}}{\partial v_{c0,j}} + c_{wj}^4 H_{pv,j},\ c_{wj}^2 = \frac{\partial P_{w0,j}}{\partial v_{wI,j}},\ c_{wj}^3 = \frac{\partial P_{w0,j}}{\partial h_{c0,j}},\ c_{wj}^4 = \frac{\partial P_{w0,j}}{\partial P_{c0,j}},$$
$$c_{wj}^5 = \frac{\partial P_{w0,j}}{\partial P_{wI,j}},\ c_{wj}^6 = \frac{\partial P_{w0,j}}{\partial h_{wI,j}},\ c_{wj}^7 = \frac{\partial P_{w0,j}}{\partial q_j}\frac{dq_j}{dp}$$

Note that Eq. (3.80) implies Eq. (3.76) since $\delta\Delta P_{cj} = \delta P_{LP,j} - \delta P_{cI,j} = \delta P_{LP}$, and Eq. (3.81) implies Eq. (F.77) since $\delta\Delta P_{wj} = \delta P_{w0,j} - \delta P_{wI,j} = \delta P_{LP} - \delta P_{wI}$. As a result, the flow perturbations satisfying the equal pressure drop boundary conditions can be determined by solving Eqs. (3.80) and (3.81). Equations (3.80) and (3.81) can be solved for $\delta v_{c0,j}$ and $\delta v_{wI,j}$ as

$$\begin{aligned}\delta v_{c0,j} &= \frac{1}{D_j}[(c_{cj}^2 c_{wj}^3 - c_{wj}^2 c_{cj}^3)\delta h_{c0} + (c_{cj}^2 c_{wj}^4 - c_{wj}^2 c_{cj}^4 - c_{cj}^2)\delta P_{LP} \\ &\quad + (c_{cj}^2 c_{wj}^5 - c_{wj}^2 c_{cj}^5)\delta P_{wI} + (c_{cj}^2 c_{wj}^6 - c_{wj}^2 c_{cj}^6)\delta h_{wI} + (c_{cj}^2 c_{wj}^7 - c_{wj}^2 c_{cj}^7)\delta p] \\ &= b_{cj}^1 \delta h_{c0} + b_{cj}^2 \delta P_{LP} + b_{cj}^3 \delta P_{wI} + b_{cj}^4 \delta h_{wI} + b_{cj}^5 \delta p\end{aligned} \tag{3.82}$$

$$\begin{aligned}\delta v_{wI,j} &= -\frac{1}{D_j}[(c_{cj}^1 c_{wj}^3 - c_{wj}^1 c_{cj}^3)\delta h_{c0} + (c_{cj}^1 c_{wj}^4 - c_{wj}^1 c_{cj}^4 - c_{cj}^1)\delta P_{LP} \\ &\quad + (c_{cj}^1 c_{wj}^5 - c_{wj}^1 c_{cj}^5)\delta P_{wI} + (c_{cj}^1 c_{wj}^6 - c_{wj}^1 c_{cj}^6)\delta h_{wI} + (c_{cj}^1 c_{wj}^7 - c_{wj}^1 c_{cj}^7)\delta p] \\ &= b_{wj}^1 \delta h_{c0} + b_{wj}^2 \delta P_{LP} + b_{wj}^3 \delta P_{wI} + b_{wj}^4 \delta h_{wI} + b_{wj}^5 \delta p\end{aligned} \tag{3.83}$$

where $D_j = c_{cj}^1 c_{wj}^2 - c_{cj}^2 c_{wj}^1$ and

$$b_{cj}^1 = (c_{cj}^2 c_{wj}^3 - c_{wj}^2 c_{cj}^3)/D_j,\ b_{cj}^2 = (c_{cj}^2 c_{wj}^4 - c_{wj}^2 c_{cj}^4 - c_{cj}^2)/D_j,$$
$$b_{cj}^3 = (c_{cj}^2 c_{wj}^5 - c_{wj}^2 c_{cj}^5)/D_j,\ b_{cj}^4 = (c_{cj}^2 c_{wj}^6 - c_{wj}^2 c_{cj}^6)/D_j,\ b_{cj}^5 = (c_{cj}^2 c_{wj}^7 - c_{wj}^2 c_{cj}^7)/D_j,$$

$$b_{wj}^1 = -(c_{cj}^1 c_{wj}^3 - c_{wj}^1 c_{cj}^3)/D_j,\ b_{wj}^2 = -(c_{cj}^1 c_{wj}^4 - c_{wj}^1 c_{cj}^4 - c_{cj}^1)/D_j,$$
$$b_{wj}^3 = -(c_{cj}^1 c_{wj}^5 - c_{wj}^1 c_{cj}^5)/D_j,\ b_{wj}^4 = -(c_{cj}^1 c_{wj}^6 - c_{wj}^1 c_{cj}^6)/D_j,\ b_{wj}^5 = -(c_{cj}^1 c_{wj}^7 - c_{wj}^1 c_{cj}^7)/D_j,$$

In the instantaneous mixing approximation, the mass conservation equations in Eqs. (3.73) can be written in terms of input parameter variations as

$$\begin{aligned}\sum_{j=1}^{J}\delta w_{cj} &= \sum_{j=1}^{J} w_{cj}\left[\frac{\delta v_{c0j}}{v_{c0,j}} + \frac{\delta\rho_{c0,j}}{\rho_{c0,j}}\right] = \sum_{j=1}^{J} w_{cj}\left[\frac{\delta v_{c0,j}}{v_{c0,j}} + \frac{\xi_{c0}}{\rho_{c0}}\delta h_{c0} + \frac{\eta_{c0}}{\rho_{c0}}\delta P_{c0}\right] \\ &= \sum_{j=1}^{J} w_{cj}(b_{fj}^1 \delta v_{c0,j} + b_{fj}^3 \delta h_{c0} + b_{fj}^4 \delta P_{LP}) = \delta w_T\end{aligned} \tag{3.84}$$

$$\sum_{j=1}^{J}\delta w_{wj}=\sum_{j=1}^{J}w_{wj}\left[\frac{\delta v_{w0\,j}}{v_{w0,j}}+\frac{\delta\rho_{w0,j}}{\rho_{w0,j}}\right]=\sum_{j=1}^{J}w_{wj}\left[\frac{\delta v_{w0,j}}{v_{w0,j}}+\frac{\xi_{w0,j}}{\rho_{w0,j}}\delta h_{w0,j}+\frac{\eta_{w0,j}}{\rho_{w0,j}}\delta P_{w0,j}\right]$$

$$=\sum_{j=1}^{J}w_{wj}\left[\frac{1}{v_{w0,j}}(c_{vj}^{1}\delta v_{c0,j}+c_{vj}^{2}\delta v_{wI,j}+c_{vj}^{3}\delta h_{c0}+c_{vj}^{4}\delta P_{LP}+c_{vj}^{5}\delta P_{wI}+c_{vj}^{6}\delta h_{wI}+c_{vj}^{7}\delta p)\right.$$

$$\left.+\frac{\xi_{w0,j}}{\rho_{w0,j}}(c_{hj}^{1}\delta v_{c0,j}+c_{hj}^{2}\delta v_{wI,j}+c_{hj}^{3}\delta h_{c0}+c_{hj}^{4}\delta P_{LP}+c_{hj}^{5}\delta P_{wI}+c_{hj}^{6}\delta h_{wI}+c_{hj}^{7}\delta p)+\frac{\eta_{w0,j}}{\rho_{w0,j}}\delta P_{LP}\right] \quad (3.85)$$

$$=\sum_{j=1}^{J}w_{wj}(b_{mj}^{1}\delta v_{c0,j}+b_{mj}^{2}\delta v_{wI,j}+b_{mj}^{3}\delta h_{c0}+b_{mj}^{4}\delta P_{LP}+b_{mj}^{5}\delta P_{wI}+b_{mj}^{6}\delta h_{wI}+b_{mj}^{7}\delta p)$$

$$=\delta w_{T}-\delta w_{dc}$$

where $\xi=\left.\frac{\partial\rho}{\partial h}\right|_{P}$, $\eta=\left.\frac{\partial\rho}{\partial P}\right|_{h}$ and

$$c_{vj}^{1}=\frac{\partial v_{w0,j}}{\partial v_{c0,j}}+c_{vj}^{4}H_{pv,j},\ c_{vj}^{2}=\frac{\partial v_{w0,j}}{\partial v_{wI,j}},\ c_{vj}^{3}=\frac{\partial v_{w0,j}}{\partial h_{c0,j}},\ c_{vj}^{4}=\frac{\partial v_{w0,j}}{\partial P_{c0,j}},$$

$$c_{vj}^{5}=\frac{\partial v_{w0,j}}{\partial P_{wI,j}},\ c_{vj}^{6}=\frac{\partial v_{w0,j}}{\partial h_{wI,j}},\ c_{vj}^{7}=\frac{\partial v_{w0,j}}{\partial q_{j}}\frac{dq_{j}}{dp}$$

$$c_{hj}^{1}=\frac{\partial h_{w0,j}}{\partial v_{c0,j}}+c_{hj}^{4}H_{pv,j},\ c_{hj}^{2}=\frac{\partial h_{w0,j}}{\partial v_{wI,j}},\ c_{hj}^{3}=\frac{\partial h_{w0,j}}{\partial h_{c0,j}},\ c_{hj}^{4}=\frac{\partial h_{w0,j}}{\partial P_{c0,j}},$$

$$c_{hj}^{5}=\frac{\partial h_{w0,j}}{\partial P_{wI,j}},\ c_{hj}^{6}=\frac{\partial h_{w0,j}}{\partial h_{wI,j}},\ c_{hj}^{7}=\frac{\partial h_{w0,j}}{\partial q_{j}}\frac{dq_{j}}{dp}$$

$$b_{fj}^{1}=\frac{1}{v_{c0,j}}+b_{fj}^{4}H_{pv,j},\ b_{fj}^{3}=\frac{\xi_{c0}}{\rho_{c0}},\ b_{fj}^{4}=\frac{\eta_{c0}}{\rho_{c0}}$$

$$b_{mj}^{1}=\frac{c_{vj}^{1}}{v_{w0,j}}+\frac{\xi_{w0,j}}{\rho_{w0,j}}c_{hj}^{1},\ b_{mj}^{2}=\frac{c_{vj}^{2}}{v_{w0,j}}+\frac{\xi_{w0,j}}{\rho_{w0,j}}c_{hj}^{2},\ b_{mj}^{3}=\frac{c_{vj}^{3}}{v_{w0,j}}+\frac{\xi_{w0,j}}{\rho_{w0,j}}c_{hj}^{3},$$

$$b_{mj}^{4}=\frac{c_{vj}^{4}}{v_{w0,j}}+\frac{\xi_{w0,j}}{\rho_{w0,j}}c_{hj}^{4}+\frac{\eta_{w0,j}}{\rho_{w0,j}},\ b_{mj}^{5}=\frac{c_{vj}^{5}}{v_{w0,j}}+\frac{\xi_{w0,j}}{\rho_{w0,j}}c_{hj}^{5},\ b_{mj}^{6}=\frac{c_{vj}^{5}}{v_{w0,j}}+\frac{\xi_{w0,j}}{\rho_{w0,j}}c_{hj}^{6},$$

$$b_{mj}^{7}=\frac{c_{vj}^{7}}{v_{w0,j}}+\frac{\xi_{w0,j}}{\rho_{w0,j}}c_{hj}^{7}$$

Similarly, the energy conservation equation in Eq. (3.74) can be written in terms of input parameter variations as

$$\delta h_{c0} w_T = \sum_{j=1}^{J} w_{wj} \delta h_{w0,j} + \sum_{j=1}^{J} (h_{w0,j} - h_{c0}) \delta w_{wj} + \delta h_{dc} w_{dc} + (h_{dc} - h_{c0}) \delta w_{dc}$$

$$= \sum_{j=1}^{J} w_{wj} (c_{hj}^1 \delta v_{c0,j} + c_{hj}^2 \delta v_{wI,j} + c_{hj}^3 \delta h_{c0} + c_{hj}^4 \delta P_{LP} + c_{hj}^5 \delta P_{wI} + c_{hj}^6 \delta h_{wI} + c_{hj}^7 \delta p)$$

$$+ \sum_{j=1}^{J} w_{wj} (h_{w0,j} - h_{c0})(b_{mj}^1 \delta v_{c0,j} + b_{mj}^2 \delta v_{wI,j} + b_{mj}^3 \delta h_{c0} + b_{mj}^4 \delta P_{LP} + b_{mj}^5 \delta P_{wI} + b_{mj}^6 \delta h_{wI} + b_{mj}^7 \delta p)$$

$$+ \delta h_{dc} w_{dc} + (h_{dc} - h_{c0}) \delta w_{dc}$$

This can be further simplified as

$$\sum_{j=1}^{J} (b_{hj}^1 \delta v_{c0,j} + b_{hj}^2 \delta v_{wI,j} + b_{hj}^3 \delta h_{c0} + b_{hj}^4 \delta P_{LP} + b_{hj}^5 \delta P_{wI} + b_{hj}^6 \delta h_{wI} + b_{hj}^7 \delta p) = \delta h_{dc} w_{dc} + (h_{dc} - h_{c0}) \delta w_{dc} \tag{3.86}$$

where

$$b_{hj}^1 = -w_{wj}[c_{hj}^1 - (h_{w0,j} - h_{c0}) b_{mj}^1],\ b_{hj}^2 = -w_{wj}[c_{hj}^2 - (h_{w0,j} - h_{c0}) b_{mj}^2],$$
$$b_{hj}^3 = w_{cj} - w_{wj}[c_{hj}^3 - (h_{w0,j} - h_{c0}) b_{mj}^3],\ b_{hj}^4 = -w_{wj}[c_{hj}^4 - (h_{w0,j} - h_{c0}) b_{mj}^4],$$
$$b_{hj}^5 = -w_{wj}[c_{hj}^5 - (h_{w0,j} - h_{c0}) b_{mj}^5],\ b_{hj}^6 = -w_{wj}[c_{hj}^6 - (h_{w0,j} - h_{c0}) b_{mj}^6],$$
$$b_{hj}^7 = -w_{wj}[c_{hj}^7 - (h_{w0,j} - h_{c0}) b_{mj}^7]$$

Substituting Eqs. (3.82) and (3.83) into Eqs. (3.84), (3.85), and (3.86) yields the system of equations for three unknowns δh_{c0}, δP_{LP}, and δP_{wI}, as

$$\begin{bmatrix} a_c^1 & a_c^2 & a_c^3 \\ a_w^1 & a_w^2 & a_w^3 \\ a_h^1 & a_h^2 & a_h^3 \end{bmatrix} \begin{bmatrix} \delta h_{c0} \\ \delta P_{LP} \\ \delta P_{wI} \end{bmatrix} = -\begin{bmatrix} a_c^5 \\ a_w^5 \\ a_h^5 \end{bmatrix} \delta p - \begin{bmatrix} a_c^4 \\ a_w^4 \\ a_h^4 \end{bmatrix} \delta h_{wI} + \begin{bmatrix} 1 \\ 1 \\ 0 \end{bmatrix} \delta w_T + \begin{bmatrix} 0 \\ -1 \\ h_{dc} - h_{c0} \end{bmatrix} \delta w_{dc} + \begin{bmatrix} 0 \\ 0 \\ w_{dc} \end{bmatrix} \delta h_{dc} \tag{3.87}$$

where

$$a_c^1 = \sum_{j=1}^{J} w_{cj} (b_{fj}^1 b_{cj}^1 + b_{fj}^3),\ a_c^2 = \sum_{j=1}^{J} w_{cj} (b_{fj}^1 b_{cj}^2 + b_{fj}^4),$$
$$a_c^3 = \sum_{j=1}^{J} w_{cj} b_{fj}^1 b_{cj}^3,\ a_c^4 = \sum_{j=1}^{J} w_{cj} b_{fj}^1 b_{cj}^4,\ a_c^5 = \sum_{j=1}^{J} w_{cj} b_{fj}^1 b_{cj}^5$$

$$a_w^1 = \sum_{j=1}^{J} w_{wj} (b_{mj}^1 b_{cj}^1 + b_{mj}^2 b_{wj}^1 + b_{mj}^3),\ a_w^2 = \sum_{j=1}^{J} w_{wj} (b_{mj}^1 b_{cj}^2 + b_{mj}^2 b_{wj}^2 + b_{mj}^4),$$
$$a_w^3 = \sum_{j=1}^{J} w_{wj} (b_{mj}^1 b_{cj}^3 + b_{mj}^2 b_{wj}^3 + b_{mj}^5),\ a_w^4 = \sum_{j=1}^{J} w_{wj} (b_{mj}^1 b_{cj}^4 + b_{mj}^2 b_{wj}^4 + b_{mj}^6),$$

$$a_w^5 = \sum_{j=1}^{J} w_{wj}(b_{mj}^1 b_{cj}^5 + b_{mj}^2 b_{wj}^5 + b_{mj}^7)$$

$$a_h^1 = \sum_{j=1}^{J}(b_{hj}^1 b_{cj}^1 + b_{hj}^2 b_{wj}^1 + b_{hj}^3),\ \ a_h^2 = \sum_{j=1}^{J}(b_{hj}^1 b_{cj}^2 + b_{hj}^2 b_{wj}^2 + b_{hj}^4),$$

$$a_h^3 = \sum_{j=1}^{J}(b_{hj}^1 b_{cj}^3 + b_{hj}^2 b_{wj}^3 + b_{hj}^5),\ \ a_h^4 = \sum_{j=1}^{J}(b_{hj}^1 b_{cj}^4 + b_{hj}^2 b_{wj}^4 + b_{hj}^6),$$

$$a_h^5 = \sum_{j=1}^{J}(b_{hj}^1 b_{cj}^5 + b_{hj}^2 b_{wj}^5 + b_{hj}^7)$$

By solving Eq. (3.87) for the unit perturbation of each external parameter, the partial derivatives of δP_{wI}, δh_{c0}, and δP_{LP} with respect to external parameters can be determined. For example, the partial derivatives $\partial P_{wI}/\partial p$, $\partial h_{c0}/\partial p$, and $\partial P_{LP}/\partial p$ can be obtained by solving Eq. (3.87) with $\delta w_T = \delta w_{dc} = \delta h_{dc} = \delta h_{wI} = \delta P_{wI} = 0$ and $\delta p = 1$. Substituting these partial derivatives into Eqs. (3.82) and (3.83), $\partial v_{c0,j}/\partial p$ and $\partial v_{wI,j}/\partial p$ are obtained. By combining these responses with the responses of state variables to the channel input parameters, the responses of state variables to the external input parameters are determined. For example, the state variable changes due to unit power change can be obtained as

$$\begin{aligned}\frac{\delta \mathbf{x}_{i,j}}{\delta p} &= \frac{\partial \mathbf{x}_{i,j}}{\partial h_{c0,j}}\frac{\partial h_{c0}}{\partial p} + \frac{\partial \mathbf{x}_{i,j}}{\partial P_{c0,j}}\frac{\partial P_{c0}}{\partial p} + \frac{\partial \mathbf{x}_{i,j}}{\partial v_{c0,j}}\frac{\partial v_{c0,j}}{\partial p} + \frac{\partial \mathbf{x}_{i,j}}{\partial h_{wI,j}}\frac{\partial h_{wI}}{\partial p} + \frac{\partial \mathbf{x}_{i,j}}{\partial P_{wI,j}}\frac{\partial P_{wI}}{\partial p} \\ &\quad + \frac{\partial \mathbf{x}_{i,j}}{\partial v_{wI,j}}\frac{\partial v_{wI,j}}{\partial p} + \frac{\partial \mathbf{x}_{i,j}}{\partial p} \\ &= \frac{\partial \mathbf{x}_{i,j}}{\partial h_{c0,j}}\frac{\partial h_{c0}}{\partial p} + \frac{\partial \mathbf{x}_{i,j}}{\partial P_{c0,j}}\frac{\partial P_{PL}}{\partial p} + \left[\frac{\partial \mathbf{x}_{i,j}}{\partial v_{c0,j}} + \frac{\partial \mathbf{x}_{i,j}}{\partial P_{c0,j}} H_{pv,j}\right]\frac{\partial v_{c0,j}}{\partial p} + \frac{\partial \mathbf{x}_{i,j}}{\partial P_{wI,j}}\frac{\partial P_{wI,j}}{\partial p} \\ &\quad + \frac{\partial \mathbf{x}_{i,j}}{\partial v_{wI,j}}\frac{\partial v_{wI,j}}{\partial p} + \frac{\partial \mathbf{x}_{i,j}}{\partial q_j}\frac{dq_j}{dp}\end{aligned} \tag{3.88}$$

In the constant mixed-mean enthalpy approximation, Eq. (3.79) needs to be satisfied instead of Eq. (3.74). As a result, Eqs. (3.82), (3.83), (3.84), and (3.85) are reduced to

$$\delta v_{c0,j} = b_{cj}^2 \delta P_{LP} + b_{cj}^3 \delta P_{wI} + b_{cj}^4 \delta h_{wI} + b_{cj}^5 \delta p \tag{3.89}$$

$$\delta v_{wI,j} = b_{wj}^2 \delta P_{LP} + b_{wj}^3 \delta P_{wI} + b_{wj}^4 \delta h_{wI} + b_{wj}^5 \delta p \tag{3.90}$$

$$\sum_{j=1}^{J} \delta w_{cj} = \sum_{j=1}^{J} w_{cj} (b_{jj}^{1} \delta v_{c0,j} + b_{jj}^{4} \delta P_{LP}) = \delta w_T \tag{3.91}$$

$$\begin{aligned} \sum_{j=1}^{J} \delta w_{wj} &= \sum_{j=1}^{J} w_{wj} (b_{mj}^{1} \delta v_{c0,j} + b_{mj}^{2} \delta v_{wI,j} + b_{mj}^{4} \delta P_{LP} + b_{mj}^{5} \delta P_{wI} + b_{mj}^{6} \delta h_{wI} + b_{mj}^{7} \delta p) \\ &= \delta w_T - \delta w_{dc} \end{aligned} \tag{3.92}$$

Substituting Eqs. (3.89) and (3.90) into Eqs. (3.91) and (3.92) yields the system of equations for two unknowns δP_{LP} and δP_{wI} as

$$\begin{bmatrix} a_c^2 & a_c^3 \\ a_w^2 & a_w^3 \end{bmatrix} \begin{bmatrix} \delta P_{LP} \\ \delta P_{wI} \end{bmatrix} = -\begin{bmatrix} a_c^5 \\ a_w^5 \end{bmatrix} \delta p - \begin{bmatrix} a_c^4 \\ a_w^4 \end{bmatrix} \delta h_{wI} + \begin{bmatrix} 1 \\ 1 \end{bmatrix} \delta w_T + \begin{bmatrix} 0 \\ -1 \end{bmatrix} \delta w_{dc} \tag{3.93}$$

By solving Eq. (3.93) for the unit perturbation of each external parameter, the partial derivatives of δP_{wI} and δP_{LP} with respect to external parameters can be determined. For example, the partial derivatives $\partial P_{wI} / \partial p$ and $\partial P_{LP} / \partial p$ can be obtained by solving Eq. (3.93) with $\delta w_T = \delta w_{dc} = \delta h_{wI} = \delta P_{wI} = 0$ and $\delta p = 1$. Substituting these partial derivatives into Eqs. (3.89) and (3.90), $\partial v_{c0,j} / \partial p$ and $\partial v_{wI,j} / \partial p$ are obtained. By combining these responses with the responses of state variables to the channel input parameters, the responses of state variables to the external input parameters are determined. For example, the state variable changes due to unit power change can be obtained as

$$\begin{aligned} \frac{\delta \mathbf{x}_{i,j}}{\delta p} = {} & \frac{\partial \mathbf{x}_{i,j}}{\partial P_{c0,j}} \frac{\partial P_{PL}}{\partial p} + \left[\frac{\partial \mathbf{x}_{i,j}}{\partial v_{c0,j}} + \frac{\partial \mathbf{x}_{i,j}}{\partial P_{c0,j}} H_{pv,j} \right] \frac{\partial v_{c0,j}}{\partial p} + \frac{\partial \mathbf{x}_{i,j}}{\partial P_{wI,j}} \frac{\partial P_{wI,j}}{\partial p} \\ & + \frac{\partial \mathbf{x}_{i,j}}{\partial v_{wI,j}} \frac{\partial v_{wI,j}}{\partial p} + \frac{\partial \mathbf{x}_{i,j}}{\partial q_j} \frac{dq_j}{dp} \end{aligned} \tag{3.94}$$

3.4. Feedbacks and System Characteristic Equation

The closed loop transfer functions and the system characteristic equations are derived by taking into account the hydraulic and reactivity feedbacks. The hydraulic feedback is determined by the boundary conditions imposed on the thermal-hydraulics equations. The reactivity feedback of a SCWR is mainly through the core-average fuel temperature, and coolant and moderator density perturbations. As discussed in Section 3.3, the inlet boundary condition perturbations are already included in determining the transfer functions in Eqs. (3.88) or (3.94). Thus, this section describes the reactivity feedback and the system characteristic equation.

3.4.1. Reactivity Feedbacks

The perturbations of coolant and water-rod state variables and fuel temperature change the core reactivity through the coolant and moderator density and Doppler reactivity feedbacks. The core reactivity perturbation in turn results in the neutron flux variation. In the point kinetics approximation employed in this study, the relation between the power (i.e. neutron flux) and reactivity perturbations is given by the so-called zero-power transfer function [18] as

$$\delta\tilde{p}(s) = \Phi(s)\delta\tilde{\rho}(s) \tag{3.95}$$

$$\Phi(s) = p_0\left[\Lambda s + \sum_{i=1}^{6}\frac{s\beta_i}{s+\lambda_i}\right]^{-1} \tag{3.96}$$

which are obtained by linearizing Eqs. (2.21) and (2.22) and subsequently applying the Laplace transformation to the resulting linearized equations. In the point kinetics approximation, the time dependence of the flux shape is neglected, and the initial flux shape is used in forming the kinetics parameters.

Substituting the state variable changes due to unit power perturbation in Eq. (3.88) or (3.94) into Eq. (3.52), the perturbation of average fuel temperature of the axial node i in channel j due to unit power perturbation is determined as

$$\frac{\delta\tilde{T}_{f,ij}^{avg}}{\delta p} = \tilde{a}_{Tf,j}^{i}\frac{\delta\tilde{h}_{ci,j}}{\delta p} + \tilde{b}_{Tf,j}^{i}\frac{\delta\tilde{P}_{ci,j}}{\delta p} + \tilde{c}_{Tf,j}^{i}\frac{\delta\tilde{v}_{ci,j}}{\delta p} + \tilde{d}_{Tf,j}^{i}f_{ij} \tag{3.97}$$

The coolant and water rod density perturbations are obtained in a similar way by substituting Eq. (3.88) or (3.94) into Eq. (3.7) as

$$\frac{\delta\tilde{\rho}_{ci,j}}{\delta p} = \xi_{ci,j}\frac{\delta\tilde{h}_{ci,j}}{\delta p} + \eta_{ci,j}\frac{\delta\tilde{P}_{ci,j}}{\delta p} \tag{3.98}$$

$$\frac{\delta\tilde{\rho}_{wi,j}}{\delta p} = \xi_{wi,j}\frac{\delta\tilde{h}_{wi,j}}{\delta p} + \eta_{wi,j}\frac{\delta\tilde{P}_{wi,j}}{\delta p} \tag{3.99}$$

The reactivity feedback is calculated with the weighted average values of these fuel temperature, and coolant and moderator density perturbations. The square of power distribution is used as the weighting function. That is, the average of a perturbation δx is computed as

$$\delta\bar{x} = \frac{\int \delta x(\mathbf{r})[p(\mathbf{r})]^2 dV}{\int [p(\mathbf{r})]^2 dV} = \frac{\sum_{j=1}^{J}\sum_{i=1}^{I} \delta x_{ij} p_{ij}^2 V_{ij}}{\sum_{j=1}^{J}\sum_{i=1}^{I} p_{ij}^2 V_{ij}} \tag{3.100}$$

where j is the index for thermal-hydraulic channels and i is the axial node index. The pin power q_j of channel j and the power density p_{ij} of the axial node i of channel j are computed as

$$q_j = \frac{f_j p}{n_j} \tag{3.101}$$

$$p_{ij} = \frac{f_{ij} q_j}{a_j \Delta z_i} = \frac{f_{ij} f_j p}{n_j a_j \Delta z_i} \tag{3.102}$$

where

p = reactor power

f_j = power fraction of channel j

f_{ij} = power fraction of axial node i in the channel j

n_j = number of fuel pins in channel j

a_j = area of fuel pellet in channel j

Δz_i = mesh interval of axial node i

Equations (3.101) and (3.102) imply the following relations:

$$\sum_{j=1}^{J} f_j = 1 \tag{3.103}$$

$$\sum_{i=1}^{I} f_{ij} = 1 \tag{3.104}$$

$$V_{ij} = n_j a_j \Delta z_i \tag{3.105}$$

Denoting the total derivatives in Eqs. (3.97) to (3.99) by G_{ij}^1, the core-average $\delta\bar{x}$ due to power perturbation δp is computed as

$$\delta\overline{x} = \frac{\sum_{j=1}^{J}\sum_{i=1}^{I} G_{ij}^{1}(f_{ij}^{2} f_{j}^{2} / n_j a_j \Delta z_i)}{\sum_{j=1}^{J}\sum_{i=1}^{I}(f_{ij}^{2} f_{j}^{2} / n_j a_j \Delta z_i)} \delta p \tag{3.106}$$

Denoting the core-average perturbations of fuel temperature, coolant density, and water rod density as

$$\delta\tilde{T}_f^{ave} = \Gamma_1^f \delta\tilde{p} \tag{3.107}$$

$$\delta\tilde{\rho}_c^{ave} = \Gamma_1^d \delta\tilde{p} \tag{3.108}$$

$$\delta\tilde{\rho}_w^{ave} = \Gamma_1^w \delta\tilde{p} \tag{3.109}$$

the total reactivity feedback can be represented as

$$\delta\tilde{\rho}_{fb} = \Gamma_1 \delta\tilde{p} = (\alpha_D \Gamma_1^f + \alpha_{Dc}\Gamma_1^d + \alpha_{Dw}\Gamma_1^w)\delta\tilde{p} \tag{3.110}$$

where α_D, α_{Dc}, and α_{Dw} are the Doppler, coolant density, and water rod density reactivity coefficients, respectively.

3.4.2. System Characteristic Equation

The net total perturbation of reactivity and power is given by the sum of the external perturbation and feedback [19]. Therefore, Eqs. (3.95) and (3.110) can be written in a matrix form as

$$\begin{bmatrix} -\Phi & 1 \\ 1 & -\Gamma_1 \end{bmatrix} \begin{bmatrix} \delta\tilde{\rho}_t \\ \delta\tilde{p}_t \end{bmatrix} = \begin{bmatrix} 0 \\ \delta\tilde{\rho}_{ext} \end{bmatrix} \tag{3.111}$$

where the subscripts t and ext denote the total and external perturbations, respectively.

Linear system instability occurs when the system becomes self-excited, which means that the system continues to oscillate in an un-damped fashion even when the external forcing function is removed. This occurs when the determinant of the matrix is zero. Therefore, the unique characteristic equation of Eq. (3.111) is given by

$$\Phi\Gamma_1 - 1 = 0 \tag{3.112}$$

This is the characteristic equation for the thermal-nuclear coupled instability. By solving Eq. (3.111), the reactivity-to-reactivity closed loop transfer function can be determined as

$$G_{\rho\rho}(s) = \frac{1}{1 - \Gamma_1(s)\Phi(s)} \tag{3.113}$$

The transient response is determined by the roots of the characteristic equation. After a sufficient time, it is dominated by the root that has the largest real part. If the real part of this dominant root is positive, the response to a perturbation would grow indefinitely and the linear system is unstable. If it is negative, the system is asymptotically stable. Oscillations introduced in the system are damped to the extent determined by the decay ratio, which is defined as the ratio between first and second peaks in the impulse response. Denoting the dominant root by λ, the decay ratio of the system can be determined as

$$R = e^{-2\pi|\mathrm{Re}(\lambda)/\mathrm{Im}(\lambda)|} \tag{3.114}$$

In this study, following the standard approach for BWR stability analysis, this decay ratio is used as the criterion for stability. The dominant root is directly searched in the complex plane using the Newton-Raphson method combined with the line search and back-track algorithm [20], as described in Appendix B.

4. Preliminary Tests

The computational models discussed above have been implemented into the frequency domain linear stability analysis code SCWRSA. The functionality of the modified program was confirmed by reproducing the previous single-channel analysis results. Preliminary tests of the new multi-channel analysis capability have been performed using two-channel models derived from the U.S. Generation IV SCWR reference design [11].

The reference SCWR design is a thermal-spectrum reactor with a rated core thermal power of 3575 MW and a rated core flow of 1843 kg/s. The planar view of SCWR is shown in Figure 4-1, and the main design parameters are summarized in Table 4-1. It is noted that no detailed core design analysis has been performed and the core performance parameters represent the design goals. For example, the total peaking factor and outlet temperature are targeted design values, and the related design parameters are derived from these target values. As mentioned in Section 2, the core includes 145 fuel assemblies, each of which has 300 fuel rods arranged in the square lattice and 36 square water rods. About 90% of feedwater flows downward through the water rods into the lower plenum, and then it is mixed with the rest of the feedwater from the downcomer in the lower plenum. The mixed coolant flows upward through the fuel channels.

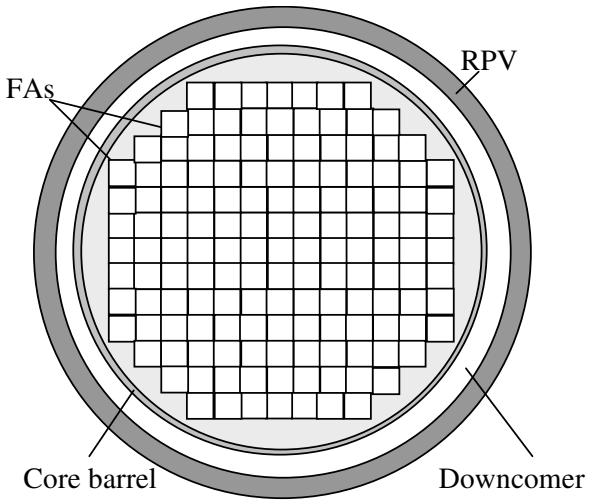

Figure 4-1 Planar View of SCWR Core

Table 4-1 Design Parameters of SCWR Reference Design

Parameter	Value
Thermal power	3575 MW
Electric power	1600 MW
Thermal efficiency	44.8%
Operating pressure	25 MPa
Reactor inlet/outlet temperature	280/500°C
Reactor flow rate	1843 kg/s
FUEL PIN	
Fuel pin OD	10.2 mm
Fuel pin pitch	11.2 mm
Cladding thickness	0.63 mm
Cladding materials	ODS steel
Fuel pellet OD	8.94 mm
Fuel composition	UO_2, 95% TD
Fuel enrichment	5% wt. average
Heated length	4.27 m
Fission gas plenum length	0.6 m
Total fuel pin height	4.87 m
Fill gas pressure at room temperature	6.0 MPa
FUEL ASSEMBLY	
Number of fuel pins per assembly	300
Number of water rods per assembly	36
Water rod side	33.6 mm
Water rod wall thickness	0.4 mm
Number of instrumentation rods per assembly	1
Number of CR fingers per assembly	16
Number of spacer grids	14
CORE	
Number of fuel assemblies	145
Equivalent diameter	3.91 m
Core barrel ID/OD	4.3/4.4 m
Average power density	69.6 kW/L
Average linear power	19.2 kW/m
Peak linear power	39 kW/m
Axial/Radial/Local/Total Peaking Factor	1.4/1.3/1.1/2.0
Core pressure drop	0.15 MPa
Water rod flow	1659 kg/s (90% of nominal flow)

Two-channel test problems composed of average and hot channel assemblies of the U.S. SCWR reference design were derived. The radial power peaking factor was assumed 1.3, and the axial power distribution was assumed a cosine shape. The active core height was assumed 4.27 m, and non-heated nodes of 0.3 m height were introduced below and above the active core, to model the lower and upper gas plenums. The inlet orifice coefficients for average and hot channels were determined such that the coolant outlet temperatures of the both channels are the same. Considering the pressure losses due to fuel pin, spacer grids, and abrupt contraction and expansion at core inlet and exit, the pressure loss coefficients of inlet orifices were estimated to maintain the targeted core pressure drop (0.15 MPa).

4.1. Iteration Scheme for Flow Splits

Several iteration schemes to determine the flow rates of individual thermal-hydraulic channels were examined prior to devising the iteration scheme described in Section 2.3.1. Since the detailed information of the US reference SCWR design is not available at this point, various two-channel models consisting of average and hot channels were tested. The iteration scheme adopted from the BWR stability analysis code LAPUR5 [21] was found unstable when applied to SCWR flow split calculations. It was also observed that separate iterations for coolant and water-rod flow rates without considering the heat transfer between coolant and water rod converge slowly and often shows small oscillatory behaviors. Therefore, a new iteration scheme was developed such that the coolant and water-rod flow rates are determined simultaneously by taking into account the heat transfer between coolant and water rod as described in Section 2.3.1.

Preliminary test results showed that the new iteration scheme converged flow rates with only five to six iterations for both the Dittus-Boelter and Jackson heat transfer correlations. As an example, the steady-state pressure and temperature solutions of a two-channel test problem are presented in Table 4-2. It was assumed that among 145 assemblies of the SCWR core, 8 assemblies average belong to the hot channel. The iteration histories of pressure drops and flow rates are also shown in Figures 4-2 and 4-3. The pressure loss coefficient of inlet orifice was 105 for the average channel and 31 for the hot channel. Initial flow rates of each channel were determined to be proportional to the channel power. A convergence criterion of 0.001 was used for the relative difference in pressure drop between two channels.

The average and hot channel pressure drops converge to each other for both the coolant channel and water rod. The boundary condition imposed on the coolant outlet pressure (25 MPa) is also satisfied. These results show that the equal pressure boundary conditions are satisfied as required. The converged pressure drop across the water rod is about five smaller than that across the coolant channel, because of much larger flow area (see Figure 2-4). As shown in Figure 4-2, to satisfy the aforementioned convergence criterion of 0.001, five and six iterations were taken for the Jackson and Dittus-Boelter correlations, respectively. However, it is noted that the Jackson and Dittus-Boelter correlations showed no difference in the number of iterations; for some other test problems, the Jackson correlation took an additional iteration than the Dittus-Boelter correlation. The Dittus-Boelter and Jackson correlations give slightly different converged pressure drops across the coolant channel and water rod. This is due to the difference in heat transfer between coolant channel and water rod. Figure 4-3 shows that the Dittus-Boelter and Jackson correlations resulted in the same coolant flow rates, but slightly different water-rod flow rates. As shown in Figure 4-4, the coolant and water-rod temperature distributions of hot channel are very similar to those of the average channel, since the orifice coefficients were determined such that the coolant outlet temperatures of the average and hot channels are the same. However, because of a higher pin power, the average fuel temperature of hot channel is significantly higher than that of average channel.

Table 4-2 Pressures and Temperatures of Two-Channel Test Problem

Heat transfer coefficient	Dittus-Boelter		Jackson	
Thermal-hydraulic channel	Average	Hot	Average	Hot
Inlet orifice coefficient	105	31	105	31
Pin power (kW)	80.89	104.27	80.89	104.27
Coolant channel flow rate (kg/s)	0.0414	0.0556	0.0414	0.0556
Pin power to flow ratio	1.9518	1.8755	1.9517	1.8758
Water rod flow rate (kg/s)	0.3157	0.3525	0.3159	0.3495
Water rod inlet pressure (MPa)	25.1110	25.1110	25.1078	25.1077
Lower plenum pressure (MPa)	25.1417	25.1417	25.1393	25.1393
Coolant outlet pressure (MPa)	25.0000	25.0000	25.0000	25.0000
Coolant pressure drop (MPa)	0.1417	0.1417	0.1393	0.1393
Water rod pressure drop (MPa)	-0.0307	-0.0307	-0.0315	-0.0316
Water rod inlet temperature (K)	553.15	553.15	553.15	553.15
Water rod outlet temperature (K)	631.29	630.84	626.50	625.97
Lower plenum temperature (K)	625.19	625.19	620.89	620.89
Coolant outlet temperature (K)	773.98	773.72	774.16	772.89

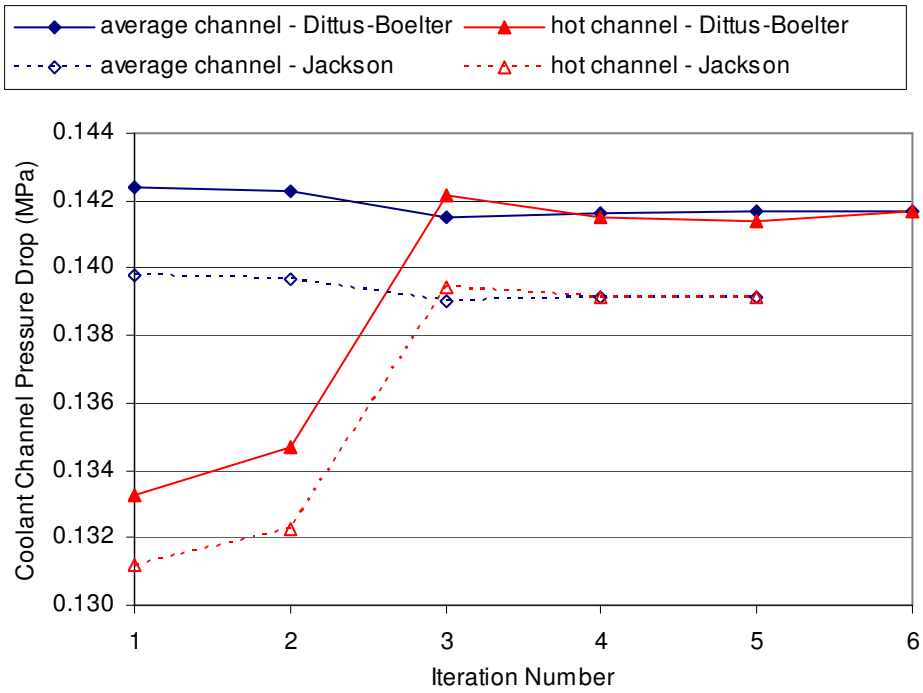

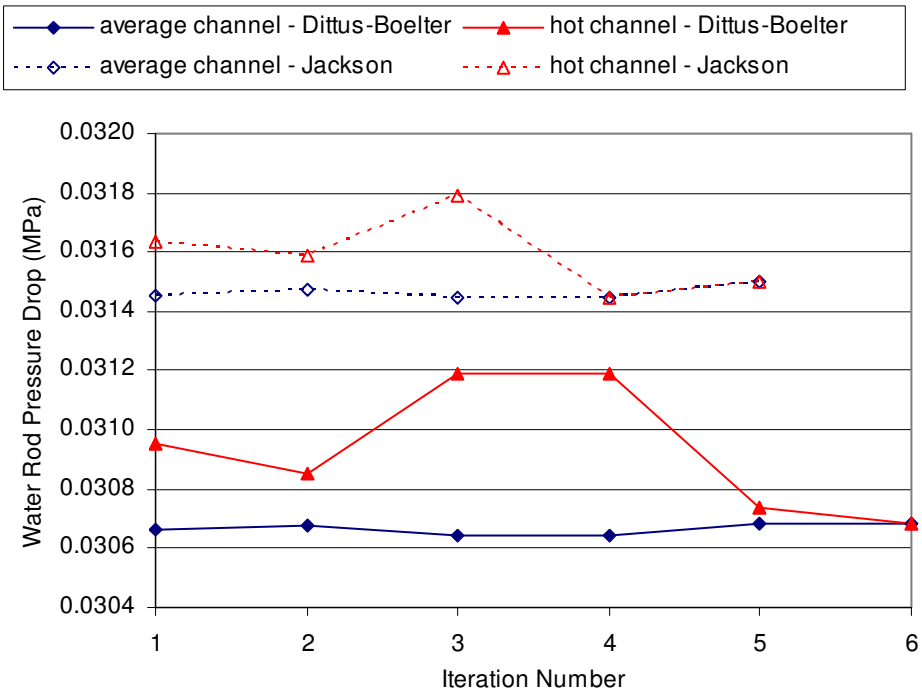

Figure 4-2 Iteration History of Pressure Drops

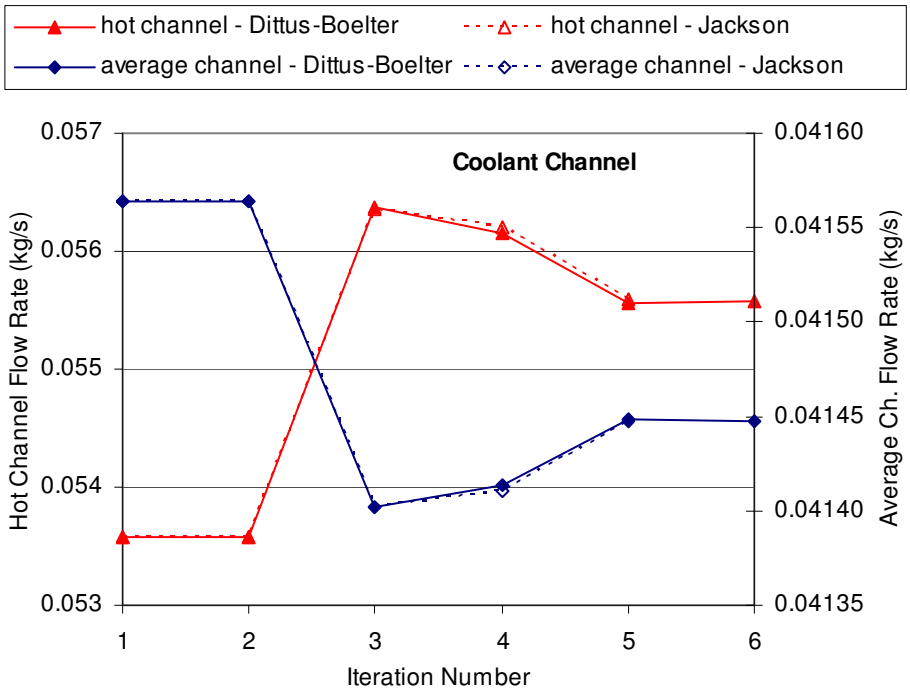

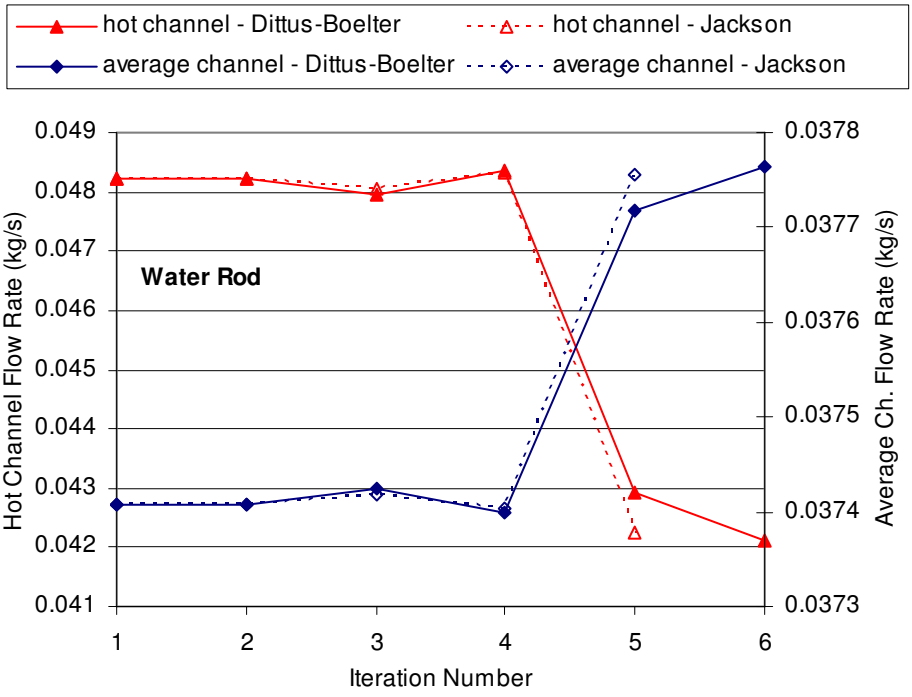

Figure 4-3 Iteration History of Flow Rates

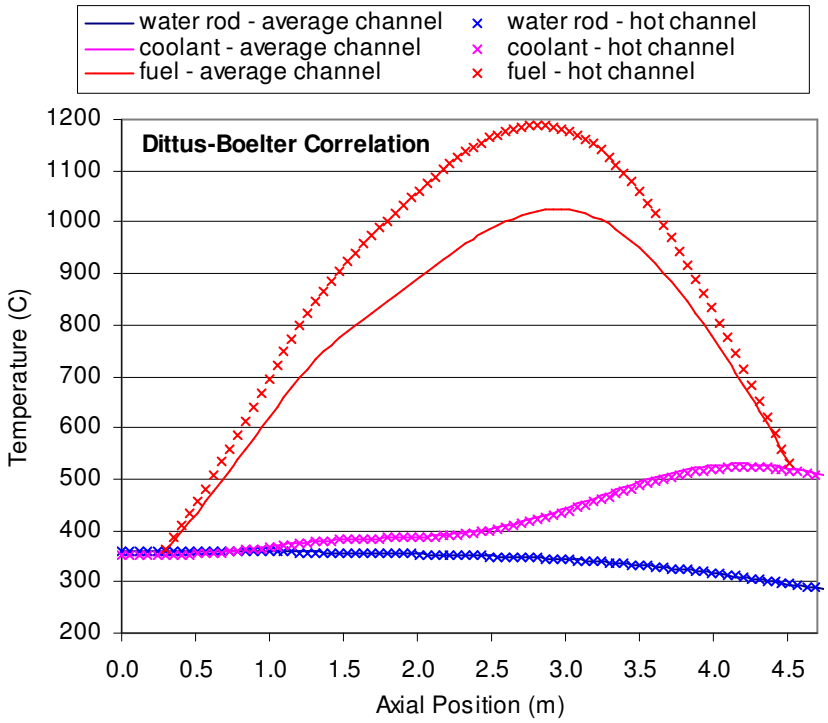

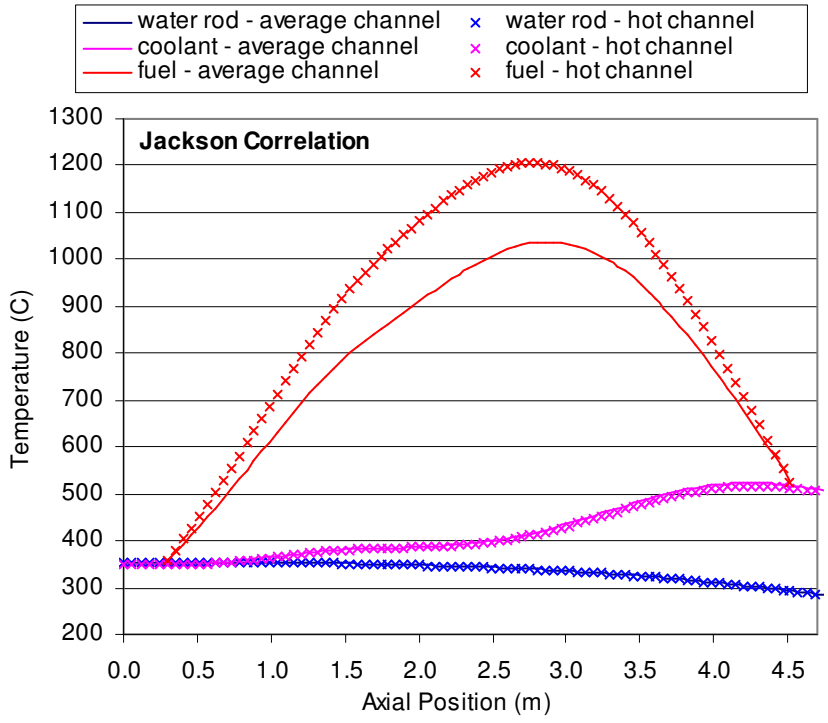

Figure 4-4 Steady State Temperature Distributions of Two-Channel Test Problem

4.2. Stability Analysis

For coupled thermal-nuclear stability analysis, the reactivity feedback coefficients were calculated using the WIMS8 lattice code [22]. Assembly calculations were performed with the method of characteristic solution option. The Doppler, coolant density, and water rod density coefficients determined with average fuel temperature, coolant density, and water rod density are -1.4×10^{-5}/°C, 1.0×10^{-5}/kg-m^{-3}, and 7.5×10^{-5}/kg-m^{-3}, respectively. Relative to a typical LWR, the Doppler coefficient is somewhat smaller due to the higher fuel enrichment. On the other hand, the coolant density coefficient is much smaller than the moderator density coefficient of LWR, since the separate water rods are the main neutron moderator. The sum of the coolant and water-rod density coefficients has the same order of magnitude as the moderator density coefficient of a conventional LWR.

Before performing the stability analyses, preliminary verification tests of the modified SCWRSA were performed using the two-channel model described in Section 4.1. The state variable responses evaluated at a near-zero frequency (10^{-8} rads/s) were compared with the steady state solution changes evaluated directly by perturbing the power by 1 %. Due to the final value theorem of the Laplace transform, the steady state value of a response to a unit step change (i.e., steady state gain) should be equal to the zero frequency response (i.e., the system transfer function evaluated at the zero frequency). Figures 4-5 and 4-6 compare the axial distributions of coolant enthalpy, water rod enthalpy, and fuel temperature changes of the average and hot channels. It can be seen that for both the Dittus-Boelter and Jackson correlations, the zero frequency responses agree very well with the steady state gains determined by direct perturbation calculation. These results suggest that the response functions are correctly calculated.

In order to investigate the effects of flow redistributions due to power perturbation, the frequency response and decay ratio of thermal-nuclear coupled stability of the above two-channel model were compared with old and new results of a single channel model. The new single channel results were obtained for the average channel model using the modified SCWRSA code with the multi-channel analysis capability. The old single channel results were obtained for the same average channel model using the previous version of SCWRSA, in which the variation of water-rod velocity due to power perturbation was not modeled. The decay ratios were

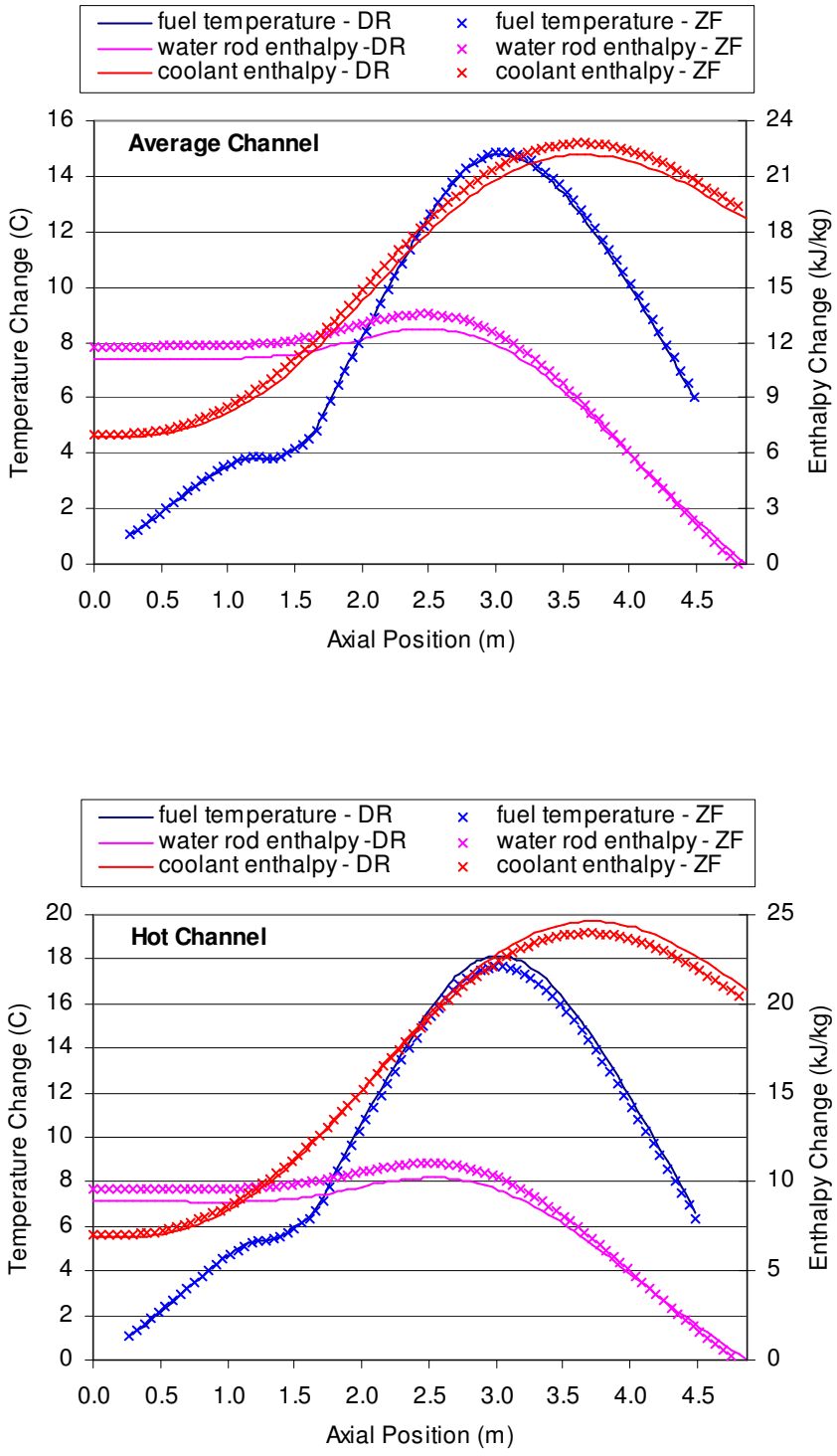

Figure 4-5 Comparison of Direct Perturbation (DP) Calculation vs. Zero Frequency (ZF) Responses of Two-Channel Test Problem (Dittus-Boelter Correlation)

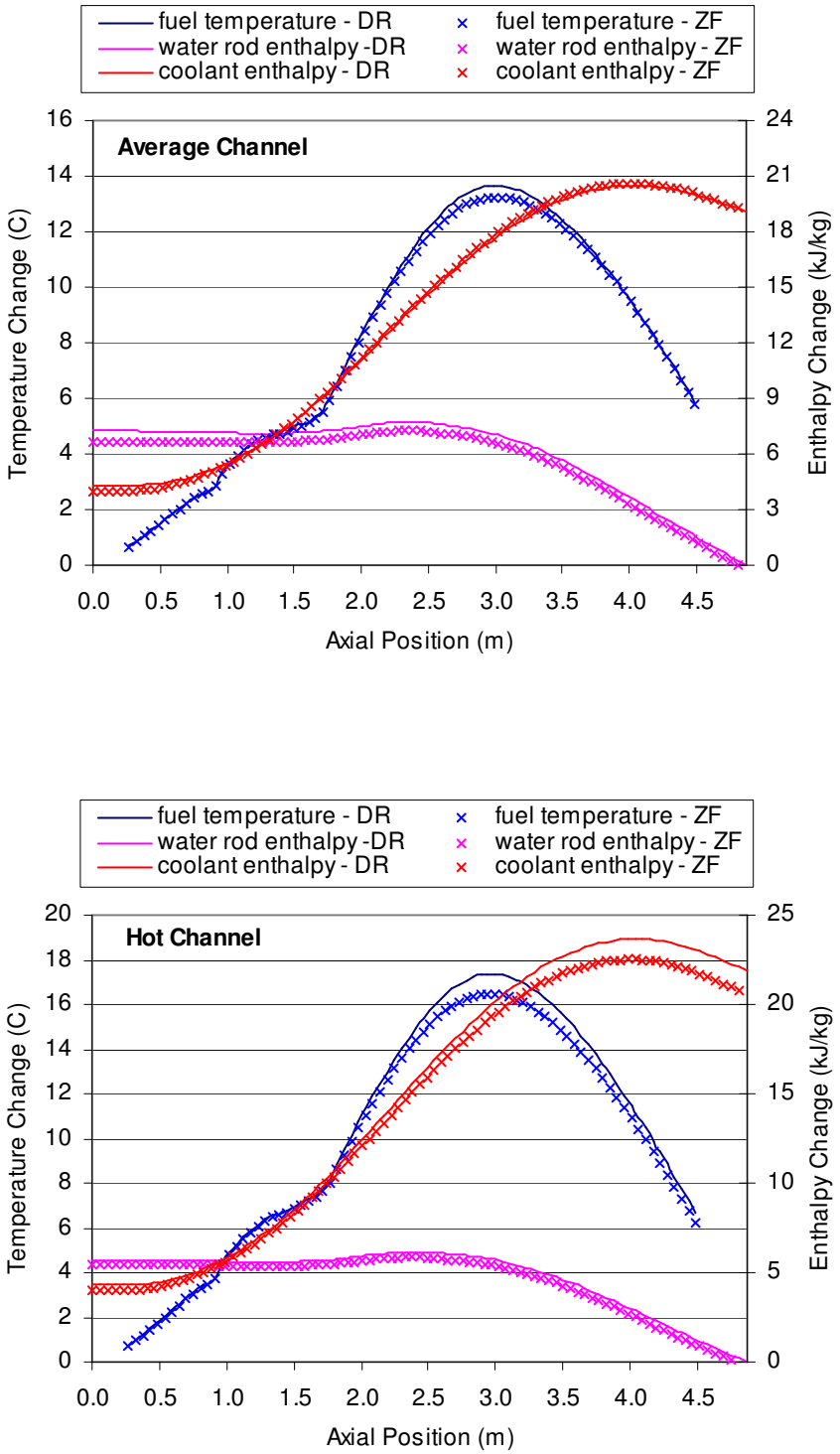

Figure 4-6 Comparison of Direct Perturbation (DP) Calculation vs. Zero Frequency (ZF) Responses of Two-Channel Test Problem (Jackson Correlation)

estimated at the full power and flow conditions. The flow rate and inlet enthalpy of feedwater were held constant, and the active core was divided into 80 axial meshes. For a consistent comparison, the instantaneous mixing approximation was used for the two-channel model.

It was observed that the delayed feedbacks of flow redistributions result in slightly higher resonant frequencies for the two-channel model. Different heat transfer correlations change the heat transfer characteristics between coolant channel and water rod and thus result in somewhat different resonant frequencies. For example, the Bode diagram in Figure 4-7 shows that the two-channel model increases the main resonant frequency from 0.51 to 0.52 rads/s for the Dittus-Boelter correlation and from 0.46 to 0.65 for the Jackson correlation. Relative to the Dittus-Boelter correlation, the Jackson correlation increases the resonant frequency more.

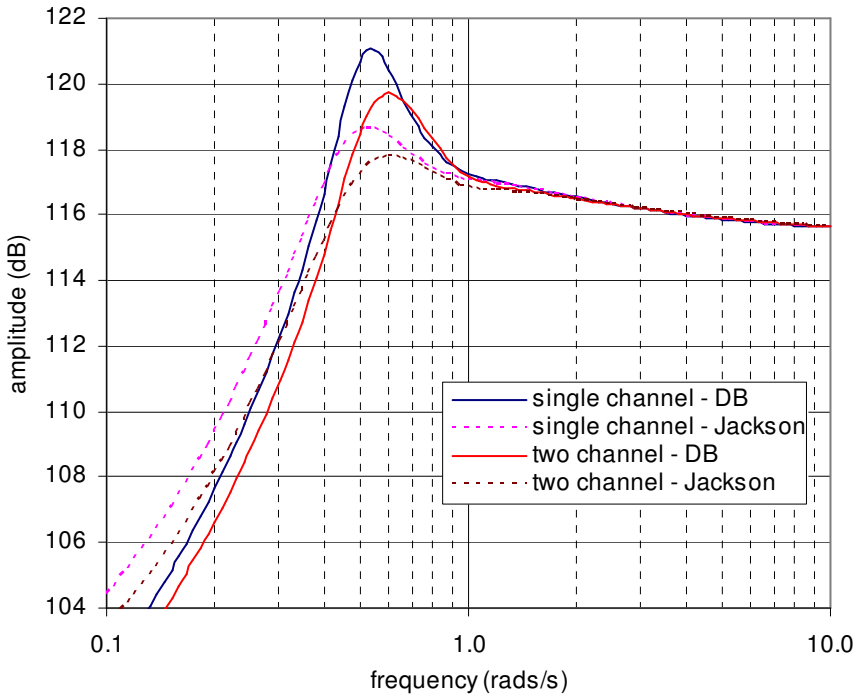

Figure 4-7 Bode Diagram for Thermal-Nuclear Coupled Stability of Two-Channel Test Problem

The roots of the system characteristic equation and the decay ratios are compared in Table 4-3. It can be seen that the water-rod velocity variation due to power perturbation increases the decay ratio slightly because of the increased delayed feedback of water-rod density variation.

As shown in the previous work [4], the delayed feedback due to water-rod density variation increases the decay ratio of thermal-nuclear coupled stability. The decay ratio of two-channel model is smaller than that of single average channel model for both Dittus-Boelter and Jackson correlations. As shown in Figures 4-5 and 4-6, the hot channel has larger variations of average fuel temperature and coolant enthalpy than the average channel, while its water rod enthalpy variation is similar to that of average channel. Thus, the hot channel introduces larger Doppler and coolant density feedbacks than the average channel. As a result, the two-channel model including hot channel assemblies results in smaller decay ratios. Compared to the Dittus-Boelter correlation, the Jackson correlation gives significantly smaller decay ratios because of reduced heat transfer from coolant to water rod that in turn decreases the delayed feedback due to water-rod density variation.

Table 4-3 Roots of System Characteristic Equation and Decay Ratios of Thermal-Nuclear Coupled Stability of Two-Channel Test Problem

Heat Transfer Correlation	Dittus-Boelter			Jackson		
Dominant Root	Real	Imaginary	Decay Ratio	Real	Imaginary	Decay Ratio
Old Single Channel	-0.1411	0.5351	0.1907	-0.1996	0.4548	0.0757
New Single Channel	-0.1175	0.5084	0.2341	-0.1759	0.4582	0.0896
Two Channel	-0.1560	0.5196	0.1517	-0.2729	0.6525	0.0722

To determine the decay ratio for zero mesh size, the effects of the axial mesh size on the dominant root and decay ratio were also investigated. As shown in Figure 4-8 for the coupled thermal-nuclear stability of the two-channel test problem, the dominant root and decay ratio significantly depend on the axial mesh size. However, it can also be seen that they are almost linear functions of mesh size when the mesh size is sufficiently small. Therefore, the decay ratio was determined by computing five values with different mesh sizes (80, 90, 100, 110, and 120 axial meshes for active core height) and by extrapolating those to the zero mesh with a linear least squares fitting.

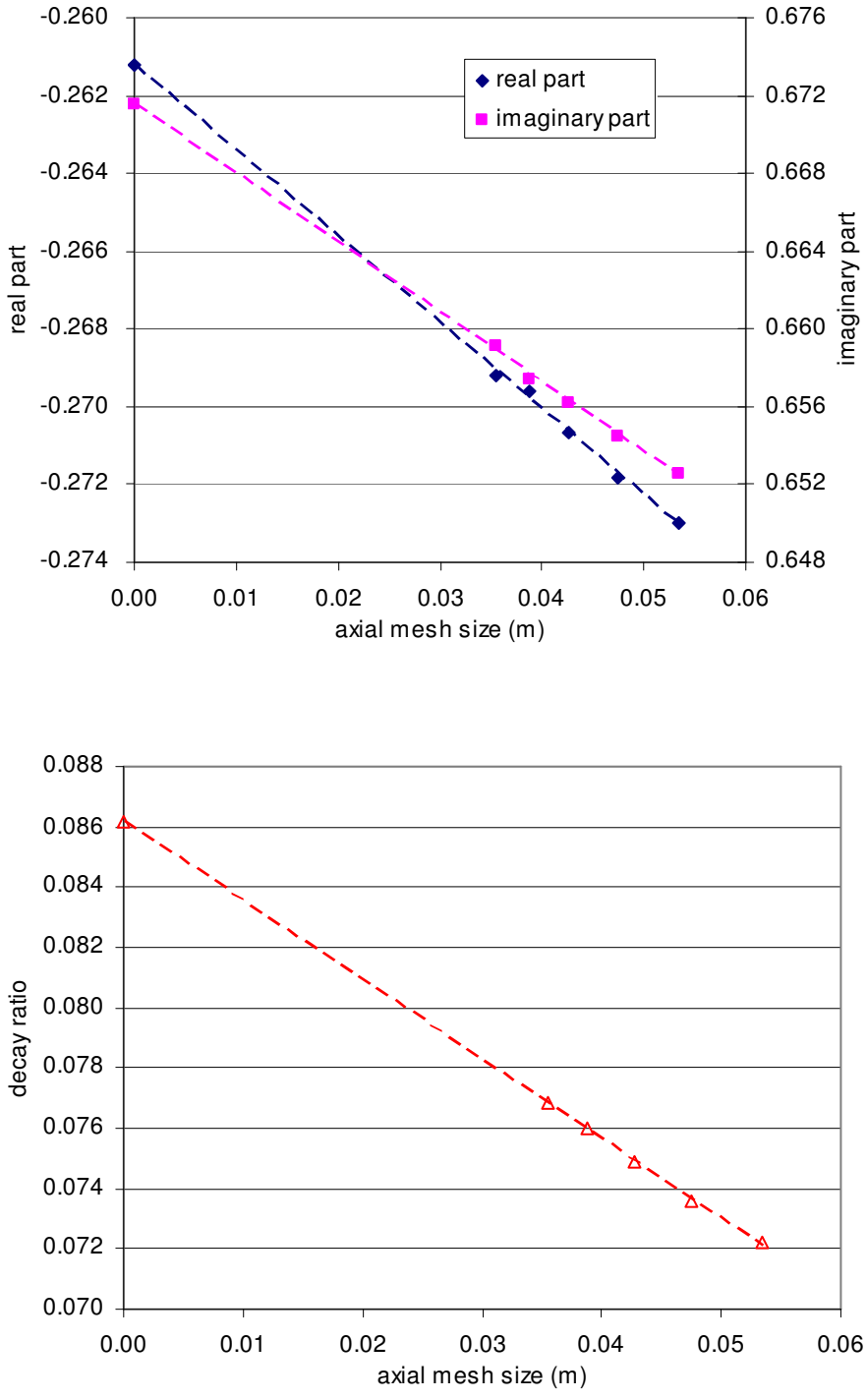

Figure 4-8 Dominant Root and Decay Ratio of Two-Channel Test Problem vs. Mesh Size (Jackson Correlation)

The decay ratios of thermal-nuclear coupled stability were estimated at full power and flow conditions. The same stability criteria for BWR were assumed for SCWR. The decay ratio for the thermal-nuclear coupled stability should be below 1.0 for all operations and below 0.25 for normal operation. The decay ratios for zero mesh size were determined by extrapolating five values obtained with 80, 90, 100, 110, and 120 axial meshes for the active core height. Table 4-4 compares the resulting decay ratios of the single average-channel and two-channel models. The dependency of decay ratio on the axial mesh size is also presented in Figure 4-9. For the two-channel model, the decay ratios were calculated for two bounding inlet boundary conditions discussed in Section 3.2.2. The instantaneous mixing boundary condition neglects the time delay of the mixing in the lower plenum, and it is equivalent to assuming that the lower plenum mass is zero. The constant mixed-mean enthalpy boundary condition assumes that the steady state mixed-mean enthalpy of water in the lower plenum is maintained during the time of interest, and it is equivalent to an assumption of infinite lower plenum mass.

Table 4-4 Roots of System Characteristic Equation and Decay Ratios of Thermal-Nuclear Coupled Stability Estimated for Zero Axial Mesh Size

Heat Transfer Correlation	Dittus-Boelter			Jackson		
Dominant Root	Real	Imaginary	Decay Ratio	Real	Imaginary	Decay Ratio
Single Average Channel	-0.1118	0.5161	0.2561	-0.1727	0.4685	0.0985
Two Channel – Instantaneous Mixing BC	-0.1484	0.5264	0.1695	-0.2612	0.6716	0.0862
Two Channel – Constant Mixed-Mean Enthalpy BC	-0.1545	0.4938	0.1397	-0.2546	0.6715	0.0917

Figure 4-9 shows that the decay ratio of the single channel model is consistently larger than that of two-channel models for both the Dittus-Boelter and Jackson correlations. As aforementioned, the hot channel introduces larger Doppler and coolant density feedbacks, which are prompt relative to the water-rod density feedback. Thus, the two-channel models that include hot channel assemblies result in smaller decay ratios. It is noted that for the Dittus-Boelter correlation, the decay ratio estimated with the single channel model is larger than the BWR stability criterion, while those obtained with two-channel models satisfy the criterion.

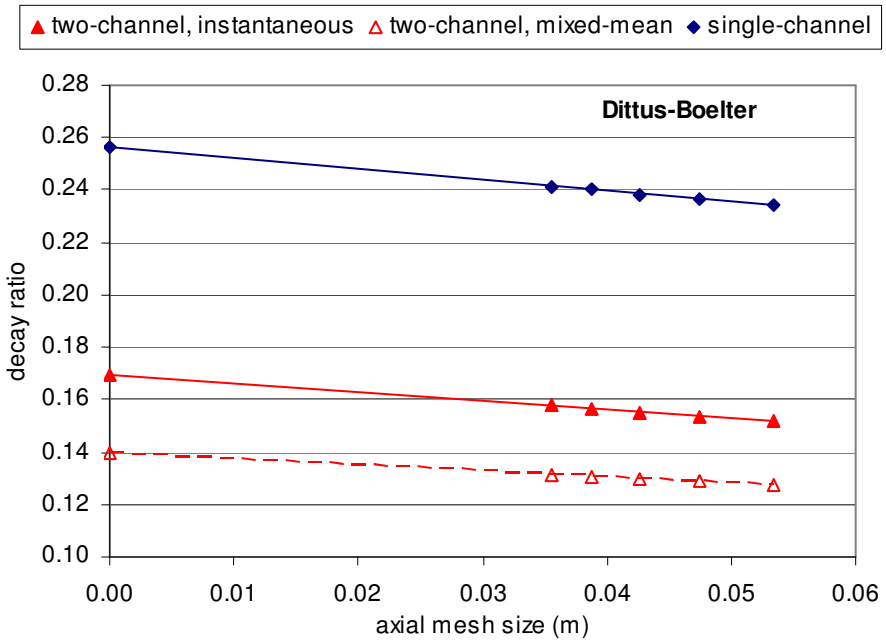

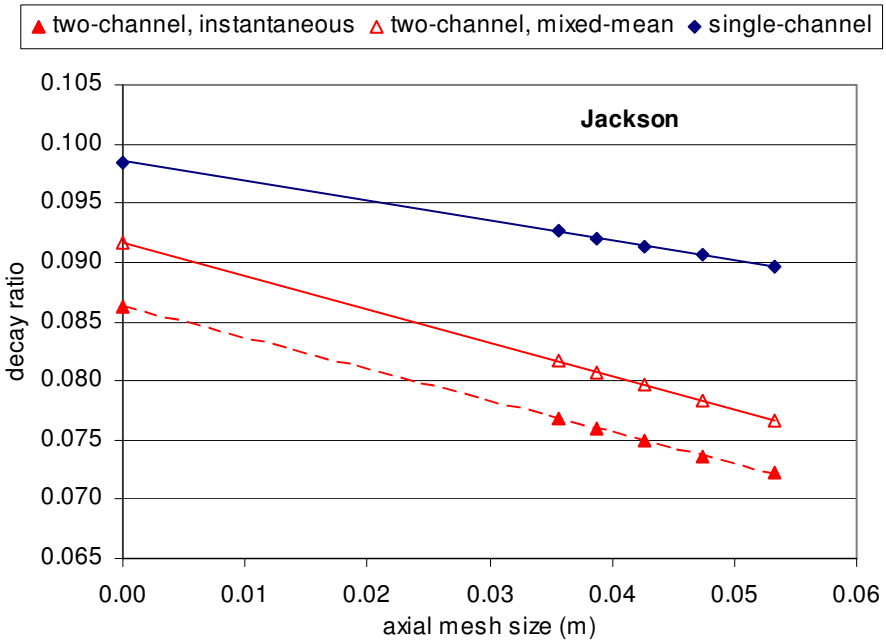

Figure 4-9 Decay Ratio of Two-Channel Test Problem vs. Mesh Size

As discussed above, the Jackson correlation produces significantly smaller decay ratios than the Dittus-Boelter correlation, because of reduced delayed feedback due to water-rod density variation. On the other hand, the effects of the inlet boundary condition are not monotonic. Compared to the constant mixed-mean enthalpy approximation, the instantaneous mixing approximation produces smaller decay ratios for the Dittus-Boelter correlation but larger decay ratios for the Jackson correlation, although the difference is not so significant.

5. Conclusions

The frequency domain linear stability analysis code SCWRSA has been extended to include the multi-channel thermal-hydraulics analysis capability. An iterative solution scheme was developed to calculate the steady state flow distribution among parallel thermal-hydraulics channels under a fixed total flow rate and the equal pressure boundary condition. This scheme determines the coolant and water-rod flow rates simultaneously by taking into account the heat transfer between coolant and water rod. Each thermal-hydraulic channel is represented by a single pin cell with a water rod. The single pin cell representation is made such that the area of water-rod wall per pin cell is preserved. For linear stability analysis, perturbation calculation models for flow redistribution among parallel channels were developed along with an efficient scheme to solve the resulting system of linear equations. Time-dependent behavior of water in the lower plenum was approximated by two bounding inlet boundary conditions: instantaneous mixing and constant mixed-mean enthalpy of water in the lower plenum. The instantaneous mixing boundary condition neglects the time delay of the mixing in the lower plenum, and the constant mixed-mean enthalpy boundary condition assumes that the steady state mixed-mean enthalpy of water in the lower plenum is maintained during the time of interest.

The functionality of the modified SCWRSA code was confirmed by reproducing the previous single-channel analysis results. Preliminary verification tests of the new multi-channel analysis capability have been performed using two-channel models derived from the U.S. Generation IV SCWR reference design. Although individual assemblies can be represented as separate channels, two-channel models were used in these tests for simplicity and because of lack of information on the core power distribution except for the target values of power peaking factors. The iteration scheme to calculate the steady state flow distribution among parallel thermal-hydraulics channels was tested. Initial verification tests for calculated response functions were performed by comparing the near-zero frequency responses with the steady state gains obtained from direct perturbation calculations. The thermal-nuclear coupled stability was estimated by using the stability criteria for BWR. The effects of two bounding inlet boundary conditions on the SCWR stability were also investigated.

Preliminary test results showed that the iteration scheme for the steady state flow distribution produces the converged solution after only a few iterations. It was observed that the heat transfer between coolant and water rod has a non-negligible effect on the steady state flow distribution. The decay ratios obtained with multi-channel models were smaller than those determined with single average-channel models, since the multi-channel model includes hot channel assemblies that introduce larger Doppler and coolant density feedbacks than average channel assemblies. The decay ratio for thermal-nuclear coupled stability estimated with two-channel models was less than 0.17, which is well below the limit traditionally imposed for BWR stability (0.25). It was also observed that the time delay in flow redistribution results in slightly higher resonant frequencies for multi-channel models. The Jackson correlation produced significantly smaller decay ratios than the Dittus-Boelter correlation, because of reduced delayed feedback due to water-rod density variation. On the other hand, the effects of the inlet boundary condition are not monotonic; compared to the constant mixed-mean enthalpy approximation, the instantaneous mixing approximation produces smaller decay ratios for the Dittus-Boelter correlation but larger decay ratios for the Jackson correlation, although the difference is not so significant. The decay ratio for thermal-nuclear coupled stability estimated with two-channel models was less than 0.17, which is well below the limit (0.25) traditionally imposed for BWR stability.

In conclusion, the modified SCWRSA code appears to be functioning correctly, although further verification and validation calculations need to be performed. Future improvements will include the implementation of additional geometry models and a time-dependent lower plenum model to extend its applicability to other SCWR design concepts different from the current reference design. In addition, a space-dependent kinetics model needs to be implemented for analysis of regional (out-of-phase) oscillations.

References

1. "A Technology Roadmap for Generation IV Nuclear Energy Systems," GIF-002-00, US DOE Nuclear Energy Research Advisory Committee and the Generation IV International Forum, 2002.

2. S. JI, H. SHIRAHAMA, S. KOSHIZUKA, and Y. OKA, "Stability Analysis of Supercritical-Pressure Light Water-Cooled Reactor in Constant Pressure Operation," *Proc. of the Ninth International Conference on Nuclear Engineering (ICONE9)*, Nice Acropolis, France, April 8-12, 2001.

3. W. S. YANG and N. ZAVALJEVSKI, "Preliminary Stability Analysis for Supercritical Water Reactor," *Proc. of Global 2003*, New Orleans, LA, November 16-20, 2003.

4. W. S. YANG and N. ZAVALJEVSKI, "Effects of Water Rods on Supercritical Water Reactor Stability," *Proc. of 2005 International Congress on Advances in Nuclear Power Plants (ICAPP05)*, Seoul, Korea, May 15-19, 2005.

5. T. T. YI, S. KOSHIZUKA, and Y. OKA "Linear Stability Analysis of a High-Temperature Supercritical-Pressure Light Water Reactor," *Proc. of Global 2003*, New Orleans, LA, November 16-20, 2003.

6. N. E. TODREAS and M. S. KAZIMI, *Nuclear Systems I Thermal Hydraulic Fundamentals*, Hemisphere Publishing Co., New York, New York, 1990.

7. A. H. HARVEY, A. P. PESKIN, and S. A. KLEIN, "NIST/ASME Steam Properties Database, version 2.2," US Department of Commerce, Technology Administration, National Institute of Standard and Technology, 1997.

8. R. H. S. WINTERTON, "Where Did the Dittus and Boelter Equation Come From," *Int. J. Heat Mass Transfer*, **41**, 809 (1998).

9. J. G. COLLIER, *Convective Boiling and Condensation*, 2nd Edition, McGraw-Hill Inc., New York, New York (1981).

10. J. D. JACKSON, "Consideration of the Heat Transfer Properties of Supercritical Pressure Water in Connection with the Cooling of Advanced Nuclear Reactors," *Proceedings of the 13th Pacific Basin Nuclear Conference*, Shenzhen, China, 21-25 October 2002.

11. J. BUONGIORNO, Personal Communication, Idaho National Engineering and Environmental Laboratory, January 2004.

12. W. S. YANG and N. ZAVALJEVSKI, "Effects of Water Rods and Heat Transfer Correlations on SCWR Stability," Gen-IV Report, Argonne National Laboratory, September 2004.

13. K. O. OTT and R. J. NEUHOLD, *Introductory Nuclear Reactor Dynamics*, American Nuclear Society, La Grange Park, Illinois, 1985.

14. S. KOSHIZUKA and Y. OKA, "Computational Analysis of Deterioration Phenomena and Thermal-hydraulic Design of SCR," *Proc. of the First International Symposium on Supercritical Water-cooled Reactors (SCR-2000)*, Tokyo, Japan, November 6-8, 2000.

15. X. CHENG and T. SCHULENBERG, "Heat Transfer at Supercritical Pressures – Literature Review and Applications to a HPLWR," FZKA 6609, Forschungszentrum Karlsruhe, April 2001.

16. J. R. HOWELL and S. H. LEE, "Convective Heat Transfer in the Entrance Region of a Vertical Tube for Water near the Thermodynamic Critical Point," *International Journal of Heat and Mass Transfer*, 42, pp. 1177-1187, 1999.

17. W. S. YANG and N. ZAVALJEVSKI, "Preliminary Investigation of Power-Flow Instabilities of Supercritical Water Reactor," Gen-IV Report, Argonne National Laboratory, September 2003.

18. D. L. HETRICK, *Dynamics of Nuclear Reactors*, American Nuclear Society, La Grange Park, Illinois (1993).

19. R. T. LAHEY, Jr. and F. J. MOODY, *The Thermal-Hydraulics of a Boiling Water Nuclear Reactor*, Second Edition, American Nuclear Society, La Grange Park, Illinois (1993).

20. W. H. PRESS, S. A. TEUKOLSKY, W. T. VETTERLING, and B. P. FLANNERY, *Numerical Recipes*, 2nd Edition, Cambridge University Press, New York, New York (1992).

21. P. J. OTADUY, J. MARCH-LEUBA, "LAPUR User's Guide," ORNL/TM-11285, Oak Ridge National Laboratory (1990).

22. "WIMS - A Modular Scheme for Neutronics Calculations, User's Guide for Version 8," ANSWERS /WIMS(99)9, The ANSWERS Software Package, AEA Technology (1999).

Appendix A. Derivatives of Heat Transfer Coefficients

The Dittus-Boelter correlation for convective heat transfer is given by the formula

$$Nu = C\,\mathrm{Re}^{n}\,Pr^{m} \tag{A.1}$$

where Nu , Re, and Pr are Nusselt , Reynolds and Prandtl numbers defined by

$$Nu = \frac{hD}{k} \tag{A.2}$$

$$Re = \frac{\rho v D}{\mu} \tag{A.3}$$

$$Pr = \frac{\mu c_p}{k} \tag{A.4}$$

with heat transfer coefficient h_w , fluid density ρ , velocity v , viscosity μ , conductivity k , specific heat c_p , and hydraulic diameter D . Differentiating Eqs. (A.1) to (A.4), we obtain

$$\begin{aligned}\frac{\delta h}{h} &= \frac{\delta Nu}{Nu} + \frac{\delta k}{k} = n\frac{\delta \mathrm{Re}}{\mathrm{Re}} + m\frac{\delta Pr}{Pr} + \frac{\delta k}{k} \\ &= (1-m)\frac{\delta k}{k} + n\frac{\delta \rho}{\rho} + (n-m)\frac{\delta \mu}{\mu} + m\frac{\delta c_p}{c_p} + n\frac{\delta v}{v}\end{aligned} \tag{A.5}$$

Thus, the partial derivatives of heat transfer can be determined as

$$\frac{1}{h}\frac{\partial h}{\partial h_b} = \frac{(1-m)}{k}\frac{\partial k}{\partial h_b} + \frac{n}{\rho}\frac{\partial \rho}{\partial h_b} + \frac{(n-m)}{\mu}\frac{\partial \mu}{\partial h_b} + \frac{m}{c_p}\frac{\partial c_p}{\partial h_b} \tag{A.6}$$

$$\frac{1}{h}\frac{\partial h}{\partial P} = \frac{(1-m)}{k}\frac{\partial k}{\partial P} + \frac{n}{\rho}\frac{\partial \rho}{\partial P} + \frac{(n-m)}{\mu}\frac{\partial \mu}{\partial P} + \frac{m}{c_p}\frac{\partial c_p}{\partial P} \tag{A.7}$$

$$\frac{1}{h}\frac{\partial h}{\partial v} = \frac{n}{v} \tag{A.8}$$

The Jackson correlation developed for forced convection heat transfer from tubes to supercritical water and supercritical carbon dioxide is given by

$$Nu_b = C\,Re_b^{n} Pr_b^{m} \left(\frac{\rho_w}{\rho_b}\right)^{l} \left(\frac{\overline{c}_p}{c_{pb}}\right)^{\alpha} \tag{A.9}$$

where $\overline{c}_p$ is defined by

$$\overline{c}_p = \frac{h_w - h_b}{T_w - T_b} \tag{A.10}$$

and the exponent α is defined as

$$\alpha = \begin{cases} 0.4 & \text{for } T_b < T_w < T_{pc} \\ 0.4 + 0.2(T_w/T_{pc} - 1) & \text{for } T_b < T_{pc} < T_w \\ 0.4 + 0.2(T_w/T_{pc} - 1)[1 - 5(T_b/T_{pc} - 1)] & \text{for } T_{pc} < T_b < 1.2T_{pc} \text{ and } T_b < T_w \\ 0.4 & \text{for } 1.2T_{pc} < T_b < T_w \end{cases} \tag{A.11}$$

where T_{pc} is the pseudo-critical temperature. Here the subscript b and w denote the properties at bulk coolant and local wall temperatures, respectively. The pseudo-critical temperature is defined as the temperature at which the specific heat capacity at constant pressure is maximized. It is obtained from the correlation of Howell and Lee

$$T_{pc} = 547.27 + 114.97\,\overline{p}_r - 15.216\,\overline{p}_r^2 \tag{A.12}$$

where T_{pc} is in degrees K and $\overline{p}_r$ is the reduced pressure, which is calculated as

$$\overline{p}_r = \frac{P}{P_c} \tag{A.13}$$

where P is the pressure and P_c is the critical pressure. By differentiating Eq. (A.9), we obtain

$$\begin{aligned} \frac{\delta h}{h} = {} & (1-m)\frac{\delta k}{k} + (n-l)\frac{\delta \rho}{\rho} + (n-m)\frac{\delta \mu}{\mu} + (m-\alpha)\frac{\delta c_p}{c_p} + n\frac{\delta v}{v} + l\frac{\delta \rho_w}{\rho_w} \\ & + \alpha\frac{\delta \overline{c}_p}{\overline{c}_p} + \delta\alpha \ln\frac{\overline{c}_p}{c_p} \end{aligned} \tag{A.14}$$

From Eqs. (A.10) to (A.13), the differentials of $\overline{c}_p$, α, and T_{pc} can be determined as

$$\frac{\delta \overline{c}_p}{\overline{c}_p} = \frac{\delta h_w - \delta h_b}{h_w - h_b} - \frac{\delta T_w - \delta T_b}{T_w - T_b} \tag{A.15}$$

$$\delta\alpha = \begin{cases} 0 & \text{for } T_b < T_w < T_{pc} \\ a_1\delta T_w + b_1\delta T_{pc} & \text{for } T_b < T_{pc} < T_w \\ a_2\delta T_w + b_2\delta T_{pc} + c_2\delta T_b & \text{for } T_{pc} < T_b < 1.2T_{pc} \text{ and } T_b < T_w \\ 0 & \text{for } 1.2T_{pc} < T_b < T_w \end{cases} \tag{A.16}$$

$$\delta T_{pc} = (114.97 - 30.432\,\overline{p}_r)\delta P / P_c \tag{A.17}$$

where

$$a_1 = \frac{0.2}{T_{pc}}, \quad b_1 = -0.2\frac{T_w}{T_{pc}^2},$$
$$a_2 = \frac{0.2}{T_{pc}}\left(6 - 5\frac{T_b}{T_{pc}}\right), b_2 = -\frac{0.2}{T_{pc}^2}(6T_w - 5T_b), \quad c_2 = -\frac{5}{T_{pc}}\left(\frac{T_w}{T_{pc}} - 1\right) \tag{A.18}$$

Combining Eqs. (A.14) to (A.18), the partial derivatives of heat transfer coefficient are obtained as

$$\frac{1}{h}\frac{\partial h}{\partial h_b} = \frac{(1-m)}{k}\frac{\partial k}{\partial h_b} + \frac{(n-l)}{\rho}\frac{\partial \rho}{\partial h_b} + \frac{(n-m)}{\mu}\frac{\partial \mu}{\partial h_b} + \frac{(m-\alpha)}{c_p}\frac{\partial c_p}{\partial h_b} - \alpha\left[\frac{1}{h_w - h_b} - \frac{1}{(T_w - T_b)c_p}\right] + \frac{\partial \alpha}{\partial h_b}\ln\frac{\overline{c}_p}{c_p} \tag{A.19}$$

$$\frac{1}{h}\frac{\partial h}{\partial P} = \frac{(1-m)}{k}\frac{\partial k}{\partial P} + \frac{(n-l)}{\rho}\frac{\partial \rho}{\partial P} + \frac{(n-m)}{\mu}\frac{\partial \mu}{\partial P} + \frac{(m-\alpha)}{c_p}\frac{\partial c_p}{\partial P} + \frac{l}{\rho_w}\frac{\partial \rho_w}{\partial P} + \frac{\alpha}{(T_w - T_b)}\left[\frac{1}{c_{pw}}\frac{\partial h_w}{\partial P}\bigg|_T - \frac{1}{c_{pb}}\frac{\partial h_b}{\partial P}\bigg|_T\right] + \frac{\partial \alpha}{\partial P}\ln\frac{\overline{c}_p}{c_p} \tag{A.20}$$

$$\frac{1}{h}\frac{\partial h}{\partial v} = \frac{n}{v} \tag{A.21}$$

$$\frac{1}{h}\frac{\partial h}{\partial T_w} = \frac{l}{\rho_w}\frac{\partial \rho_w}{\partial T_w} + \alpha\left[\frac{c_{pw}}{h_w - h_b} - \frac{1}{T_w - T_b}\right] + \frac{\partial \alpha}{\partial T_w}\ln\frac{\overline{c}_p}{c_p} \tag{A.22}$$

using the following relations

$$\frac{\partial T}{\partial h}\bigg|_P = \frac{1}{c_p} \tag{A.23}$$

$$\frac{\partial T}{\partial P}\bigg|_h = -\frac{1}{c_p}\frac{\partial h}{\partial P}\bigg|_T \tag{A.24}$$

The partial derivatives of the exponent α are given by

$$\frac{\partial \alpha}{\partial h_b} = \begin{cases} 0 & \text{for } T_b < T_w < T_{pc} \\ 0 & \text{for } T_b < T_{pc} < T_w \\ c_2 / c_{pb} & \text{for } T_{pc} < T_b < 1.2T_{pc} \text{ and } T_b < T_w \\ 0 & \text{for } 1.2T_{pc} < T_b < T_w \end{cases} \tag{A.25}$$

$$\frac{\partial \alpha}{\partial P} = \begin{cases} 0 & \text{for } T_b < T_w < T_{pc} \\ b_1 \dfrac{\partial T_{pc}}{\partial P} & \text{for } T_b < T_{pc} < T_w \\ b_2 \dfrac{\partial T_{pc}}{\partial P} - \dfrac{c_2}{c_p} \dfrac{\partial h_b}{\partial P}\bigg|_T & \text{for } T_{pc} < T_b < 1.2T_{pc} \text{ and } T_b < T_w \\ 0 & \text{for } 1.2T_{pc} < T_b < T_w \end{cases} \tag{A.26}$$

$$\frac{\partial \alpha}{\partial T_w} = \begin{cases} 0 & \text{for } T_b < T_w < T_{pc} \\ a_1 & \text{for } T_b < T_{pc} < T_w \\ a_2 & \text{for } T_{pc} < T_b < 1.2T_{pc} \text{ and } T_b < T_w \\ 0 & \text{for } 1.2T_{pc} < T_b < T_w \end{cases} \tag{A.27}$$

Appendix B. Iterative Search Scheme for Dominant Root of Characteristic Equation

The system characteristic equation described in Section 3.4.2 can be represented by a nonlinear equation in complex domain as

$$F(s) = 1 + G(s) = X(\sigma, \omega) + jY(\sigma, \omega) = 0 \tag{B.1}$$

where

$$s = \sigma + j\omega \tag{B.2}$$

This equation can be solved using the Newton-Raphson method, which derives from the Taylor series expansion of a function in the neighborhood of the present point,

$$F(s + \delta s) = F(s) + F'(s)\delta s + \frac{1}{2}F''(s)(\delta s)^2 + \cdots \tag{B.3}$$

For small enough values of δs, and for well-behaved functions, the terms beyond linear are unimportant, hence $F(s + \delta s) = 0$ implies

$$\delta s = -\frac{F(s)}{F'(s)} \tag{B.4}$$

By evaluating this Newton step at a trial solution s_i, the next trial solution is determined as

$$s_{i+1} = s_i + \delta s_i \tag{B.5}$$

until this change becomes negligible.

Since an analytic function satisfies the Cauchy-Riemann equation, the derivative $F'(s)$ is given by

$$F'(s) = \frac{\partial X}{\partial \sigma} + j\frac{\partial Y}{\partial \sigma} = \frac{\partial Y}{\partial \omega} - j\frac{\partial X}{\partial \omega} \tag{B.6}$$

Thus, the Newton step is explicitly determined only with the derivatives with respect to frequency as

$$\delta s = \delta\sigma + j\delta\omega \tag{B.7}$$

where

$$\delta\sigma = -\frac{1}{|F'(s)|^2}\left(\frac{\partial Y}{\partial \omega}X - \frac{\partial X}{\partial \omega}Y\right) \tag{B.8}$$

$$\delta\omega = -\frac{1}{|F'(s)|^2}\left(\frac{\partial X}{\partial \omega}X + \frac{\partial Y}{\partial \omega}Y\right) \tag{B.9}$$

$$| F'(s) |^2 = \left(\frac{\partial X}{\partial \omega} \right)^2 + \left(\frac{\partial Y}{\partial \omega} \right)^2 \tag{B.10}$$

When a trial solution s_i differs from the true root s by ε_i, $F(s_i)$ and $F'(s_i)$ can be expressed in terms of ε_i and derivatives at the root itself as

$$\begin{aligned} F(s_i) &= F(s+\varepsilon_i) = F'(s)\varepsilon_i + \frac{1}{2}F''(s)\varepsilon_i^2 + \cdots \\ F'(s_i) &= F'(s+\varepsilon_i) = F'(s) + F''(s)\varepsilon_i + \cdots \end{aligned} \tag{B.11}$$

since $F(s) = 0$. Thus a recurrence relation for the deviation of the trial solution can be determined as

$$\varepsilon_{i+1} = s_{i+1} - s = s_i + \delta s_i - s = \varepsilon_i - \frac{F(s_i)}{F'(s_i)} = -\frac{\varepsilon_i^2}{2}\frac{F''(s)}{F'(s)} \tag{B.12}$$

This shows that the Newton-Raphson method converges quadratically near a root, and hence the number of significant digits approximately doubles with each step.

However, far from a root where the higher order terms are important, the Newton-Raphson formula can give grossly inaccurate, meaningless corrections. For instance, the initial guess for the root might be so far from the true root as to let the search interval include a local maximum or minimum of the function. If iteration places a trial guess near such a local extreme, so that the first derivative nearly vanishes, then Newton-Raphson sends its solution off to a limbo, with vanishingly small hope of recovery. In other words, its global convergence property is poor, and hence it often diverges if the initial guess is not sufficiently close to the root. Therefore, it is desirable to combine the rapid local convergence of Newton's method with a globally convergent strategy that will guarantee some progress towards the solution at each iteration.

The characteristic equation given in Eq. (B.1) is equivalent to the equation $| F | = 0$. However, when the old point s_i is not close enough to the root, taking the full Newton step δs need not make the new point s_{i+1} reduce $| F |$ and closer to the root. Therefore, in order to guarantee some progress towards the solution at each iteration, the new step is determined such

that it decreases $|F|$. This is the same requirement we would impose if we were trying to minimize the function

$$f(s) = \frac{1}{2}|F(s)|^2 \tag{B.13}$$

Every solution to Eq. (B.1) minimizes Eq. (B.13), but there may be local minima of Eq. (B.13) that are not solutions to Eq. (B.1).

Representing the complex variable s and the characteristic function $F(s)$ as two dimensional vectors as

$$\mathbf{s} = (\sigma, \omega)^T \tag{B.14}$$

$$\mathbf{F}(\mathbf{s}) = [X(\mathbf{s}), Y(\mathbf{s})]^T \tag{B.15}$$

the characteristic equation in Eq. (B.1) is represented as a set of equations as

$$\mathbf{F}(\mathbf{s}) = 0 \tag{B.16}$$

The Newton step for this set of equations is given by

$$\delta\mathbf{s} = (\delta\sigma, \delta\omega)^T = -\mathbf{J}^{-1} \cdot \mathbf{F} \tag{B.17}$$

Here $\mathbf{J}$ is the Jacobian matrix

$$\mathbf{J} = \begin{bmatrix} \frac{\partial X}{\partial \sigma} & \frac{\partial X}{\partial \omega} \\ \frac{\partial Y}{\partial \sigma} & \frac{\partial Y}{\partial \omega} \end{bmatrix} = \begin{bmatrix} \frac{\partial Y}{\partial \omega} & \frac{\partial X}{\partial \omega} \\ -\frac{\partial X}{\partial \omega} & \frac{\partial Y}{\partial \omega} \end{bmatrix} \tag{B.18}$$

whose inverse is

$$\mathbf{J}^{-1} = \frac{1}{\left(\frac{\partial X}{\partial \omega}\right)^2 + \left(\frac{\partial Y}{\partial \omega}\right)^2} \begin{bmatrix} \frac{\partial Y}{\partial \omega} & -\frac{\partial X}{\partial \omega} \\ \frac{\partial X}{\partial \omega} & \frac{\partial Y}{\partial \omega} \end{bmatrix} \tag{B.19}$$

In this representation, the function $f(s)$ defined in Eq. (B.13) is given by

$$f(\mathbf{s}) = \frac{1}{2}\mathbf{F} \cdot \mathbf{F} \tag{B.20}$$

A global method can be developed by minimizing $f(s)$ along the Newton direction $\delta\mathbf{s}$ in Eq. (B.17) by taking Newton steps designed to bring $\mathbf{F}$ to zero. To utilize the quadratic convergence of Newton method near the root, the full Newton step is first tried. However, it is

checked at each iteration that the proposed step reduces f. If not, the Newton direction is backtracked until an acceptable step is found. In other words, a new point along the Newton direction $\delta\mathbf{s}$ is determined as

$$\mathbf{s}_{i+1} = \mathbf{s}_i + \lambda\delta\mathbf{s}, \quad 0 < \lambda \le 1 \tag{B.21}$$

by finding λ so that $F(\mathbf{s}_{i+1})$ has decreased sufficiently. It is guaranteed to find an acceptable step by backtracking, since the Newton step is a descent direction for f

$$df = \nabla f \cdot \delta\mathbf{s} = (\mathbf{F}\cdot\mathbf{J})\cdot(-\mathbf{J}^{-1}\cdot\mathbf{F}) = -\mathbf{F}\cdot\mathbf{F} < 0 \tag{B.22}$$

The parameter λ can be determined such that it exactly minimizes f in the direction $\delta\mathbf{s}$. However, it is extremely wasteful of function evaluation. A better strategy is obtained by requiring the average rate of decrease of f to be at least some fraction α of the initial rate of decrease $\nabla f \cdot \delta\mathbf{s}$

$$f(\mathbf{s}_{i+1}) \le f(\mathbf{s}_i) + \alpha\nabla f \cdot (\mathbf{s}_{i+1} - \mathbf{s}_i), \quad 0 < \alpha < 1 \tag{B.23}$$

and by requiring the rate of decrease of f at $\mathbf{s}_{i+1}$ to be greater than some fraction β of the rate of decrease of f at $\mathbf{s}_i$. By defining a function $g(\lambda)$

$$g(\lambda) = f(\mathbf{s}_i + \lambda\delta\mathbf{s}) \tag{B.24}$$

so that

$$g'(\lambda) = \nabla f \cdot \delta\mathbf{s} \tag{B.25}$$

A practical backtracking algorithm is derived as follows:

(1) The first step is always the Newton step, $\lambda = 1$.

(2) If this step is not acceptable, $g(\lambda)$ is approximated by a quadratic polynomial.

(3) Using available values $g(0) = F(\mathbf{s}_i)$, $g'(0) = \nabla f(\mathbf{s}_i)\cdot\delta\mathbf{s}_i < 0$, and $g(1) = F(\mathbf{s}_{i+1})$, $g(\lambda)$ is approximated as

$$g(\lambda) \approx [g(1) - g(0) - g'(0)]\lambda^2 + g'(0)\lambda + g(0) \tag{B.26}$$

(4) λ is determined by minimizing this quadratic

$$\lambda = -\frac{g'(0)}{2[g(1) - g(0) - g'(0)]} \tag{B.27}$$

(5) Since the Newton step failed, $g(1) > g(0) + \alpha g'(0)$ and hence $\lambda < [2(1-\alpha)]^{-1}$. However, we need to guard against too small a value of λ to avoid taking steps that are

too small. $\lambda_{\min} \approx 0.1$

(6) On the second and subsequent backtracks, $g(\lambda)$ is approximated by a cubic polynomial. Using the previous $g(\lambda_1)$ and the second most recent value $g(\lambda_2)$, $g(\lambda)$ is approximated as

$$g(\lambda) = a\lambda^3 + b\lambda^2 + g'(0)\lambda + g(0) \tag{B.28}$$

$$a = \frac{1}{\lambda_1 - \lambda_2}\left\{\frac{1}{\lambda_1^2}[g(\lambda_1) - g'(0)\lambda_1 - g(0)] - \frac{1}{\lambda_2^2}[g(\lambda_2) - g'(0)\lambda_2 - g(0)]\right\} \tag{B.29}$$

$$b = \frac{1}{\lambda_1 - \lambda_2}\left\{-\frac{\lambda_2}{\lambda_1^2}[g(\lambda_1) - g'(0)\lambda_1 - g(0)] + \frac{\lambda_1}{\lambda_2^2}[g(\lambda_2) - g'(0)\lambda_2 - g(0)]\right\} \tag{B.30}$$

(7) λ is determined by minimizing this cubic

$$\lambda = \frac{-b + \sqrt{b^2 - 3ag'(0)}}{3a} \tag{B.31}$$

(8) Enforce λ to lie between $\lambda_{\max} = 0.5\lambda_1$ and $\lambda_{\min} = 0.1\lambda_1$. The initial guesses σ_0 and ω_0 are determined as follows:

(9) σ_0 is set to zero since the frequency responses are calculated for a given interval of frequencies.

(10) ω_0 is determined by the value among the initial frequencies used in evaluating the frequencies that minimizes f. Since this ω_0 is generally a very good approximation to the resonant frequency, the maximum step length for line search is limited by ω_0. This restriction avoids an excessive step change in the first iteration, which seems to result in one of non-dominant roots.